NASA CONTRACTOR REPORT

NASA CR-2247

NASA CR-2247

THE ELEVATION, SLOPE, AND CURVATURE SPECTRA OF A WIND ROUGHENED SEA SURFACE

by Willard J. Pierson, Jr., and Robert A. Stacy

Prepared by
SCHOOL OF ENGINEERING AND SCIENCE
NEW YORK UNIVERSITY
University Heights, Bronx, N.Y. 10453
for Langley Research Center

NATIONAL AERONAUTICS AND SPACE ADMINISTRATION • WASHINGTON, D. C. • DECEMBER 1973

1. Report No.	2. Government Accession No.	3. Recipient's Catalog No.
NASA CR-2247		

4. Title and Subtitle	5. Report Date
THE ELEVATION, SLOPE, AND CURVATURE SPECTRA OF A WIND ROUGHENED SEA SURFACE	December 1973
	6. Performing Organization Code

7. Author(s)	8. Performing Organization Report No.
Willard J. Pierson, Jr., and Robert A. Stacy	
	10. Work Unit No.

9. Performing Organization Name and Address	11. Contract or Grant No.
New York University School of Engineering and Science Department of Meteorology and Oceanography University Heights, Bronx, New York 10453	NAS1-10090
	13. Type of Report and Period Covered
12. Sponsoring Agency Name and Address	Contractor Report
National Aeronautics and Space Administration Washington, D.C. 20546	14. Sponsoring Agency Code

15. Supplementary Notes

This is a final report.

16. Abstract

The elevation, slope and curvature spectra of a wind roughened sea surface are deduced from an analysis of a wide variety of reports and data sources and verified to a large extent by means of both these sources and other independent sources. The spectra are defined as a function of wave number and depend on u_* (the friction velocity). There are five wave number ranges of definition called the gravity wave-gravity equilibrium range, the isotropic turbulence range, the connecting range due to Leykin and Rosenberg, the capillary range, and the viscous cutoff range. The higher wave number ranges are strongly wind speed dependent, and there is no equilibrium (or saturated) capillary range, at least for winds up to 30 meters/sec.

Some properties of the angular variation of the spectra are also found. For high wave numbers, especially in the capillary range, the results are shown to be consistent with the Rayleigh-Rice backscattering theory (Bragg scattering), and certain properties of the angular variation are deduced from backscatter measurements.

17. Key Words (Suggested by Author(s))	18. Distribution Statement
Sea-surface wind roughness wave spectra backscattering theory	Unclassified - Unlimited

19. Security Classif. (of this report)	20. Security Classif. (of this page)	21. No. of Pages	22. Price*
Unclassified	Unclassified	128	Domestic, $4.50 Foreign, $7.00

*For sale by the National Technical Information Service, Springfield, Virginia 22151

Table of Contents

	Page
Introduction	1
Definitions and notation (equations 1.1 to 1.16)	10
An analytic representation of the spectrum of a wind roughened sea (equations 2.1 to 2.14)	14
Wind profile relationships (equations 3.1 and 3.2)	17
The gravity wave-gravity equilibrium spectral range (equation 4.1)	21
The capillary spectral range (equations 5.1 to 5.7)	25
The Cox viscous cutoff (equations 6.1 to 6.4)	48
The Kitaigorodskii and Leykin-Rosenberg wave number ranges (equations 7.1 to 7.20)	54
Graphical representations (equations 8.1 to 8.4)	68
Anisotropy, sun glitter and radar backscatter (equations 9.1 to 9.43)	82
Conclusion	120
Acknowledgements	121
References	122

INTRODUCTION

Literature and data sources

The literature on the properties and spectra of ocean waves and water waves that have been generated by the wind is substantial. Beginning with "Ocean Wave Spectra" and continuing through Kinsman (1965), Neumann and Pierson (1966), Phillips (1966), and Hess, Hidy and Plate (1969), various texts and review papers have presented summaries and interpretations of the data and their analysis. Additional material subsequent to these analyses has become available from observations in wind tunnels made by Toba*, Sutherland (1967), and at New York University, from measurements in the Black Sea by Leykin and Rosenberg (1970, 1971) and from numerous investigations of the gravity wave spectrum for open ocean conditions.

Most of this work has concentrated on measuring the time variation of elevation at a point, but other studies such as Coté et al.(1960), Schooley,** Schule, Simpson and DeLeonibus (1971), and Dobson (1970) have reported on measurements of elevation as a function of position either on a rectangular grid or along a line. Cox (1958) has measured high frequency slopes in the upwind-downwind direction for very short fetches as a function of time.

For an appropriate spectral definition and a modest range of speeds, the wave number spectrum can range from 10^{8} (or so) cm^{3} at a peak to 10^{-5} (or so) cm^{3} near the viscous cutoff region and the wave numbers can

---

*Personal communication of data.

**Personal communication of data.

range from $2\pi\ 10^{-5}$ cm^{-1} (a wavelength of 1 kilometer) to $2\pi\ 10$ cm^{-1} (a wavelength of 0.1 cm). There are thus more than thirteen orders of magnitude in spectral values to be covered in attempting to understand the spectrum of a wind-roughened sea which in turn covers about six orders of magnitude in the wave numbers involved.

Two reports by Martin (1966, 1969) were particularly helpful at the start of this investigation. Martin attempted to recover wave number spectra from the limited amount of data available to him so as to apply them to problems in underwater sound. These efforts resulted in an indication of strong variation with wind speed in the capillary wave portion of the spectra and an indication of the need for some transitional region to connect the gravity wave portion to the capillary portion.

Measurements under natural conditions

This entire set of published material is not totally consistent for many reasons. Wave recording systems on ships and on offshore towers such as those once at Argus Island have to be rugged enough to withstand stormy seas and therefore cannot respond to, and measure, the high frequency part of the spectrum. The Tucker shipborne wave recorder (Tucker, 1956) more or less cuts out about $\omega = 2\pi/4$ and various artifacts have had to be employed to handle the calibration and digitization noise problem that develops when wave records taken by this instrument are analyzed as in Moskowitz, Pierson and Mehr (1962, 1963). The laser altimeter data of Schule, Simpson and DeLeonibus (1971), for example, cuts out a wave number of 0.36 m^{-1} corresponding to a wavelength of about 17 meters. Additional open ocean wave data given by Saenger (1972) provide data of value on the frequency spectrum from $f = 0.35$ to 0.7 hertz by means of

data obtained with a very accurate version of the NIO heave, pitch and roll buoy.

Although many open ocean, marginal sea, lake, reservoir, and wind-water tunnel records of waves generated by the wind have been spectrally analyzed and reported in the literature, not too much has been said about the calibration and frequency response of the recorder systems that were used. A notable exception is the field study by Kinsman (1960) in which every step of the calibration and recording process was checked and described. These data were of such high quality that they were used to document the non-Gaussian probability density function for wave elevation. These non-Gaussian properties are important enough to consider in refined theories of wave properties, but it is still important to determine the wave spectrum as the resolution of the variance of the wavy surface into frequency and direction bands, or into vector wave number space.

Measurements in wind-water tunnels

Measurements of the high frequency, high wave number, portion of the wave spectrum have been carried out in wind-water tunnels under more easily controlled conditions and with more sensitive instrumentation. It is, of course, then necessary to assume that these short waves as measured in a wind tunnel superimpose on the long waves measured on open water. The formulas for the generation of wave spectra due to Miles (1957, 1959a, 1959b, 1962) and Phillips (1957, 1966) involve the spectra of the advected turbulent wind fluctuations. These spectra might differ from one facility to another and from what occurs on the open ocean, where, for example, there are scales of gustiness that are long compared to the time constants involved in the generation and decay of capillary waves. This

does not seem to be what happens when differences in the nature of the winds over the ocean compared to winds in wind-water tunnels are accounted for in a reasonable way.

The gap in the data

The study of these various sources of data, along with recognition of the problem of instrument calibration for some of the data, led to the realization that a portion of the frequency band (or wave number band) that had to be covered was not well measured in either the field data or in the laboratory data. The laboratory data do not yield low enough frequencies because of the limited fetches, and the field data do not extend to the higher frequencies.

This data gap has, however, just recently been removed by the work of Leykin and Rosenberg (1970), who made measurements in the Black Sea covering frequencies from 1 to 7 hertz for a variety of wind speeds with a recording system whose calibration was known and checked in the laboratory. The recording system was such that the high frequencies were pre-whitened, which resulted in more reliable results.

These measurements, plus wind tunnel measurements, make it possible for the first time to obtain theoretical spectra that are consistent with the results obtained in the classical study of sea surface slopes as a function of wind speed made near the Hawaiian Islands by Cox and Munk (1954). The slope statistics of Cox and Munk have been verified over a limited range of wind speeds from spacecraft photographs of glitter patterns, the difficulty being that such patterns are usually available only in the trade wind areas of the subtropics for a modest range of wind speeds.

An idealized spectrum for idealized conditions

The concept of a wind generated sea whose properties are solely determined in a neutrally stratified atmosphere by the direction and speed of the wind that has blown a sufficiently long time over a sufficiently large area of the ocean has been questioned. Apart from the fact that large enough areas and long enough durations do not occur for the high winds, and that the waves are modified by swell and left-over dead seas for low winds, it is believed by some scientists that the spectrum of the waves will continuously grow toward low frequencies if a constant wind continues to blow over a long fetch (Phillips, 1966).

The main reasons for questioning this belief are the characteristics of the trade wind seas, which seem to be in equilibrium with the winds over vast areas, and the fact that the lowest frequencies observed in ocean wave spectra correspond to periods of about 24 seconds and never seem to get lower. Such a continuous growth toward lower frequencies ought to produce these low frequencies, if they were possible.

For these reasons, in this study, a fully developed wind wave spectrum that is solely a function of u_* and $U_{19.5}$, as related to u_* through the theory of a logarithmic wind profile in a neutral atmosphere, is given. The actual spectrum for a particular area of the ocean will depart from this theoretical spectrum for a variety of reasons.

For the lower frequencies (and longer wavelengths), the spectral components require a relatively long time to be generated and lag the build up of a local wind. Once they are generated, they persist as a "dead" sea and propagate into areas of lighter winds as swell. Moreover, there is increasing observational support from both the JONSWAP study (Barnett, 1970) and from spectra obtained by the Tucker shipborne wave recorder, Hoffman*

*Personal communication.

(unpublished), that nonlinear interactions as proposed by Phillips (1960, 1966) and studied by Hasselmann (1962, 1963) and Mitsuyasu (1968) modify the spectra by exporting spectral energy from the central frequency bands both to low frequencies so that the spectral peak becomes more pronounced (and perhaps shifts to lower frequencies) and to high frequencies where spectral saturation causes breaking and the destruction of the organized wave energy.

Our impression at present is that the fully developed spectrum given by Pierson and Moskowitz (1964) probably applies as long as the wind continues to act on the waves because the middle band will continuously be regenerated. However, once the wind decreases, the spectra will die down in the middle gravity band and increase in the low frequency band. The spectral energy transported to the high frequency gravity band will be destroyed by breaking.

Measurements in the high frequency gravity band and on into the capillary band made in a variety of ways with a variety of instruments for both field conditions and in wind-water tunnels all show that the spectrum at high frequencies is strongly variable as a function of wind speed. There is no equilibrium range in the capillary spectrum. There is a range of frequencies in the gravity wave range that have an equilibrium value, but this range is wind-speed dependent and shifts toward lower frequencies with increasing wind.

For a given area of the ocean at a given time, the spectrum of the waves in that area will differ from the spectrum given here in a number of ways. The low frequency, low wave number, portion will often correspond to higher waves with swell bands when the winds are very light. If the winds

have died down from, say, 20 m/s to 10 m/s over a large area, the spectrum will develop, with time, a sharper low frequency peak and a deficit at middle frequencies. The higher frequency gravity portion will be in equilibrium with an equilibrium range over a portion of the band and with the wind over another portion, probably with the wind corresponding to the properly averaged synoptic wind.

The capillary portion of the spectrum will be in practically instantaneous equilibrium with the gusts and lulls of the turbulent wind over areas with dimensions of 10's of meters. These scales of wave response were described by Pierson and Moore (1972) in interpreting the variability of radar backscatter measurements made under the MSC earth resources program. The spectrum in the capillary range will also have angular properties that respond to the lateral variation of the turbulent wind about the average wind direction.

It is thus possible to imagine that the actual spectra of wind-roughened seas will have shapes roughly like the ones proposed at low wave numbers but depart from the theoretical form because of the variations in time and space of synoptic scale winds and because of swell. At middle wave numbers, the spectra will be in equilibrium with the local wind as averaged over 20 minutes or so. At high wave numbers, the spectra will be in practically instantaneous equilibrium with the turbulent gusts and lulls of the wind.

Analysis procedures and the fundamental hypothesis of this investigation

The analysis procedures used in this study are the standard procedures for the analysis of stationary time series data in terms of spectra, where the statistical term "time series" also includes the extension to space

series and two-dimensional surfaces. Fast Fourier Transforms were used, if needed, to sharpen up the analysis. When appropriate, the analysis procedures are given in greater detail in the various sections of this study.

The fundamental hypothesis in this study is, however, very different from the hypotheses made by many other scientists in the study of similar data. The hypothesis is simply that once the effect of fetch, as some multiple of the wavelength involved, is overcome so that the spectral component is generated, its value is solely determined by the speed of the wind. This hypothesis assumes, then, that waves with lengths of 10 meters do not change properties for fetches of one kilometer or 100 kilometers. Waves with lengths of 10 cm do not change properties for fetches of 100 meters or 10 kilometers. This hypothesis, as tested against a wide variety of data sources, makes it possible to demonstrate that the higher wave numbers, and higher frequencies, are strongly dependent on wind speed.

Analysis procedures that normalize the frequencies in the spectra to f/f_{max} where f_{max} is the frequency of the spectral peak or that use non-dimensional frequencies of the form $u_* f/g$ and that then use non-dimensional fetches of the form gF/u_*^2 relocate the same true frequency in different places in the normalized spectra and in the analysis. Such procedures may lead to strange conclusions such as the one that the spectral constant in the so-called equilibrium range decreases with increasing fetch.

Wave spectra and radar backscatter

The reason for this study is that there is a need for a better definition of the spectrum of a wind-roughened sea surface for use in the interpretation of radar sea return measurements. There is also need

for improved theories of radar sea return, especially for measurements near vertical incidence and out to 30°, or so, off the vertical.

Wright (1968), for example, used the available literature to reason that both the high frequency gravity waves and the capillary waves were saturated (with perhaps different spectral constants) and did not change with wind speed, and concluded from Bragg scattering theory that the measurements of radar backscatter should also saturate at a relatively low wind speed. As will be shown, the high wave number region of the wave spectrum varies strongly with wind speed and Bragg scattering theory can thus be used to relate these wind speed dependent wave number regions to radar backscatter measurements. Radar sea return measurements should not saturate with increasing wind speed, as far as the spectrum is concerned. Whitecapping and foam are not treated in this analysis and could alter the real situation at high wind speeds.

Beginning with the work of Chia (1968), it has become clear that a better definition of the wave spectrum is required for improved theories of sea return. The need for an improved wave spectrum becomes particularly acute in the recent theoretical work of Jackson (1973), which extended the work of Chia. This theory for radar sea return requires a vector wave number spectrum with fourth moments in both ℓ and m (to be defined later), and the spectrum proposed by this study has these moments. A final task in this Langley AAFE Program as described by Pierson, Jackson, Stacy and Mehr (1972) is to evaluate the equations given by Jackson (1972) using the spectra given in this report so as to determine theoretical sea return values for the near vertical.

DEFINITIONS AND NOTATION

Spectral forms

Given a large area of the ocean in which the sea surface elevation is known as a function of x^* and y^* as $\eta(x^*, y^*)$ then the covariance function can be defined as equation (1.1), as L becomes large.

$$R(x, y) = \frac{1}{L^2} \int_{x^*-L/2}^{x^*+L/2} \int_{y^*-L/2}^{y^*+L/2} \eta(x^*, y^*)\, \eta(x^*+x, y^*+y)\, dx^*\, dy^* \qquad (1.1)$$

It is assumed that the wind is blowing in the positive x-direction.

The Fourier transform of $R(x, y)$ defines the wave number spectrum $S^*(\ell, m)$ or $S(\vec{k})$ where $|k| = (\ell^2 + m^2)^{\frac{1}{2}}$

$$S^*(\ell, m) = \frac{1}{\pi^2} \int_{-\infty}^{\infty} \int_{0}^{\infty} R(x, y) \cos(\ell x + my)\, dx\, dy \qquad (1.2)$$

under the assumption that $S^*(\ell, m) = 0$ if $\ell < 0$ because of the assumed wind direction.

With $\ell = k \cos\Phi$ and $m = k \sin\Phi$, it follows that $S^*(\ell, m)\, d\ell\, dm$ can be transformed to

$$S^*(k \cos\Phi,\ k \sin\Phi)\, k\, dk\, d\Phi = S^*(k, \Phi)\, k\, dk\, d\Phi \qquad (1.3)$$
$$= S(k, \Phi)\, dk\, d\Phi$$

Furthermore, if positive x is in the wind direction and if $S(\ell, m) = 0, \quad \ell < 0,$

$$\int_{-\pi/2}^{\pi/2} S(k, \Phi)\, d\Phi = S(k) \qquad (1.4)$$

The integral from 0 to ∞ of S(k) is the variance of the random process and equals R(0, 0). Equations for $S(k, \Phi)$ will be given below according to the above definitions.

Now, if the sea surface can be represented by a stationary linear Gaussian process, it is possible to discuss the spectra of slopes and curvatures. The spectrum of $\partial\eta(x, y)/\partial x$, for example, is given by $\ell^2 S(\ell, m)$ and the spectrum of $\partial\eta(x, y)/\partial y$ is given by $m^2 S(\ell, m)$. The spectrum of the total slope of the sea surface is thus

$$S_s(\ell, m) = (\ell^2 + m^2)\, S(\ell, m) \tag{1.5}$$

which transforms to

$$S_s(k) = k^2 S(k) \tag{1.6}$$

upon integrating out Φ, and for example

$$\sigma^2 = \sigma_x^2 + \sigma_y^2 = \sigma_u^2 + \sigma_c^2 = \int_0^\infty k^2 S(k)\, dk \tag{1.7}$$

should be related to the measurements of slope variance made by Cox and Munk (1954).

It can be shown that a similar measure of curvature is given by

$$S_c(k) = k^4 S(k) \tag{1.8}$$

This function will also be discussed along with the validity of the assumption that the sea surface can be thought of as a linear Gaussian process for such operations.

Wave number - frequency relationships

The relationship between frequency and wave number for the full range of frequency and wave number is given by equation (1.9).

$$\omega = \omega(k) = \left(gk + \frac{\tau}{\rho} k^3\right)^{\frac{1}{2}} \tag{1.9}$$

or by

$$\omega = \omega_m \frac{\sqrt{2}}{2} \left[\frac{k}{k_m} + \frac{k^3}{k_m^3}\right]^{\frac{1}{2}} \tag{1.10}$$

where

$$k_m = (g\rho/\tau)^{\frac{1}{2}} \tag{1.11}$$

and

$$\omega_m = \sqrt{2g}\,(g\rho/\tau)^{\frac{1}{4}} \tag{1.12}$$

and where τ is the surface tension.

The inverse of equation (1.10) is equation (1.13).

$$k = k(\omega) = 3\omega^2/gF(\omega/\omega_m) \tag{1.13}$$

where
$$F(\omega/\omega_m) = 1 + \left[1 + B(\omega) + (B(\omega)(2 + B(\omega)))^{\frac{1}{2}}\right]^{\frac{1}{3}} + \left[1 + B(\omega) - (B(\omega)(2 + B(\omega)))^{\frac{1}{2}}\right]^{\frac{1}{3}} \tag{1.14}$$

and where $B(\omega) = 54(\omega/\omega_m)^4$ as given, for example, in Neumann and Pierson (1966).

Some questions have been raised about the validity of using these relationships in the presence of possible currents in the water. A time history, $\eta(t)$, yields a spectrum $S(\omega)$ that it would be desirable to transform to $S(k)$ by means of

$$S(k)\,dk = S(\omega(k))\frac{d\omega(k)}{dk}\,dk \tag{1.15}$$

If the waves are being translated on a true current in the wind direction, the frequency at a fixed point would be higher than the true frequency that goes with a given wave number. However, there can be currents in the water due to Stokes' drift as shown by Chang (1968) for gravity waves and yet the relationship between frequency and wave number would still be the one given above. Equations (1.9) and (1.13) will be used to transform spectra back and forth as needed from wave number space to frequency space. The various data sources support the validity of this procedure, as will be shown.

It should be pointed out that systems of measuring and analyzing wave elevation along lines, or on a rectangular grid, do not yield spectra that are easily related to S(k). For example, the measurement of sea surface elevation along a line parallel to the wind direction yields a spectrum of the form

$$S(\ell^*) = \int_{-\infty}^{\infty} S(\ell, m)\,dm \tag{1.16}$$

This expression is not easily related to S(k), and various complex expressions result when $S(\ell, m)$ is wind speed dependent and defined in different ways over various ranges of k. Schule, Simpson and DeLeonibus (1971) have studied how spectra of this form in the gravity wave range can be related to directional spectra under various assumptions for the angular spread of the spectrum.

AN ANALYTIC REPRESENTATION OF THE SPECTRUM OF A WIND ROUGHENED SEA

For a friction velocity, u_* greater than some minimum value, $u_{*m} = 12$ cm/sec, the spectrum can be defined by the following equations.

$$S(k,\Phi) = S(k)\,F(k,\Phi)\ ; \qquad 0 < k < \infty\ ,\ -\frac{\pi}{2} < \Phi < \frac{\pi}{2} \tag{2.1}$$

$$S(k,\Phi) = 0\ ; \qquad 0 < k < \infty\ ,\ \frac{\pi}{2} < \Phi < \pi\ ,\ -\pi < \Phi < -\frac{\pi}{2} \tag{2.2}$$

$$F(k,\Phi) = \frac{8}{3\pi}(\cos\Phi)^4\left[1 - e^{-g^2/2k^2(U(u_*))^4}\right] + \frac{1}{\pi}\left[1 - \frac{A}{2} + A(\cos\Phi)^2\right]e^{-g^2/2k^2(U(u_*))^4} \tag{2.3}$$

where $0 < A < 2$ and A could be a function of k and u_* if needed.

$$S(k) = \begin{cases} S_1(k)\ ; & 0 < k < k_1 \\ S_2(k)\ ; & k_1 < k < k_2 \\ S_3(k)\ ; & k_2 < k < k_3 \\ S_4(k)\ ; & k_3 < k < k_\nu \\ S_5(k)\ ; & k_\nu < k < \infty \end{cases} \tag{2.4}$$

$$S_1(k) = \frac{\alpha}{2k^3}\,e^{-\beta(g^2/(U_{19.5}(u_*))^4 k^2)} \qquad \text{for } 0 < k < k_1 = \frac{k_2 u_{*m}^2}{u_*^2} \tag{2.5}$$

$$S_2(k) = \frac{\alpha}{2k_1^{1/2}k^{5/2}} \qquad \text{for } k_1 < k < k_2 \tag{2.6}$$

$$S_3(k) = \frac{aD(u_*)}{2k_3^p k^{3-p}} \qquad \text{for } k_2 < k < k_3 \tag{2.7}$$

$$S_4(k) = \frac{aD(u_*)}{2k^3} \qquad \text{for } k_3 < k < k_\nu \tag{2.8}$$

$$S_5(k) = \frac{Eu_*^3 k_m^6}{\nu g k^9} \qquad \text{for } k_\nu < k < \infty \tag{2.9}$$

where $S_1(k_1) = S_2(k_1)$; $S_2(k_2) = S_3(k_2)$; $S_3(k_3) = S_4(k_3)$ and $S_4(k_\nu) = S_5(k_\nu)$; and where $a = 8.1 \times 10^{-3}$, $\beta = 0.74$, $E = 1.445 \times 10^{-3}$, $\frac{E}{\nu g} = 1.473 \times 10^{-4}$, $k_2 = k(6\pi) \cong 0.359$, $k_3 = k(10\pi) \cong 0.942$ $k_m = (g\rho/\tau)^{\frac{1}{2}} \cong 3.63$ (τ is the surface tension), $u_{*m} = 12$ cm/sec,

$$p = \frac{\log_{10}(D(u_*)/(u_*/u_{*m}))}{\log_{10}(k_3/k_2)} \tag{2.10}$$

$$k_\nu = \left[\frac{2Eu_*^3}{\nu g\, aD(u_*)}\right]^{1/6} \qquad k_m = \frac{.5756\ u_*^{\frac{1}{2}} k_m}{[D(u_*)]^{1/6}} \tag{2.11}$$

$$D(u_*) = (1.274 + .0268\, u_* + 6.03 \times 10^{-5} u_*^2)^2 \tag{2.12}$$

and $U_{19.5}(u_*)$ is the wind at 19.5 meters for a friction velocity of u_* in a neutral atmosphere. $U(u_*)$ will often be used for $U_{19.5}(u_*)$.

These five ranges of definition can be substantiated by means of data obtained under a wide variety of conditions. $S_1(k)$ can be named the gravity wave-gravity equilibrium spectral range; $S_2(k)$ is the Kitaigorodskii spectral range; $S_3(k)$ can be called the Leykin-Rosenberg spectral range; $S_4(k)$ is the capillary spectral range; and $S_5(k)$ is the Cox viscous cut-off region.

Anisotropy

The definition of $F(k,\Phi)$ given by equation (2.3) was based on the work of Coté et al. (1960) in project SWOP. It turns out to be inadequate for the higher wave number ranges, such as the capillary range. For these higher wave numbers not much was known then about the angular properties of the spectrum.

For these high wave numbers, the exponential term in equation (2.3) is one, and the second term can be rewritten as equation (2.13).

$$\frac{1}{\pi}\left[1 - \frac{A}{2} + A(\cos\Phi)^2\right] = \frac{1}{\pi}\left[1 + \frac{A}{2}\cos 2\Phi\right] = \frac{1}{\pi}\left[1 + a_1(k)\cos 2\Phi\right] \qquad (2.13)$$

In this form, it is seen that this term represents the first term in the even Fourier series representation of $F(k,\Phi)$ over $-\frac{\pi}{2} < \Phi < \frac{\pi}{2}$ and that a more general representation would be given by equation (2.14).

$$F(k,\Phi) = \frac{1}{\pi}\left[1 + \sum_{n=1}^{N} a_n(k; u_*)\cos 2n\Phi\right] \qquad (2.14)$$

Some results on the first two coefficients of this series $a_1(k_1, u_*)$ and $a_2(k, u_*)$ can be obtained and will be given in a later section.

WIND PROFILE RELATIONSHIPS

The average wind varies with elevation in the planetary boundary layer. Since different experimenters use anemometers at different elevations for free atmosphere measurements, and since data obtained in wind-water tunnels have to be interpreted for open ocean conditions, the procedures for interrelating the various measurements have to be given.

The spectra are given in terms of u_* and $U_{19.5}(u_*)$ where u_* is the friction velocity defined by $u_* = \sqrt{\tau/\rho}$, where τ is the wind stress and where $U_{19.5}(u_*)$ is the wind measured at 19.5 meters in a neutrally stratified atmosphere. The equations relating these quantities according to Cardone (1969) are given by equations (3.1) and (3.2).

$$U_z = \frac{u_*}{k'} \ln(z/z_o) \tag{3.1}$$

$$z_o = \frac{.684}{u_*} + 4.28 \times 10^{-5} u_*^2 - .0443 \tag{3.2}$$

where z is the height of interest in centimeters (1950 in this case), k' is von Karman's constant (= 0.4) and U and u_* are expressed in centimeters/sec.

Also since many measurements are referred to an elevation of 10 meters, the interrelationship between u_*, $U_{10}(u_*)$ and $U_{19.5}(u_*)$ is needed. Table 3.1 gives the values of these quantities, and Figure 3.1 is a graph of $U_{19.5}$ and U_{10} as a function of u_* for a neutral atmosphere. The range from 5 cm/sec to 138 cm/sec corresponds to wind speeds at 19.5 meters of 1.25 m/s (2.4 knots) to 27.0 m/s (52.4 knots).

The wind at these two anemometer heights would be greater than the amount tabulated for a stable atmosphere to produce the same u_* at

Table 3.1 Wind speed at 19.5 meters and 10 meters in meters/sec as a function of u_* in cm/sec for a neutral atmosphere.

u_*	U_{10}	$U_{19.5}$	u_*	U_{10}	$U_{19.5}$
5	1.16	1.24	72	15.45	16.65
6	1.43	1.53	75	15.92	17.17
10	2.62	2.78	78	16.38	17.68
12	3.26	3.46	80	16.69	18.02
15	4.28	4.53	84	17.29	18.69
18	5.30	5.61	85	17.44	18.86
20	5.93	6.27	90	18.18	19.68
24	6.98	7.38	95	18.91	20.49
25	7.21	7.63	96	19.05	20.65
30	8.24	8.74	100	19.62	21.29
35	9.18	9.77	102	19.90	21.61
36	9.37	9.97	105	20.32	22.08
40	10.10	10.75	108	20.74	22.54
42	10.45	11.15	110	21.01	22.85
45	10.98	11.73	114	21.56	23.47
48	11.51	12.31	115	21.70	23.62
50	11.85	12.69	120	22.37	24.37
54	12.53	13.43	125	23.03	25.12
55	12.70	13.62	126	23.15	25.27
60	13.53	14.53	130	23.68	25.85
65	14.34	15.43	132	23.54	26.15
66	14.50	15.62	135	24.33	26.58
70	15.14	16.31	138	24.71	27.01

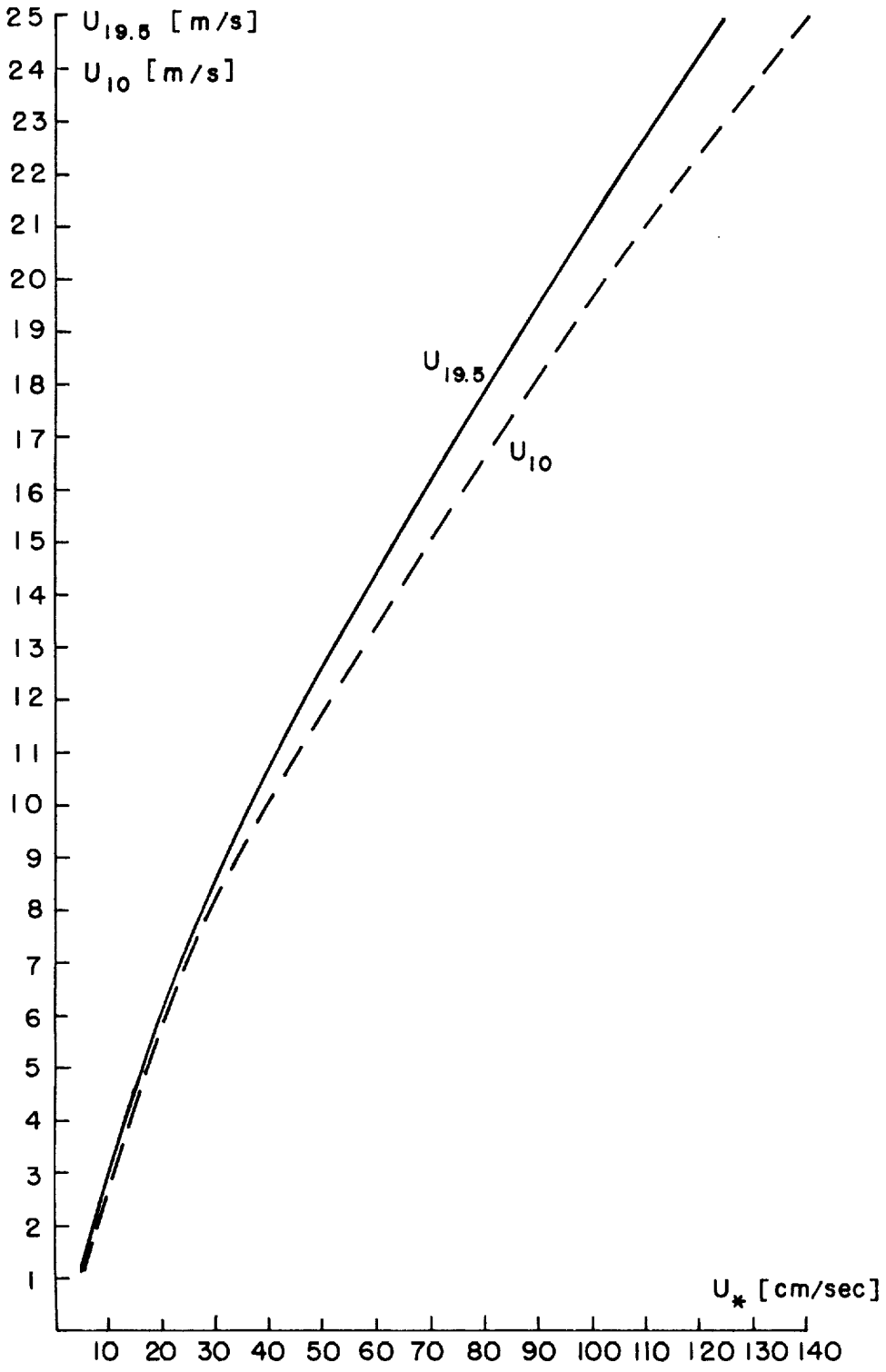

Fig. 3.1 $U_{10}(u_*)$ and $U_{19.5}(u_*)$ as a function of u_* in a neutrally stratified atmosphere.

the surface and less than the amount tabulated for an unstable atmosphere. If possible, where needed, corrections for the effects of atmospheric stability have been made in interpreting the data.

THE GRAVITY WAVE-GRAVITY EQUILIBRIUM SPECTRAL RANGE

Source

The spectral range defined by equation (2.5) is obtained from the results of Moskowitz (1964), Pierson and Moskowitz (1964) and Pierson (1964) by transforming the frequency spectra given by them to wave number spectra. $U = U_{19.5}(u_*)$ represents the wind at 19.5 meters as described above.

The equilibrium constant

The equilibrium constant is usually found by attempting to fit the high frequency portion of a gravity wave spectrum to a curve with a slope of -5 on a double log plot under the assumption that

$$S(\omega) = \alpha g^2/\omega^5 \tag{4.1}$$

in this range. There has been some discussion concerning the possibility that the constant α in the Phillips equilibrium gravity wave range is fetch dependent as, for example, in Longuet-Higgins (1969), and Mitsuyasu (1969). For open ocean conditions, the preponderance of the data now suggests that α is a constant very nearly given by 8.1×10^{-3} as obtained by Pierson and Moskowitz (1964).

Longuet-Higgins et al. (1963) gave a value of α equal to 8×10^{-3} for open ocean conditions and a large fetch.

Ewing (1969) found that $\alpha = 8 \times 10^{-3}$ fitted spectra obtained from a series of observations taken with the NIO buoy.

Schule, Simpson, and DeLeonibus (1971) in a study of laser altimeter wave records in wave number space found that α equalled 8.4×10^{-3}. The value of α does not seem to depend on fetch because the

fetch varied over one order of magnitude in their measurements.

More recently, DeLeonibus et al. (1973) have summarized results obtained at Argus Island and by using a bow-mounted wave height sensor in the Norwegian Sea. For Argus Island data, α was found to equal $(7.8 \pm 1.6) \times 10^{-3}$ and for the Norwegian Sea a value of 8.3×10^{-3} was found.

A recent study by Saenger (1972) also supports a value of α equal to 8.1×10^{-3}, or 8.0×10^{-3}, with one important exception to be described below. The wave recording instrument used was a heave acceleration, pitch and roll buoy with extremely carefully designed sensing elements. The high quality data obtained yield S(f), or equivalently, $S(\omega)$, from 0.5 hertz (f) to 1.0 hertz with a small roll-off in frequency response beyond about 0.7 hertz. Spectra were obtained for winds of 3, 6, 6.5, 9.5, 11, 13.5, 14.5, 15, 17 and 18 knots. Over the frequency range from 0.35 to 0.7 hertz, and for winds of 9.5 knots, or more, the spectra coincide within sampling variability and correspond to $\alpha = 8.1 \times 10^{-3}$ within the accuracy of the plots. The spectra for the waves when the winds were 6 knots and 3 knots were well below this value with $\alpha = 3.2 \times 10^{-3}$ for 6 knots and 1.6×10^{-3} for 3 knots.

This result is important because something even more dramatic happens to capillary waves at a wind speed of about 3.5 m/s (7 knots). The Phillips' equilibrium gravity wave range may only exist if the winds exceed 3.5 m/s in a neutral atmosphere.

In summary, for winds greater than about 3.5 m/s, Pierson and Moskowitz (1969) gave 8.1×10^{-3} for α, Longuet-Higgens et al. (1963) gave 8×10^{-3}, Ewing (1969) gave 8×10^{-3}, Schule et al. (1971) gave

8.4×10^{-3} (or its equivalent in wave number space), DeLeonibus et al. (1973) gave $(7.8 \pm 1.6) \times 10^{-3}$ and 8.3×10^{-3}, and data from Saenger (1972) are consistent with 8.1×10^{-3}.

A value of 8.1×10^{-3} is used here with a variation from 7.8 to 8.4×10^{-3}, implying a 4 percent change in spectral values. If the spectral shapes were unchanged, this would imply a completely undetectable (due to sampling variability) change in significant wave height of plus or minus 2 percent if the upper or lower ranges of this value were used.

The SWOP project (Coté et al, 1960) is often cited for a value of α equal to 13.3×10^{-3}. This value depends on the adequate calibration of a wave buoy that moved up and down in the water and may perhaps be in error for this reason.

Other values of α often cited are 14.8×10^{-3} for a 70 meter fetch due to Burling (1959), 12.1×10^{-3} for a 55 meter fetch due to Hicks (1960), and 10.4×10^{-3} for a 2.5 km fetch due to Kinsman (1960). An explanation for these higher values will be given later in this study.

Relationship to wave forecasting methods

This portion of the spectrum is based on a selected subset of many hundreds of ocean wave records obtained by the Tucker shipborne wave recorder (Tucker, 1956) as analyzed by Moskowitz, Pierson and Mehr (1962, 1963). Fully developed seas with a spectrum given by this form are not frequent over the open ocean. This form, however, is the basis for the numerical spectral wave forecasting model described by Pierson, Tick and Baer (1966) and more recently by Pierson (1971) and Pierson and Cardone (1971). Papers by Cardone (1969), and Adamo, Baer and Hosmer (1968) describe features of this hindcasting and forecasting model.

An earlier version of this model has been tested on simulated forecasts with results described by Bunting (1970) and Bunting and Moskowitz (1970). Both observations and these simulated forecasts show that the wave spectra depart considerably from the spectrum that would be present as calculated from the instantaneous local wind.

Tests have shown, however, that this portion of the wave spectrum can be both forecasted and hindcasted with considerable accuracy on the basis of the wind field as it varies from hour to hour over the oceans. If the low wave number, low frequency part of the wind wave and swell spectrum had any effect on the amount of backscattered radiation in radar measurements, then these forecasts and hindcasts can provide the required information on this part of the spectrum.

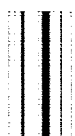

THE CAPILLARY SPECTRAL RANGE

Data sources

The capillary spectral range given by equation (2.8) has been determined from data obtained in three different wind water tunnels for a variety of fetches. A range of friction velocities from 3.3 to 170 cm/sec corresponding to winds over the ocean varying from nearly calm to more than 29 m/s were covered by the data.

The three data sources consisted of a set of wave records in digitized form obtained at New York University, a second set of records in graphical form provided by Dr. Yoshiaki Toba of the Geophysical Institute of Tohoku University, which were originally obtained at Kyoto University, and a third set of digitized records obtained by Dr. A. J. Sutherland and provided by the Department of Civil Engineering of Stanford University. The first set were for fetches of 2.3 to 6.4 meters and friction velocities of 3.3 to 19 cm/sec. The second set were for fetches of 4.5 to 13.6 meters and friction velocities of 33 to 115 cm/sec. The third set were for fetches of 1.1 to 18 meters and friction velocities of 45 to 170 cm/sec, with data actually used having been for fetches of 8.7 to 18 meters. The Nyquist frequencies for the three sets of data were 78, 125 and 125 radians/sec respectively.

A critical friction velocity

The New York University data covered a range of friction velocities from nearly calm to 19 cm/sec. For the lower wind speeds, the wind hardly ruffled the surface, but slight disturbances could be detected that were capable of being recorded on a high gain oscillograph. At a

critical friction velocity of about 12 cm/sec the waves grew rather suddenly, and the data on their properties merge with the data from the other two sources as will be shown.

The problem remains though as to what the spectrum would be of a fully developed sea for winds corresponding to friction velocities less than 12 cm/sec. Our results will be definitive only for $u_* > 12$ cm/sec. Perhaps winds less than this can only ruffle the surface and equation (5.1) given by Pierson and Moskowitz (1964),

$$\overline{H}_{\frac{1}{3}} = 0.0212\ U^2_{19.5} \qquad (5.1)$$

where $\overline{H}_{\frac{1}{3}}$ is in meters and $U_{19.5}$ is in meters/sec only holds for winds greater than about 3.5 m/s at 19.5 meters, corresponding to a significant wave height of 0.25 meters or 11 inches.

For wind speeds less than the wind that corresponds to a friction velocity of 12 cm/sec, the gravity wave spectrum may be very low under the idealization that a constant wind has blown for a long time over a large fetch. The minute undulations that were measured for these light winds yielded spectra for the capillary range that corresponded to disturbances one one-hundredth the height of the waves that were measured after the friction velocity exceeded 12 cm/sec. The data from Saenger (1972) could lead to the conclusion that the waves for a fully developed sea would be 5 inches high instead of 8 inches for a 6 knot wind and only about 1 inch high in the gravity range for a 3 knot wind . There will, of course, be swell present.

A capillary equilibrium range?

Phillips (1966) has discussed the possibility of two different equilibrium ranges: one for gravity waves and the other for capillary waves. In the previous section of this paper, a possible equilibrium range in the gravity wave portion of this spectrum was shown with a constant equal to 8.1×10^{-3} for winds above 3.5 m/s.

Phillips (1966) wrote that the capillary spectrum should be of the form $B^*/\vec{k}^4$, or in polar coordinates after integrating out the angle variable, B/k^3, where B is a constant. Phillips (1966), page 117, can be quoted as follows:

> "It should be noted that an infinitesimal capillary wave cannot be in a state of stable equilibrium in which the energy flux from the wind balances the viscous dissipation. For according to the linear theory, these two energy fluxes are in fixed proportion, each being proportional to the square of the wave amplitude. A disturbance either dies away or grows until it is limited by one or the other of these finite amplitude effects."

The data described in this section establish that there is no equilibrium range in the capillary spectrum as computed from wave records obtained in a wind-water tunnel. This fact was recognized by Sutherland (1967) who wrote that "the present data do not show a true equilibrium range as predicted by Phillips (1958)."

The capillary spectrum is a function of wind speed. An adequate theory for this portion of the spectrum of a wind roughened sea is lacking. The suggestion given by Pierson, Jackson, Stacy and Mehr (1971) is not adequate because spectral components with the least viscous effect grow the most slowly.

Data analysis

If the capillary spectrum is of the form given by equation (5. 2)

$$S(k)\,dk = \frac{B}{k^3}\,dk \tag{5.2}$$

and if there are no currents, the use of equation (1. 13) can transform the wave number spectrum to a frequency spectrum as in equation (5. 3).

$$S(\omega)\,d\omega = \frac{B}{(k(\omega))^3}\,\frac{dk(\omega)}{d\omega}\,d\omega \tag{5.3}$$

Let the constant B be assumed to be equal to 4.05×10^{-3}, and let the spectra estimated from the records described above be designated by $\hat{S}(\omega; u_*, F)$. If then the capillary spectrum is of the form given by equation (5.3) the function of ω given by equation (5.4) ought to equal some constant over some portion of the capillary range of frequencies in the spectrum.

$$H(\omega; u_*, F) = \frac{\hat{S}(\omega, u_*, F)(k(\omega))^3}{(a/2)(dk(\omega)/d\omega)} \tag{5.4}$$

The function, $H(\omega; u_*, F)$ was computed and graphed for a wide range of estimated spectra $\hat{S}(\omega; u_*, F)$, for the ranges of u_* and F given above. $H(\omega; u_*, F)$, in general, was small for low values of ω, increased sharply to some constant value at some ω_1, and leveled off to nearly a constant value after that ω. To determine this constant value, the quantity D was computed as in equation (5. 5).

$$D(u_*, F) = \frac{1}{\omega_N - \omega_1} \int_{\omega_1}^{\omega_N} H(\omega; u_*, F)\,d\omega \tag{5.5}$$

The value of ω_1 varied as a function of both u_* and F. If $F_2 > F_1$ and u_* was constant, then $\omega_{12} < \omega_{11}$. Also, if $u_{1*} < u_{2*}$, and if $F_1 = F_2$, then $\omega_{12} < \omega_{11}$. The spectra of the waves in the wind water tunnel grew toward lower frequency with both increasing fetch for the same friction velocity and with increasing friction velocity for the same fetch.

Selected graphs of $H(\omega; u_*, F)$ are shown from the Sutherland data in Figure 5.1 for different fetches and values of u_*. The values of ω_1 and ω_N, which is where the effect of digitization noise resulted in the upper cut-off value, are shown along with the resulting value of $D(u_*)$. The plotted points as connected by a zigzag line are the result of 21-point non-overlapping averages of the Fast Fourier transform of the data. The 90% confidence interval is shown, and the variability of $H(\omega; u_*, F)$ is consistent with this confidence interval. The value of $D(u_*)$ is insensitive to the exact choice of ω_1.

A total of 67 spectra were obtained for varying friction velocities and fetches, 27 from N. Y. U., 23 from Dr. Toba, and 17 from Dr. Sutherland (1967). These spectra were processed to obtain $H(\omega; u_*, F)$ and $D(u_*, F)$.

The values of u_*, F, $(u_*^2/gF)^{\frac{1}{2}}$, D, and $D^{\frac{1}{2}}$ are shown in Table 5.1.

Sutherland (1967) stated that the spectra he obtained were not good at high frequencies. This point was overlooked in the initial analysis of the data so that the values of D as plotted by Pierson, Jackson, Stacy and Mehr (1971) came out, without a needed correction, to be higher than the values obtained from the Toba data.

It was found that the Sutherland data had white noise at high frequencies, probably caused by digitization effects. This white noise was easily removed by finding its magnitude at the high frequencies and

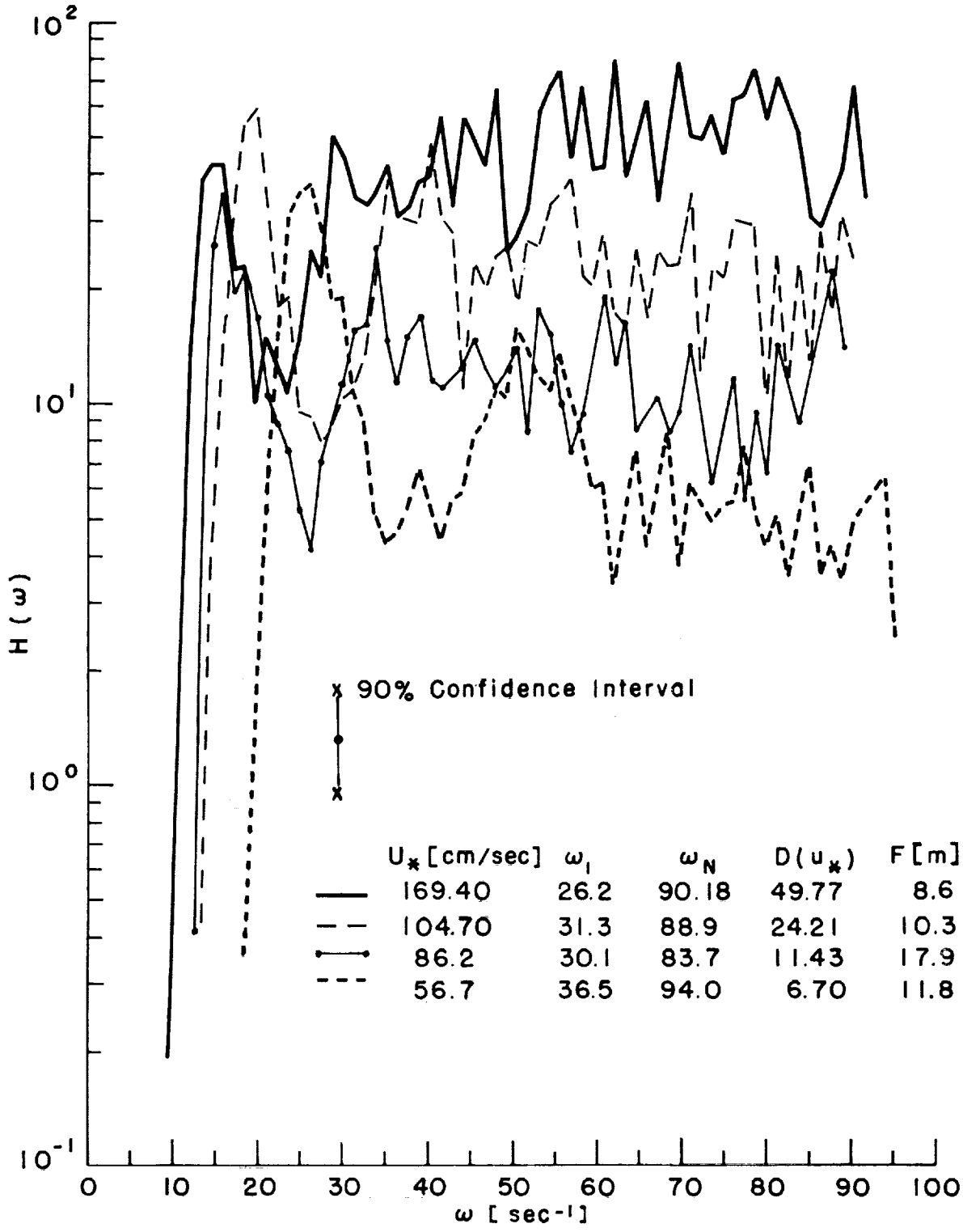

Fig. 5.1 Selected graphs of $H(\omega; u_*, F)$ from Sutherland data.

Table 5.1

Values of u_* (cm/sec), F (meters), $(u_*^2/gF)^{\frac{1}{2}}$, D, and $D^{\frac{1}{2}}$ for the N. Y. U., Toba, and Sutherland data sets.

	Data set	u_*	F	$(u_*^2/gF)^{\frac{1}{2}}$	D	$D^{\frac{1}{2}}$
1.	NYU	3.3	2.3	6.9×10^{-3}	3.8×10^{-5}	--
2.	"	3.3	4.8	4.8×10^{-3}	4.5×10^{-5}	--
3.	"	3.3	6.4	4.2×10^{-3}	7.2×10^{-5}	--
4.	"	4.7	2.3	9.9×10^{-3}	9.6×10^{-5}	--
5.	"	4.7	4.8	6.9×10^{-3}	6.9×10^{-5}	--
6.	"	4.7	6.4	5.9×10^{-3}	8.5×10^{-5}	--
7.	"	5.9	2.3	1.2×10^{-2}	2.4×10^{-4}	--
8.	"	5.9	4.8	8.7×10^{-3}	9.5×10^{-5}	--
9.	"	5.9	6.4	7.5×10^{-3}	1.35×10^{-4}	--
10.	"	7.4	4.8	1.1×10^{-2}	7.75×10^{-4}	--
11.	"	7.4	4.8	1.1×10^{-2}	1.22×10^{-4}	--
12.	"	7.4	6.4	9.4×10^{-3}	1.38×10^{-4}	--
13.	"	9.2	4.8	1.36×10^{-2}	4.32×10^{-4}	--
14.	"	9.2	6.4	1.15×10^{-2}	1.42×10^{-4}	--
15.	"	9.2	6.4	1.15×10^{-2}	1.26×10^{-4}	--
16.	"	9.9	6.4	1.25×10^{-2}	3.14×10^{-4}	--
17.	"	9.8	6.4	1.25×10^{-2}	2.68×10^{-4}	--
18.	"	12.1	4.8	1.79×10^{-2}	7.8×10^{-3}	--
19.	"	12.1	6.4	1.53×10^{-2}	1.56×10^{-1}	--
20.	"	12.3	6,4	1.55×10^{-2}	2.78	1.67
21.	"	13.3	4.8	1.94×10^{-2}	2.76	1.66
22.	"	13.8	6.4	1.74×10^{-2}	3.08	1.75

[continued]

Table 5.1 (cont.)

	Data set	u_*	F	$(u_*^2/gF)^{\frac{1}{2}}$	D	$D^{\frac{1}{2}}$
23.	NYU	14.2	4.8	2.07×10^{-2}	2.50	1.58
24.	"	14.2	6.4	1.79×10^{-2}	3.20	1.79
25.	"	16.2	2.3	3.41×10^{-2}	1.69	1.30
26.	"	16.2	4.8	2.36×10^{-2}	3.48	1.86
27.	"	16.2	6.4	2.04×10^{-2}	3.64	1.91
28.	"	18.9	2.3	3.98×10^{-2}	1.19	1.09
29.	"	18.9	6.4	2.39×10^{-2}	5.68	2.42
30.	Toba	33.4	4.5	5.03×10^{-2}	4.40	2.10
31.	"	33.5	10.0	3.38×10^{-2}	4.19	2.05
32.	"	36.7	13.6	3.18×10^{-2}	4.48	2.12
33.	"	38.9	13.6	3.37×10^{-2}	4.00	2.00
34.	"	45.2	6.9	5.49×10^{-2}	6.50	2.55
35.	"	48.9	13.6	4.23×10^{-2}	7.58	2.75
36.	"	49.3	6.9	5.99×10^{-2}	9.76	3.12
37.	"	56.5	6.9	6.87×10^{-2}	7.15	2.67
38.	"	61.5	13.6	5.33×10^{-2}	7.15	2.67
39.	"	63.2	6.9	7.68×10^{-2}	9.68	3.11
40.	"	64.8	10.0	6.54×10^{-2}	12.16	3.49
41.	"	73.7	13.6	6.38×10^{-2}	13.68	3.70
42.	"	77.4	4.5	1.17×10^{-1}	15.5	3.94
43.	"	78.6	6.9	9.55×10^{-2}	16.56	4.07
44.	"	88.1	6.9	1.07×10^{-1}	27.41	5.24

[continued]

Table 5.1 (cont.)

	Data set	u_*	F	$(u_*^2/gF)^{\frac{1}{2}}$	D	$D^{\frac{1}{2}}$
45.	Toba	92.6	13.6	8.02×10^{-2}	14.9	3.68
46.	"	102.0	4.5	1.54×10^{-1}	29.10	5.39
47.	"	104.0	10.0	1.05×10^{-1}	23.90	4.89
48.	"	112.0	10.0	1.13×10^{-1}	32.4	5.69
49.	"	114.0	13.6	9.87×10^{-1}	21.7	4.66
50.	"	115.0	4.5	1.73×10^{-1}	24.2	4.92
51.	Sutherland	37.2	18.0	2.8×10^{-2}	7.44	2.73
52.	"	40.3	11.9	3.73×10^{-2}	6.20	2.49
53.	"	40.1	10.3	3.99×10^{-2}	9.25	3.04
54.	"	40.3	14.8	3.35×10^{-2}	6.57	2.56
55.	"	52.4	17.9	3.95×10^{-2}	6.30	2.51
56.	"	56.5	10.3	5.62×10^{-2}	7.98	2.82
57.	"	56.7	11.8	5.27×10^{-2}	6.70	2.59
58.	"	56.7	14.9	4.69×10^{-2}	6.60	2.57
59.	"	84.2	10.3	8.38×10^{-2}	11.8	3.44
60.	"	84.8	11.8	7.88×10^{-2}	12.60	3.55
61.	"	85.8	14.9	7.10×10^{-2}	12.58	3.55
62.	"	86.2	17.9	6.51×10^{-2}	11.43	3.38
63,	"	102.4	8.7	1.11×10^{-1}	22.07	4.70
64.	"	104.7	10.3	1.04×10^{-1}	24.21	4.92
65.	"	105.8	11.8	9.84×10^{-2}	23.46	4.84
66.	"	169.4	8.6	1.84×10^{-2}	49.47	7.06
67.	"	170.2	10.3	1.69×10^{-1}	60.96	7.81

subtracting it from the spectrum before calculating $H(\omega; u_*, F)$ and $D(u_*)$.

The Toba data were provided to us in the form of strip charts of wave height as a function of time. These charts were magnified by projecting them on a wall across the room and the data were read off very accurately. There was no need for a correction for white noise digitization errors in the Toba data processed in this way.

The variation of $D(u_*)$ as a function of u_* is shown on a double log plot in Figure 5.2. There are three anomalous points for D greater than one in the NYU data. For u_* less than 12 cm/sec, D increases from values near 5×10^{-4} to values near 4×10^{-3} at u_* equal to 10 cm/sec. Near 12 cm/sec, values of D scatter over four orders of magnitude, and for u_* just greater than 12 cm/sec the values of D cluster around three. Since the wind at anemometer level is not a very good measure of u_* when the winds are light, because atmospheric stability plays an important role, this plot suggests a reason for those radar measurements that found strong effects of varying wind speed on radar sea return for light winds. The coded points attributed to Bradley (1971) will be discussed in a later section.

There is a data gap between 20 and 30 cm/sec. Above 30 cm/sec the Toba and Sutherland data would be indistinguishable were it not for the coded points. The data show a constant increase in D from 4 to 60 as the friction velocity increases from 33 to 170 cm/sec.

Although the frequency at which $H(\omega; u_*, F)$ first levels off to a constant value is fetch dependent, the value of D does not appear to be fetch dependent. This is shown by Figure 5.3 in which D is plotted against $(u_*^2/gF)^{\frac{1}{2}}$ on roughly the same horizontal spacing. The scatter in the points is increased compared to Figure 5.2, whereas if fetch were

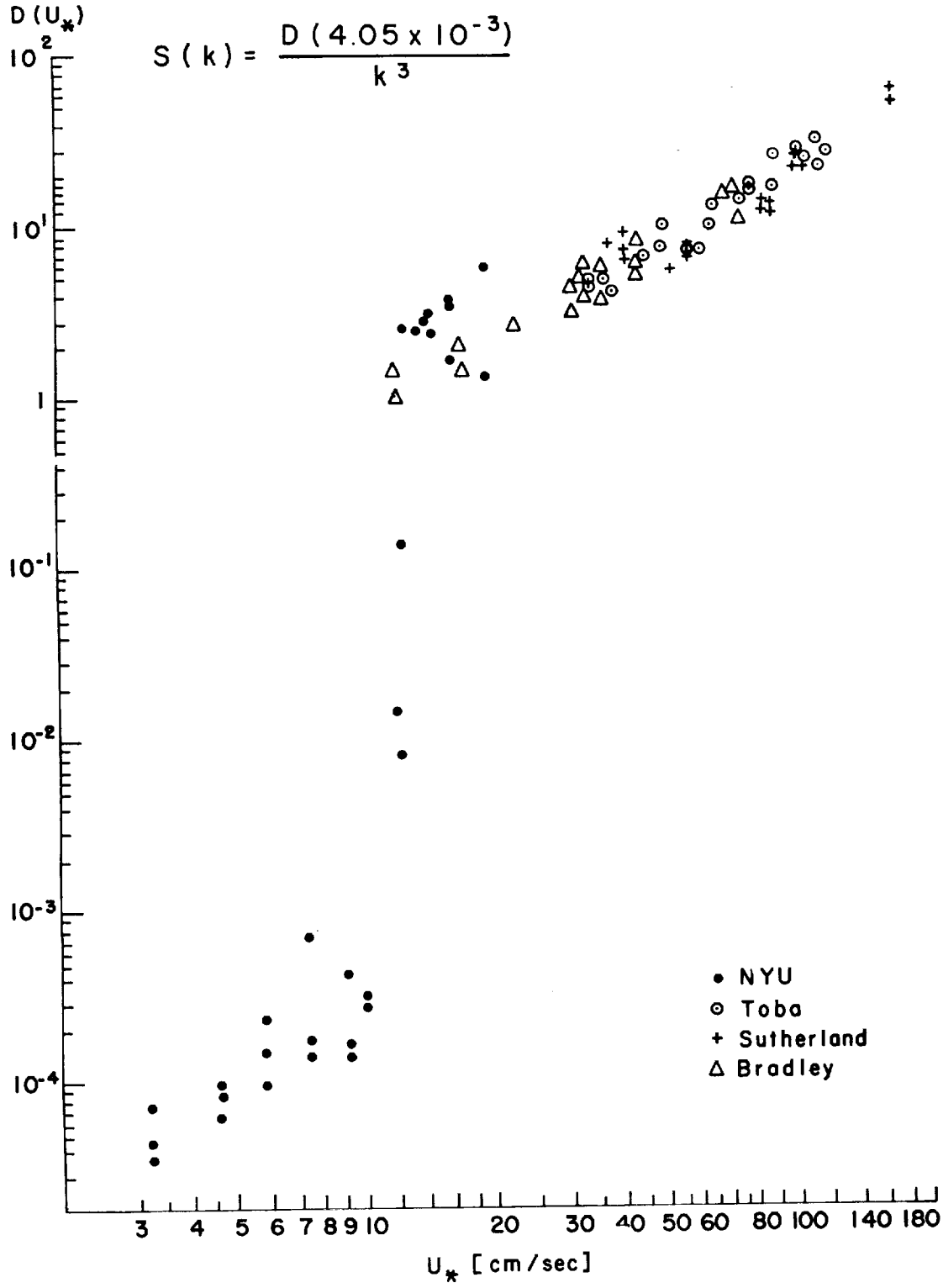

Fig. 5.2 $D(u_*)$ versus u_*.

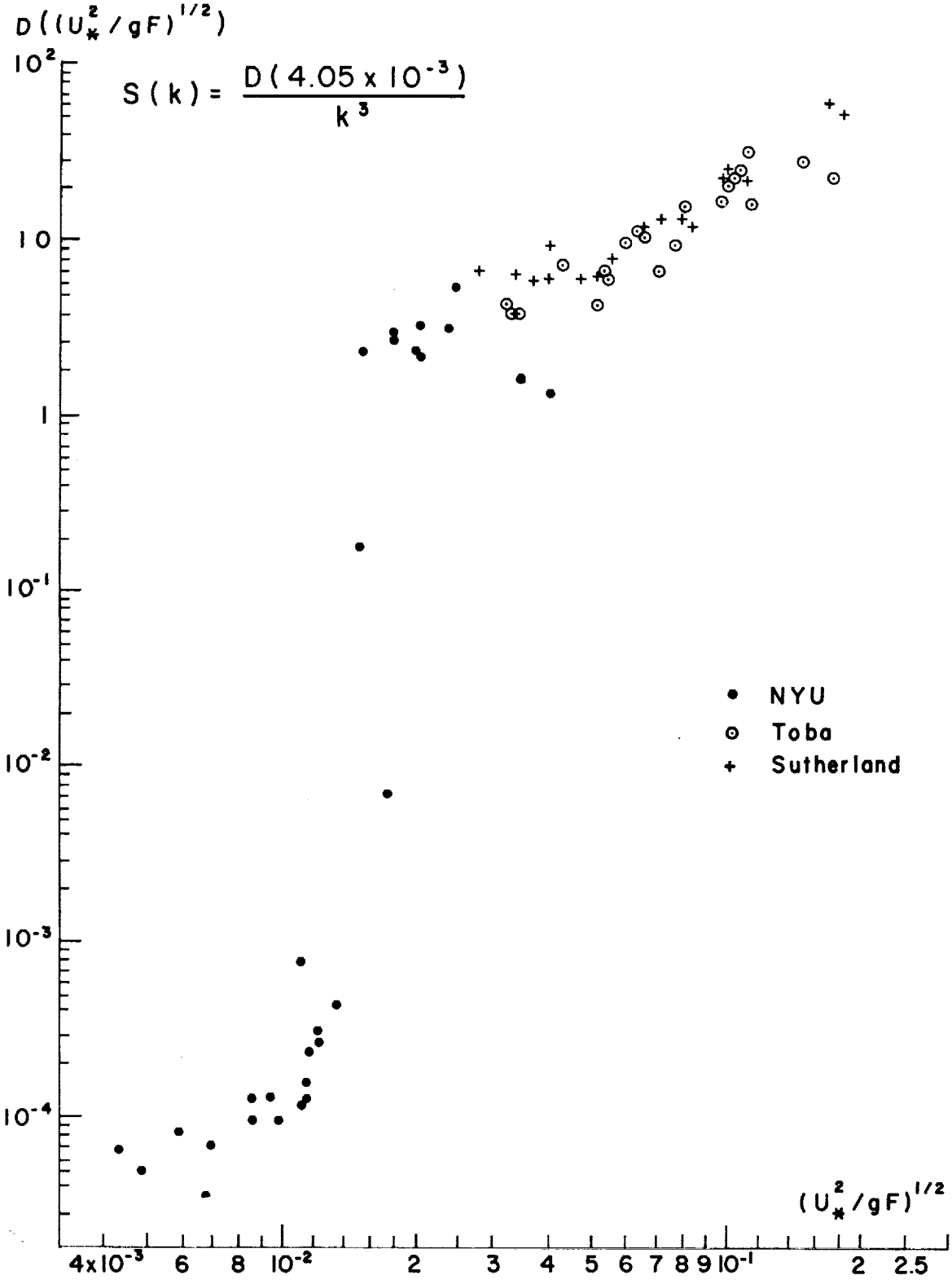

Fig. 5.3 $D((u_*^2/gF)^{\frac{1}{2}})$ versus $(u_*^2/gF)^{\frac{1}{2}}$

truly involved, the scatter should have decreased. The square root of the reciprocal of the dimensionless fetch varies over nearly two orders of magnitude. One could interpret this plot to infer that D is proportional to $((u_*^2/gF)^{\frac{1}{2}})^q$ for $(u_*^2/gF)^{\frac{1}{2}}$ greater than 1.2×10^{-2}. Only the increased scatter when compared with figure 5.2 leads to the preference to a wind speed dependence only. Some high quality measurements of waves for a fetch of one kilometer or so for the same frequency range could settle the question completely.* Note that the coded points attributed to Bradley (1971) in Figure 5.2 are not shown on this figure.

A relationship between D and u_* is needed to provide an analytical representation for the spectrum. It should be recalled that the primary measurement was wave elevation as a function of time, and that spectra are related to squares of wave elevation. Since the spectrum for a long enough fetch is more or less defined over a constant wave number range the square root of D would be a measure of the wave height in this band.

Figure 5.4 shows a plot of $(D(u_*))^{\frac{1}{2}}$ versus u_* on linear scales. The significant height of the capillary waves can be given approximately by equation (5.6) because the wave number range for the capillary portion of the spectrum extends from 0.92 radians/cm to about 10 radians/cm on the basis of results to be given later. An upper limit of the integral ranging from 6 to 12 has only a small effect.

$$H_{1/3} \cong 4\left[\int_{0.94}^{10} \frac{4.05 \times 10^{-3}\, D(u_*)\, dk}{k^3}\right] \cong 0.195\,(D(u_*))^{\frac{1}{2}} \qquad (5.6)$$

A second vertical scale shows that the variation of $(D(u_*))^{\frac{1}{2}}$ from 1 to 8

* See page 81.

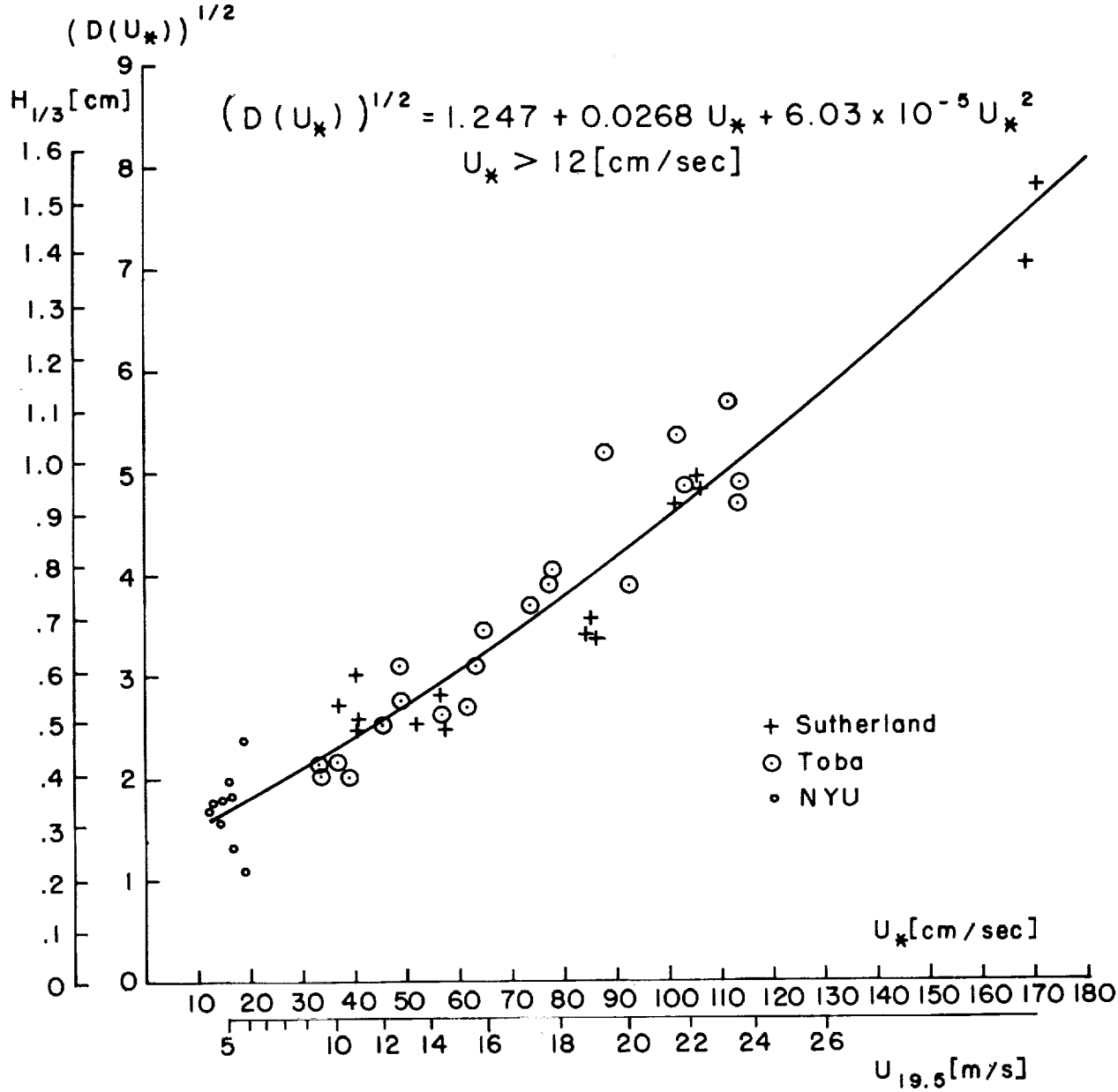

Fig. 5.4 $(D(u_*))^{\frac{1}{2}}$ versus u_* on linear scales. The additional vertical scale shows the significant height of the capillary waves.

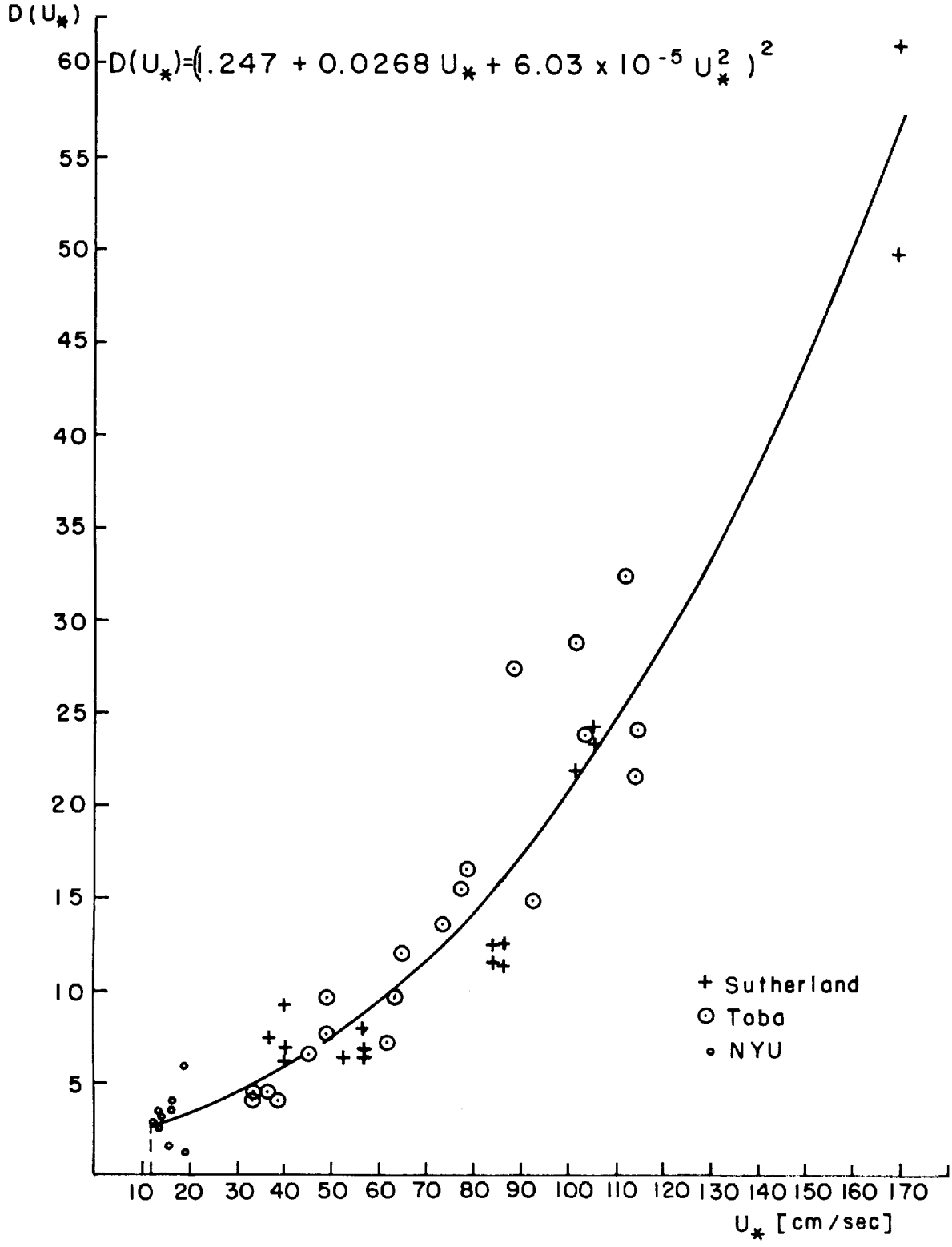

Fig. 5.5 $D(u_*)$ versus u_* on linear scales.

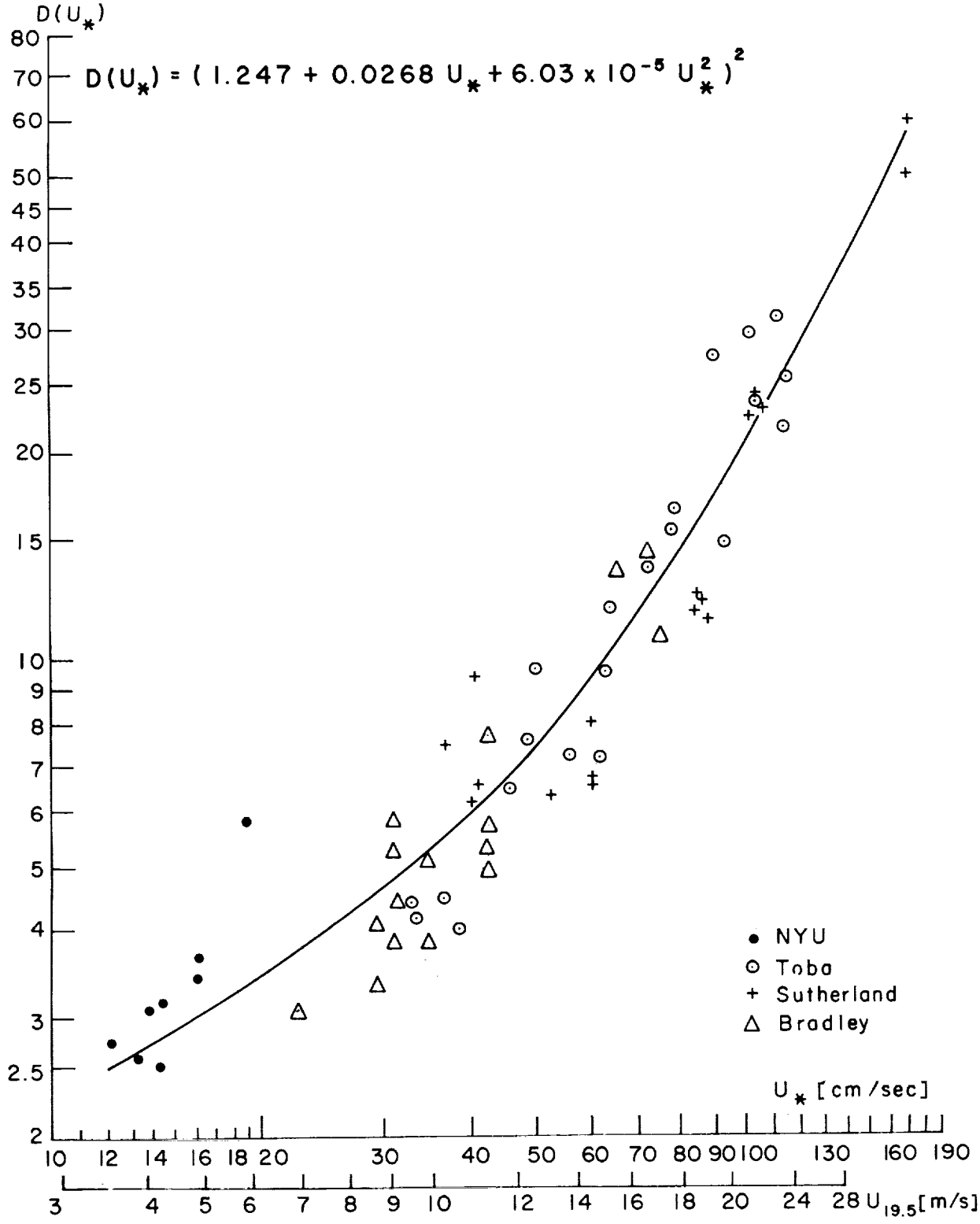

Fig. 5.6 $D(u_*)$ versus u_* on logarithmic scales for restricted ranges.

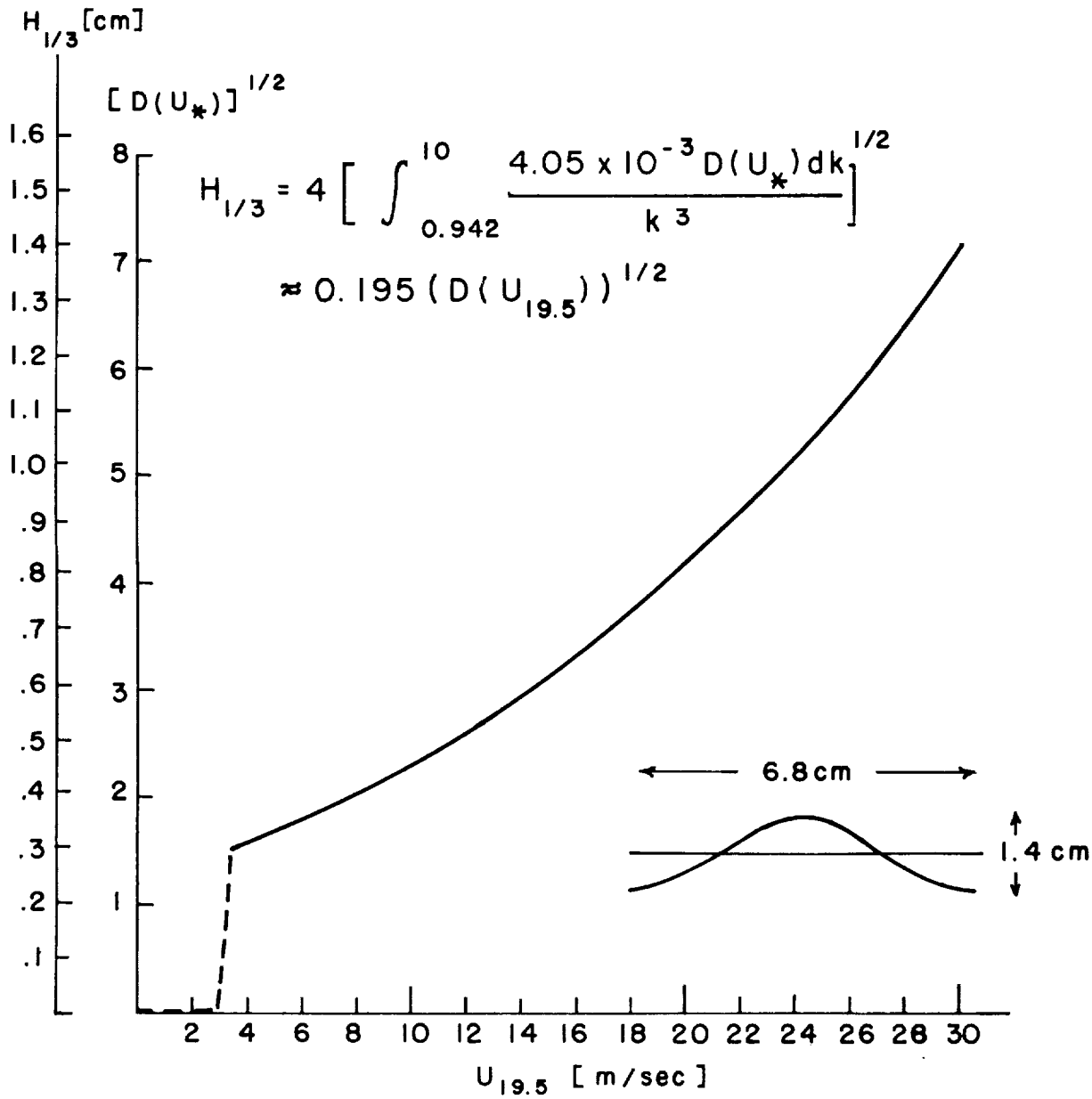

Fig. 5.7 $(D(u_*))^{\frac{1}{2}}$ versus $U_{19.5}$ for a neutrally stratified atmosphere. Also shown are the corresponding significant wave heights.

corresponds to a variation in significant wave height† from 0.3 to 1.6 cm.

The least squares regression of $[D(u_*)]^{\frac{1}{2}}$ on u_* is shown in Figure 5.4 for $u_* > 12$ cm/sec.

The defining equation for $[D(u_*)]^{\frac{1}{2}}$ is given on the figure and by equation (5.7) (or equation (2.12)) for $u_* > 12$ cm/sec. The three outrider points in the NYU data are included. Their omission would not change the equation very much.

$$(D(u_*))^{\frac{1}{2}} = 1.247 + 0.0268(u_*) + 6.03 \times 10^{-5}(u_*)^2 \qquad (5.7)$$

This form of presentation also shows something about the size of the scatter. The significant capillary wave height scatters by about plus or minus 0.1 cm about the regression line over the full range of u_* from 12 to 170 cm/sec.

There would have been other ways to obtain an expression for $D(u_*)$ as a function of u_*, but the way chosen appears to fit $D(u_*)$ as given in equation (5.7) versus u_* on both linear and double log scales almost as well as if the regression curves had been derived to fit the data on these scales as shown in Figures 5.5 and 5.6. Note the coded points attributed to Bradley (1971) in Figure 5.6, which will be discussed later.

Given the relationship between u_* and $U_{19.5}$, $D^{\frac{1}{2}}$ can be plotted against $U_{19.5}$ as in Figure 5.7. $D^{\frac{1}{2}}$ varies from about 1.5 at 3.5 m/s to 7 at 30 m/s and the wave height varies from 0.3 to 1.4 cm. A wave 6.8 cm long and 1.4 cm high is shown as an insert. Figure 5.7 also shows the sharp increase in wave height near 3.5 m/s. Slightly below

---

†The significant wave height is defined to be the average of the heights of one-third highest waves in a wave record, in this case after the other wave number ranges have been filtered out.

this speed, the capillary wave height decreases sharply from 0.3 cm to 0.003 cm for this range of wave numbers.

Photographs of capillary waves

Figures 5.8, 5.9 and 5.10 show 32 cm long photographs of the waves generated at Kyoto as furnished by Dr. Toba for nominal wind tunnel speeds varying from 5.1 to 12.1 m/s and for fetches of 4.5, 6.9, and 10.0 meters. The high wave number, short wave, structure of the surface becomes rougher with increasing wind speed at all three fetches, and this short wave structure is nearly the same for a given wind speed at all three fetches. The figures also show the crossing capillary waves in the proper locations as described theoretically by Longuet-Higgins (1963) for the lower wind speeds, and as predicted by Phillips (1957) in the resonant theory of wave generation. These crossing waves at low winds will play an interesting role in providing a refined version of equation (2.3) in a later section. The surface becomes uniformly rough for the higher speeds. It is difficult to imagine any reason why these scales of capillary waves should become lower for open ocean conditions. Moreover, these photographs support the procedures used in going back and forth from frequency to wave number space. The wave number spectrum clearly grows with increasing wind speed for waves between 6.8 and 0.63 cm in length.

Catspaws

One of the interesting features of these results, in particular Figure 5.2, is that they can be used to explain "catspaws". Catspaws are patches of roughened water scattered over a relatively smooth surface. They form, move along for a short distance, and disappear to be replaced

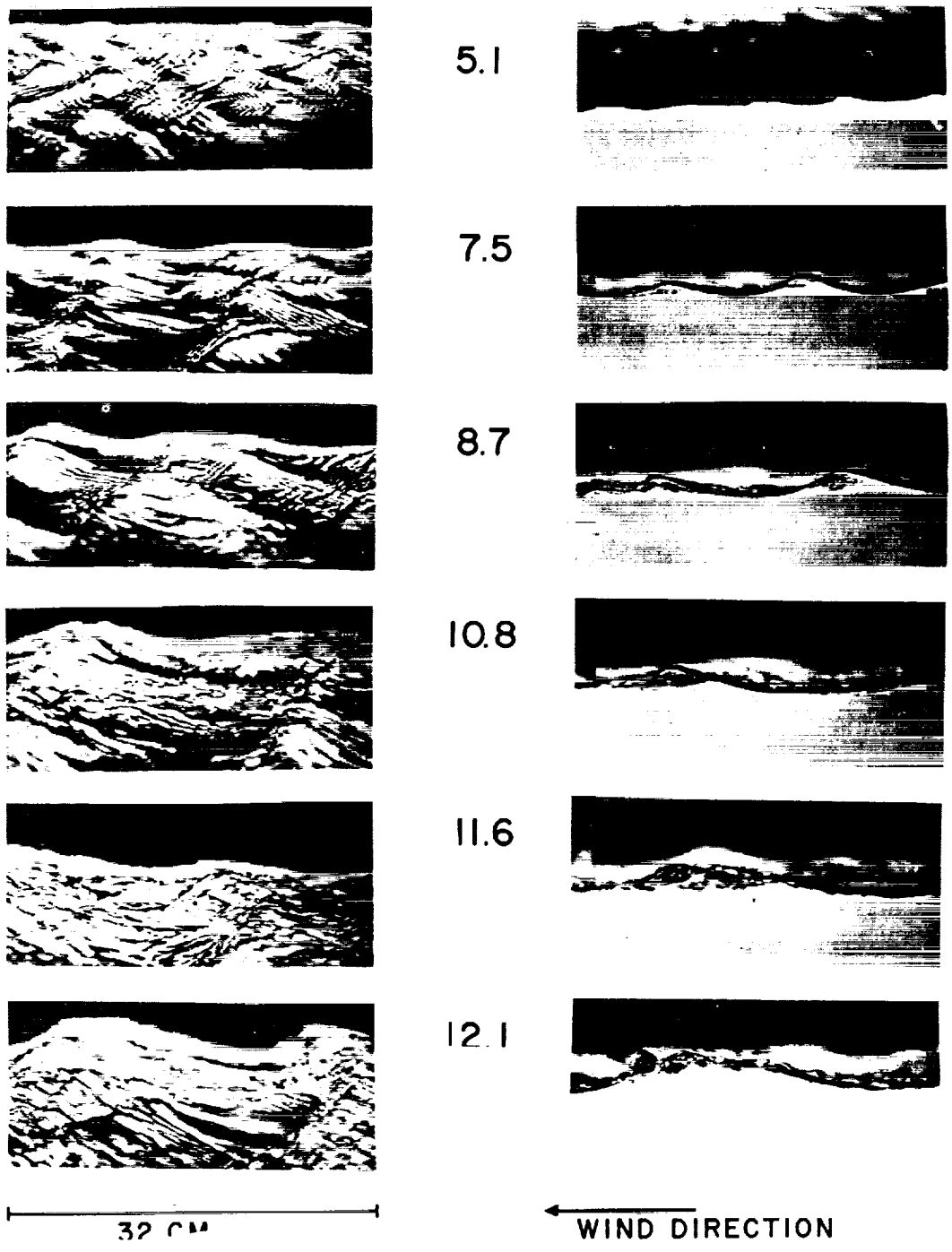

Fig. 5.8 Photographs of waves in a wind tunnel for a fetch of 4.5 meters. (Courtesy of Dr. Yoshiaki Toba.)

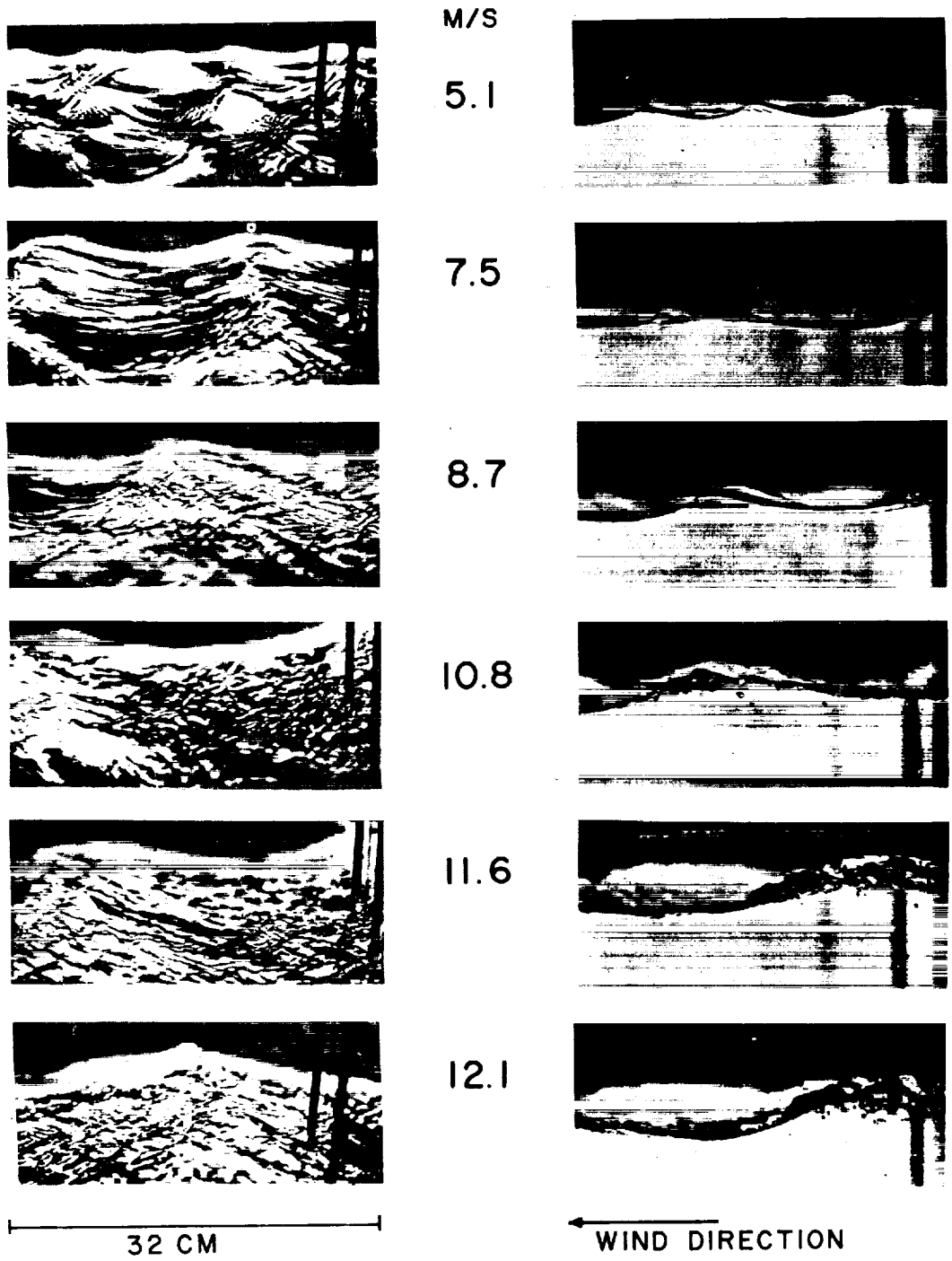

Fig. 5.9 Photographs of waves in a wind tunnel for a fetch of 6.9 meters. (Courtesy of Dr. Yoshiaki Toba.)

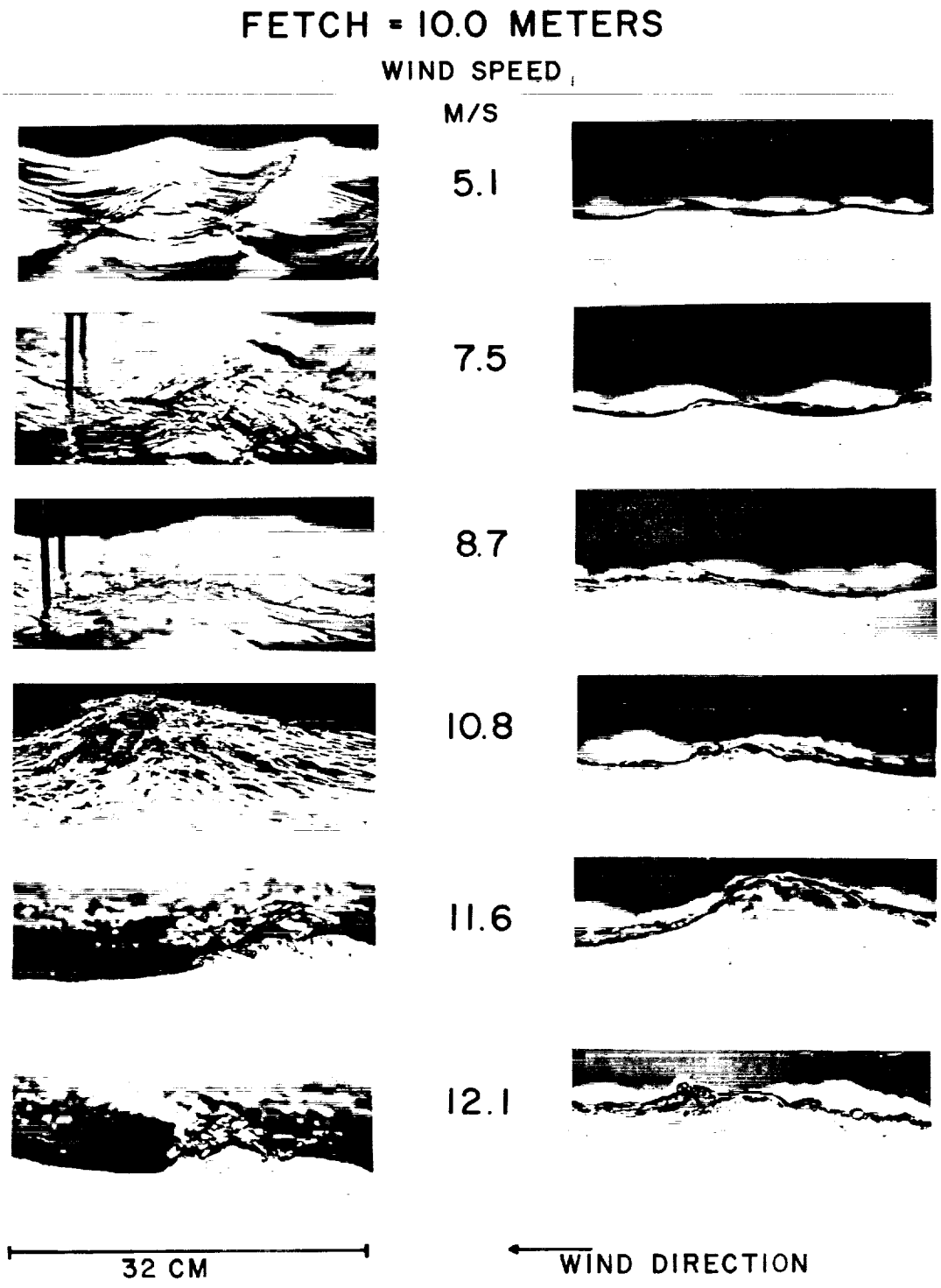

Fig. 5.10 Photographs of waves in a wind tunnel for a fetch of 10.0 meters. (Courtesy of Dr. Yoshiaki Toba.)

by other "catspaws" somewhere else over the water. If the wind over the water is describable as "light air", the friction velocity at the surface will be less than 12 cm/sec over nearly the whole surface. Turbulent gusts will produce small isolated patches over the water where u_* will exceed u_{*m} (12 cm/sec). The spectrum of the capillary waves in these patches will be four orders of magnitude higher than the spectrum of the low undulations in the nearby areas. The waves in the "catspaws" will be 100 times higher than the waves outside the catspaws.

Wave number spectra in the capillary range

Dr. Alan Schooley provided us with photographs for two different wind speeds of the wavy surface along the glass side of a small wind-water tank. The fetch was very short. The elevation as a function of distance along the glass side was read off and two wave number spectra were computed. The spectra varied as $(\ell^*)^{-3}$ (see equation (1.16) and the discussion in the section on the Leykin-Rosenberg range) with the one for the higher wind speed being considerably higher than the one for the lower wind speed at all values of ℓ^*. Since u_* was not known, exact quantitative agreement with the preceding equations could not be obtained, but the spectra behaved as the theory would predict and the photographs in this section show they should.

THE COX VISCOUS CUTOFF

Cox (1958) measured the upwind-downwind slope of capillary waves as a function of time at a fixed point in a small wind-water tunnel with a fetch of 2.14 meters. He was able to determine the spectrum of the slope of the waves out to very high frequencies. For the lowest wind speed for which data were obtained there was a sharp falloff of the slope spectrum by three orders of magnitude from 200 radians/sec to 800 radians/sec. For the next highest wind speed the three orders of magnitude falloff occurred between frequencies of 800 radians/sec and 2000 radians/sec.

From the available information, which consisted of a large size copy of the original plot of the data sent to us by Dr. Cox, it was possible to fit a function to the sharp cutoff region of these data. It was found that equation (6.1) described this portion of the spectrum. The constant A equals 0.792 and is not dimensionless.

$$fS_s(f) = \frac{A u_*^3}{f^4} \tag{6.1}$$

The frequencies, $\omega > 200$, were so high that the capillary relationships for wave number and frequency could be used. Equation (6.1) can be put in the form given by equation (6.2) where A^* is dimensionless.

$$S_s(f) = \frac{A^* k_m \omega_m^2 u_*^3}{\nu f^5} \tag{6.2}$$

Then by means of $\omega = 2\pi f$, $\omega = \frac{2g^{3/2}}{\omega_m^2} k^{3/2}$, and $\omega_m = (2gk_m)^{\frac{1}{2}}$, it is possible to find $k^2 S(k)$ and finally $S(k)$. The result is equation (6.3), (or equation (2.9)).

$$S_5(k) = 3(2\pi)^4 A^* \frac{u_*^3}{\nu g} \frac{k_m^6}{k^9} = E \frac{u_*^3}{\nu g} \frac{k_m^6}{k^9} \tag{6.3}$$

The dimensionless form $u_*^3/\nu g$ has been constructed with ν as one of the parameters because it yields a dimensionless result; obviously other combinations of k_m, g, ν, and ω_m could also have been used.

It would be more desirable to obtain both $\partial\eta(t)/\partial x$ and $\partial\eta(t)/\partial y$ and proceed from it to $S_5(k)$, but such data are not presently available so that the procedure used will have to suffice. As far as the viscous cut-off region is concerned, the function $k^2(\cos\Phi)^2 S(k) F(k,\Phi)$ has effectively been treated as if it were $k^2 S(k) F(k,\Phi)$.

If $S_4(k_\nu)$ is set equal to $S_5(k_\nu)$, the wave number at which the k^{-3} behavior shifts to the k^{-9} behavior can be found. The value of k_ν is given by equation (6.4).

$$k_\nu = \left[\frac{2E u_*^3}{\nu g a D(u_*)} \right]^{1/6} k_m \tag{6.4}$$

Over the range of u_* corresponding to realistic winds k_ν increases slowly with increasing u_*. The value of k_ν is typically near 10 and actually varies from 6 to 12, or so, as u_* varies from 12 to 48. The wavelength that corresponds to k = 10 is 0.63 cm which yields the upper limit of the integral in equation (5.6).

Cox (1958) also found the equivalent of the threshold u_* at about 12 cm/sec described above. The change in boundary layer characteristics at the input end of the wind water tunnel seems to have produced a slight fetch effect. The 10 meter wind at which the waves were observed to increase suddenly, with appropriate remarks about the unreliability of the calculation, was found to be given by 2.9, 2.5,

and 2.3 m/s as the fetch varied from 1.47 through 2.14 to 3.12 meters. These values would correspond to values of u_* between 9 and 11 cm/sec if the estimates were correct. If they were more nearly 3.5 m/sec, then the value of u_* would agree with the value deduced in the preceding analyses of the capillary range.

The measurements made by Cox (1958) of the upwind-downwind slope as a function of time at a point were made for values of u_* of 284 cm/sec, 217 cm/sec, 144 cm/sec, and 31 cm/sec. These correspond to 19.5 meter average winds of 45.6 m/s, 37.6 m/s, 27.9 m/s, and 8.98 m/s; and, in turn, the first two of these speeds corresponds to a wind in excess of hurricane speed and to a wind of nearly hurricane speed. The Sutherland (1967) data on elevation spectra for longer fetches only extends to about 180 cm/sec for comparison.

Figures 6.1 and 6.2 show graphs of $fS_s(f)$ versus f as found by Cox (1958) plotted along with the theoretical graphs for the same quantity for an infinite fetch for these four different values of u_*. The agreement is poor for $u_* = 284$ cm/sec both because there is no particular reason why the equation for $D(u_*)$ should be valid for such an extreme wind and because the fetch is so short that the waves might not have been generated anyway.

For $u_* = 217$ cm/sec, the viscous cut-off range agrees fairly well but the observed spectrum is low compared to the computed one. For $u_* = 144$, the viscous cut-off range is correctly located and the spectra agree over portions of their range of definition within a factor of two.

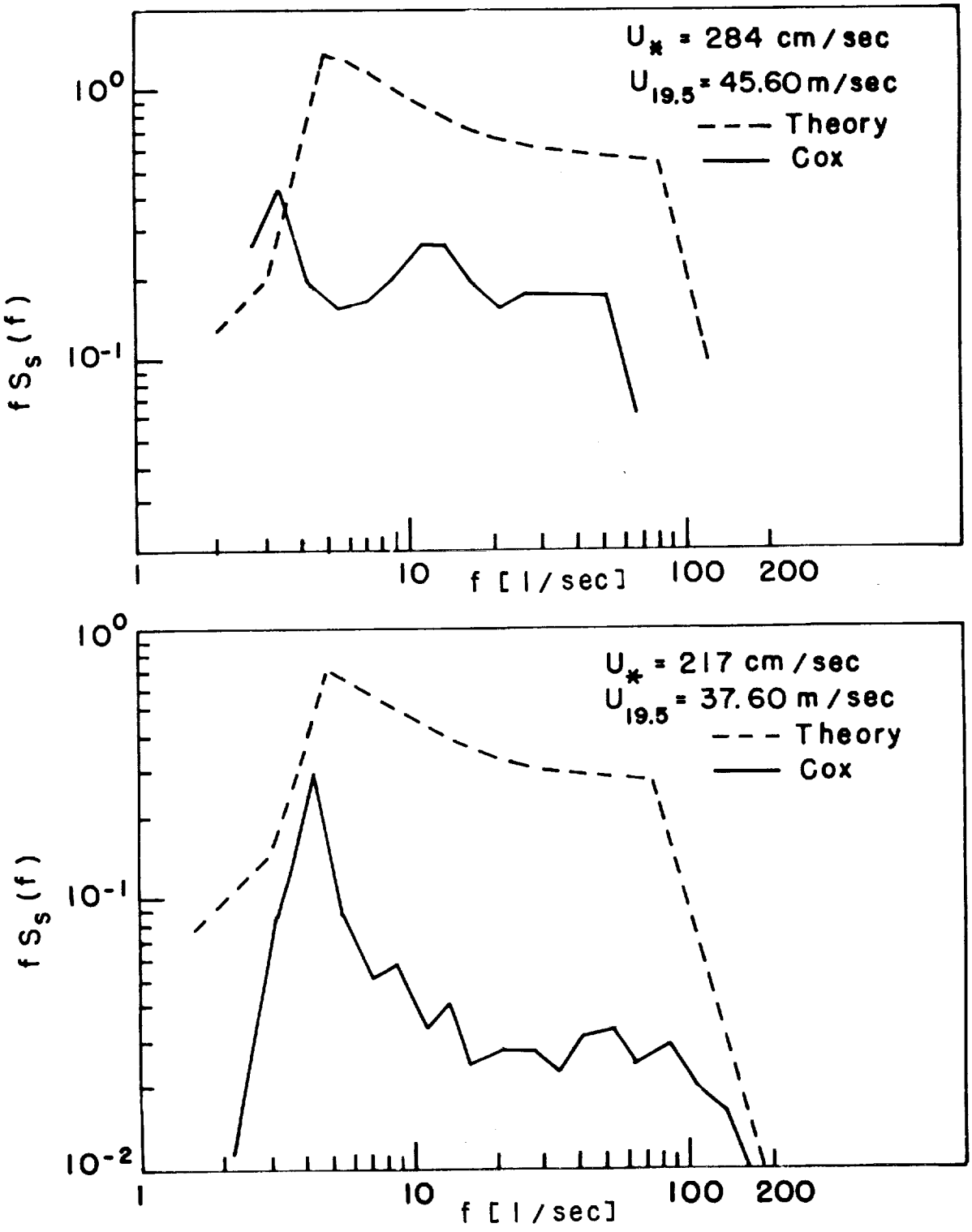

Fig. 6.1 Theoretical and observed graphs of $fS_s(f)$ versus f for high values of u_*.

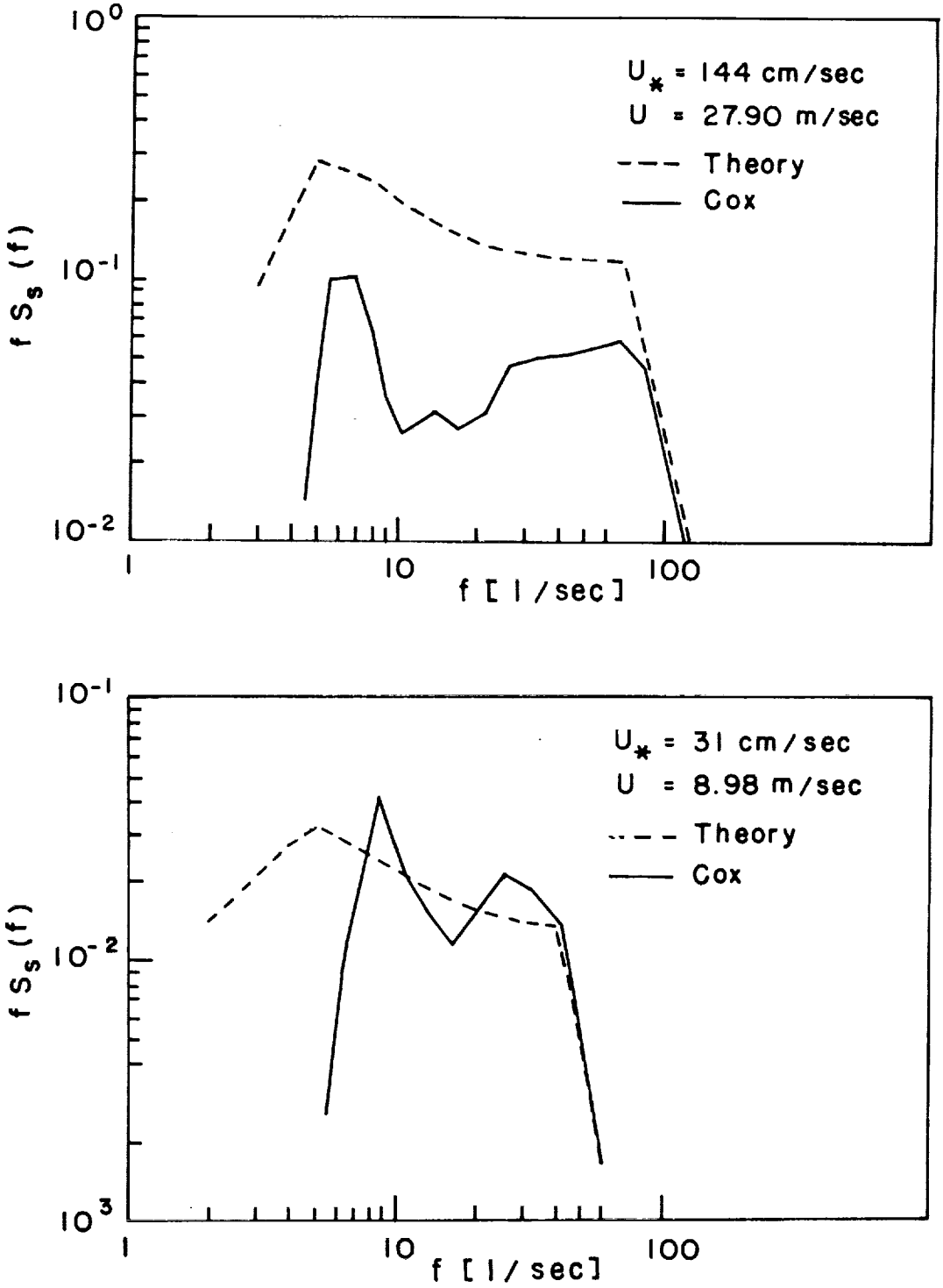

Fig. 6.2 Theoretical and observed graphs of $fS_s(f)$ versus f for moderate values of u_*.

For $u_* = 31$, the agreement is really quite good over one order of magnitude in f. The fetch is simply too short to generate those components with frequencies less than 6 hertz.

The further investigation of the slope spectrum over a more modest range of wind speeds for longer fetches should provide useful refinements in the definition of the viscous cut-off range. Research on this problem by others is under way at the present time and the results can be used to improve on the analysis given here.

THE KITAIGORODSKII AND LEYKIN-ROSENBERG WAVE NUMBER RANGES

The need to connect the gravity wave and capillary ranges

From the preceding sections, a gravity wave spectrum has been obtained that has the property that

$$S_1(k) \cong \frac{a}{2k^3} \tag{7.1}$$

for some high wave number part of the gravity wave spectrum, $0 < k < k_1$.

A capillary spectrum given by

$$S_4(k) = \frac{a}{2} \frac{D(u_*)}{k^3} \tag{7.2}$$

for $k_3 < k < k_\nu$ has also been found.

If $u_* = 50$, for example, corresponding to a 19.5 meter wind of 12.7 m/s, then $D(u_*)$ equals 6.5 and $S_4(k)$ is 6.5 times higher than the continuation of $S_1(k)$ into the interval, $k_3 < k < k_\nu$. Similarly, if $u_* = 100$ cm/sec, corresponding to a 19.5 meter wind of 21 m/s, $D(u_*)$ equals 20 and $S_4(k)$ is 20 times higher than the continuation of $S_1(k)$ into the interval, $k_3 < k < k_\nu$.

It thus becomes necessary to connect the Phillips equilibrium gravity wave range with this highly variable capillary range and to determine the values for k_1, k_2 and k_3. Equations (2.6) and (2.7) represent the Kitaigorodskii range and the Leykin-Rosenberg connecting range respectively.

The Kitaigorodskii range

The range defined by equation (2.6) was first proposed by Kitaigorodskii (1961) who discussed an interval of small-scale isotropic

turbulence postulated to follow (in frequency) the Phillips equilibrium range. A quotation from this source is:

> "We advance the additional hypothesis that at a frequency somewhat above the equilibrium interval the small-scale turbulent motions are such that they are affected only negligibly by the force of gravity, g. A region of the corresponding scale of magnitude is still not affected by surface tension and molecular viscosity. Then
>
> $$S(\omega) = f(\varepsilon_{max}, \omega) \tag{7.3}$$
>
> whence
>
> $$S(\omega) \sim \varepsilon_{max} \omega^{-4} \approx \frac{G u_* g}{\omega^4} \tag{7.4}$$
>
> "Equation (7.4) can serve as the essential particularization of [the spectrum] at high frequencies (somewhat above the equilibrium interval)."

This interval of isotropic turbulence grows like u_*, whereas the capillary range grows like $D(u_*)$ as shown previously. Moreover, it is not yet clear where one interval begins and the other ends.

The Leykin-Rosenberg results

Leykin and Rosenberg (1970) seem to have answered the question of how to connect the gravity wave range to the capillary range by means of observations made in the Black Sea at a point 50 meters from the shore in a water depth of 15 meters for situations where fetch effects did not influence the shape of the spectra. Thirty-two wave spectra were obtained "of which 19 were in absolute values and 13 in relative values".

The data show a clear increase of the spectrum at 3, 5, and 7 hertz as the wind speed at a 20 meter anemometer height varied from 0 to 11 meters/second. A plot of $S(f) \times f^4$ with the area under $S(f)$ normalized

to one from 1 to 7 hertz is shown for data grouped in wind speed ranges of 0 to 0.5 m/s, 0.5 to 2 m/s, 2 to 4 m/s, 4 to 8 m/s, and 8 to 11 m/s. Neither an f^{-4} nor an f^{-5} law is strictly correct over this full frequency range for the controlling parameters are wave number dependent and not frequency dependent and the frequencies span those for gravity waves and capillary waves. The low frequency end for low winds appears to follow an f^{-5} law because of the absence of the Kitaigorodski range. All plots of the normalized function $S(f) \times f^4$ show a relative minimum at f = 3 hertz and all but one show a maximum at f = 5 hertz with $S(f)\, f^4$ increasing between 3 and 5 hertz.

Beyond the 5 hertz peak the different spectra all still increase with wind speed roughly in the way the capillary range described above increased in the spectra studied from the wind-water tunnel.

Leykin and Rosenberg (1970) make several pertinent observations about their results. One is quoted as follows:

> " ... At wind velocities V > 0.5 m/sec, a spectral density peak appears in the spectra $S_{rel}(f)$ at a frequency of 4 to 6 Hz. With an increase in the wind velocity from 0.5 to 11 m/sec the peak increases more than twofold, while its location on the frequency axis remains practically unchanged. ..."

A second is quoted as follows:

> "In order to ascertain the uniqueness of the relation between S(f) and the wind velocity, we carried out several series of consecutive swell [wave] measurements; each series of measurements lasted several hours; during this time the parameters of the low-frequency swell [wave] components remained [invariant], while the wind velocity varied. The results of the measurements confirmed the decisive effect of the wind velocity on the variation of S(f)."

A third is quoted as follows:

> "The observed increase in the spectral density of S(f) with increasing wind velocity may be attributed either to amplification of nonlinear interactions in the low-frequency range of the spectrum or to direct transfer of wind energy to the high-frequency range [according to Phillips]. Since the frequency range considered was, as a rule, located far from the energy-carrying maximum (f_o= 0.1 to 0.2 Hz), and taking into account the decisive effect of the wind velocity on the variation of S(f), we may apparently give preference to the second of the above-mentioned mechanisms."

A final quotation is:

> "...All the results considered correspond to wind directions at which sufficient fetch paths were ensured for all the wave components; therefore the effect of the fetch path on the change in the shape of the spectra may be neglected."

These observations seem therefore to confirm the belief that the high wave number, high frequency portion of a wind roughened sea responds quickly, and rather uniquely, to variations of u_*. The upper range of wind speeds covered by the data was only 8 to 11 meters/sec so that open water verification of the wind-water tunnel results for higher wind speeds is still required. There is a discrepancy between this paper and the wind tunnel data on the critical wind speed because changes are reported in the ranges of 0 to 0.5 m/s and 0.5 to 2 m/s that would not compare with wind tunnel results.

The variations in the data, the minimum at 3 hertz, and the maximum at 5 hertz all suggest that the highest wave number for the interval of small-scale isotropic turbulence should be given by $k = k(\omega) = k(6\pi)$, and that the lowest wave number in the capillary range should be given by

$k = k(\omega) = k(10\pi)$. These values correspond to wave numbers of about 0.35 and 0.92 or wavelengths of about 18 cm and 6.8 cm. The interval between 0.36 and 0.94 can be called the Leykin-Rosenberg range. The value, 0.94, for k_3 determines the lower limit of the integral in equation (5.6).

For $u_* = 12$, the capillary range is still higher than the Phillips equilibrium range in the gravity wave spectrum. The u_* dependent range should perhaps disappear so that $k_1 = k_2$. The Leykin-Rosenberg range could be made to connect the gravity range to the capillary range by a straight line on a double log plot of S(k) versus k.

At $k = k_2$, $S_2(k)$ should grow linearly with u_*. From (7.4),

$$S_2(\omega) = \frac{G g u_*}{\omega^4} \tag{7.5}$$

and by means of $\omega^2 = gk$ one obtains

$$S_2(k) = \frac{G u_*}{2 g^{\frac{1}{2}} k^{2.5}} \tag{7.6}$$

At $k_1 = k_2$, and $u_* = 12 = u_{*m}$,

$$S_2(k) = \frac{G u_{*m}}{2 g^{\frac{1}{2}} k_2^{2.5}} = \frac{\alpha}{2 k_2^3} \tag{7.7}$$

so that

$$G = \frac{\alpha\, g^{\frac{1}{2}}}{u_{*m}\, k_2^{\frac{1}{2}}} \tag{7.8}$$

and $S_2(k)$ has the form

$$S_2(k) = \frac{a}{2 k_2^{\frac{1}{2}}} \frac{u_*}{u_{*m}} \frac{1}{k^{2.5}} \tag{7.9}$$

This curve will intersect the curve defining $S_1(k)$ at $k = k_1$, and imposing this condition, one finds that

$$\frac{a}{2k_1^3}\exp\left[-\beta\left(\frac{g^2}{k_1^2(U(u_*))^4}\right)\right] = \frac{a}{2}\frac{u_*}{(u_{*m})}\frac{1}{k_2^{\frac{1}{2}}}\frac{1}{k_1^{2.5}} \tag{7.10}$$

The exponential term can be neglected as typical values of the exponent work out to be 10^{-3} or so, so that the term is essentially unity. It follows that

$$k_1 = \left(\frac{u_{*m}}{u_*}\right)^2 k_2 \tag{7.11}$$

and that k_1 decreases with increasing wind speed as also given following equation (2.5).

At $k = k_2 = k\,(6\pi)$, the value of $S_2(k)$ is now given by

$$S_2(k_2) = \frac{a}{2}\frac{u_*}{u_{*m}}\frac{1}{k_2^3} \tag{7.12}$$

and at $k = k_3 = k\,(10\pi)$, the value of $S_4(k)$ is given by equation (7.13).

$$S_4(k_3) = \frac{a}{2}\frac{D(u_*)}{k_3^3} \tag{7.13}$$

The Leykin-Rosenberg range will be defined by connecting the two points $S_2(k_2)$, k_2, and $S_4(k_3)$, k_3 by a straight line on a double log plot. The result is

$$\frac{\log_{10} S_3(k) - \log_{10} S_4(k_3)}{\log_{10} k - \log_{10} k_3} = \frac{\log_{10} S_2(k_2) - \log_{10} S_4(k_3)}{\log_{10} k_2 - \log_{10} k_3} \tag{7.14}$$

This result can be written in the number of forms such as equation (7.15).

$$\log_{10}\left(\frac{S_3(k)}{S_4(k_3)}\right) = \frac{\log_{10}\frac{k}{k_3}}{\log_{10}\frac{k_2}{k_3}}\left[\log_{10}\left(\frac{S_2(k_2)}{S_4(k_3)}\right)\right] \tag{7.15}$$

and equation (7.16)

$$\frac{S_3(k)}{S_4(k_3)} = (k/k_3)^P \tag{7.16}$$

where $P = \dfrac{\log_{10}(S_2(k_2)/S_4(k_3))}{\log_{10}(k_2/k_3)}$. From the definitions of $S_2(k_2)$ and $S_4(k_3)$, equation (7.16) can be put into a final form given by

$$S_3(k) = \frac{a}{2} \frac{D(u_*)}{k_3^P k^{3-P}} \tag{7.17}$$

where

$$P = \frac{\log_{10}(D(u_*)/(u_*/u_{*m}))}{\log_{10}(k_3/k_2)} \tag{7.18}$$

for $k_2 < k < k_3$. When $k = k_3$, equation (7.17) equals $S_4(k)$ and from equation (7.14), when $k = k_2$, it equals $S_3(k_2)$.

Comparison of Kitaigorodskii range with data from Kinsman

Kinsman (1960) carried out extensive measurements of waves in Chesapeake Bay and documented the results thoroughly so as to show certain non-Gaussian features of the probability density function of wave elevation. The observations were of such high quality that Longuet-Higgins (1963) used the data to verify a theory he derived on the non-Gaussian distribution of wave elevation. Kinsman (1961) reported on the results of his measurements and concluded that he could find no consistent evidence of an equilibrium range like ω^{-5}. In fact, the average of all the spectra, normalized to f/f_{max}, came out like $\omega^{-4.5}$.

The literature of that period for studies carried out in reservoirs, and other smaller bodies of water, with wave recording systems that could acquire data out to 1.5 Hz, or so, gave values such as $\omega^{-4.7 \pm 0.5}$ from

Hicks (1960) and $\omega^{-4.5}$ for Burling (1959). An equilibrium law according to $\alpha g^2 \omega^{-5}$ was not clearly documented in these studies. Part of the difficulty was that some of the spectra were normalized to f/f_{max} and that the Tukey methods of spectral analysis smooth over a fairly large frequency range with a triangular weighting function.

Four of the original data sets of wave elevation time histories as tabulated by Kinsman (1960) were augmented by adding on zeros at the end, computing a properly corrected Fast Fourier Transform, and finding non-overlapping averages so that the spectral estimates were independent for a square shouldered spectral window. The data sets were for records 017, 018, 093 and 094, with the first two corresponding to a u_* of 15.9 cm/sec and the second two to a u_* of 41.2 cm/sec. These records were chosen because they corresponded to the lowest observed u_* and the highest observed u_* after correction for atmospheric stability effects according to the methods described by Cardone (1969). The pairs of spectra were averaged to obtain a single spectrum for the two different u_* values.

These two spectra are shown on Figure 7.1 as labeled. The heavy line shows $\alpha g^2 \omega^{-5}$ for $\alpha = 8.1 \times 10^{-3}$. The dashed line shows $S_2(\omega)$ as given by equation (7.19), which is the transformation of equation (7.9) to frequency space, for $u_* = 41.2$. The capillary effects do not cause $S_2(\omega)$ to depart from the theoretical gravity form.

$$S_2(\omega) = \alpha g^{3/2} u_* / k_2^{\frac{1}{2}} (12) \omega^4 \qquad (7.19)$$

The dashed line is the Kitaigorodskii range for $u_* = 41.2$. The Kitaigorodskii range for $u_* = 15.9$ cm/sec hardly shows up at all the lower right corner of the figure and is not graphed.

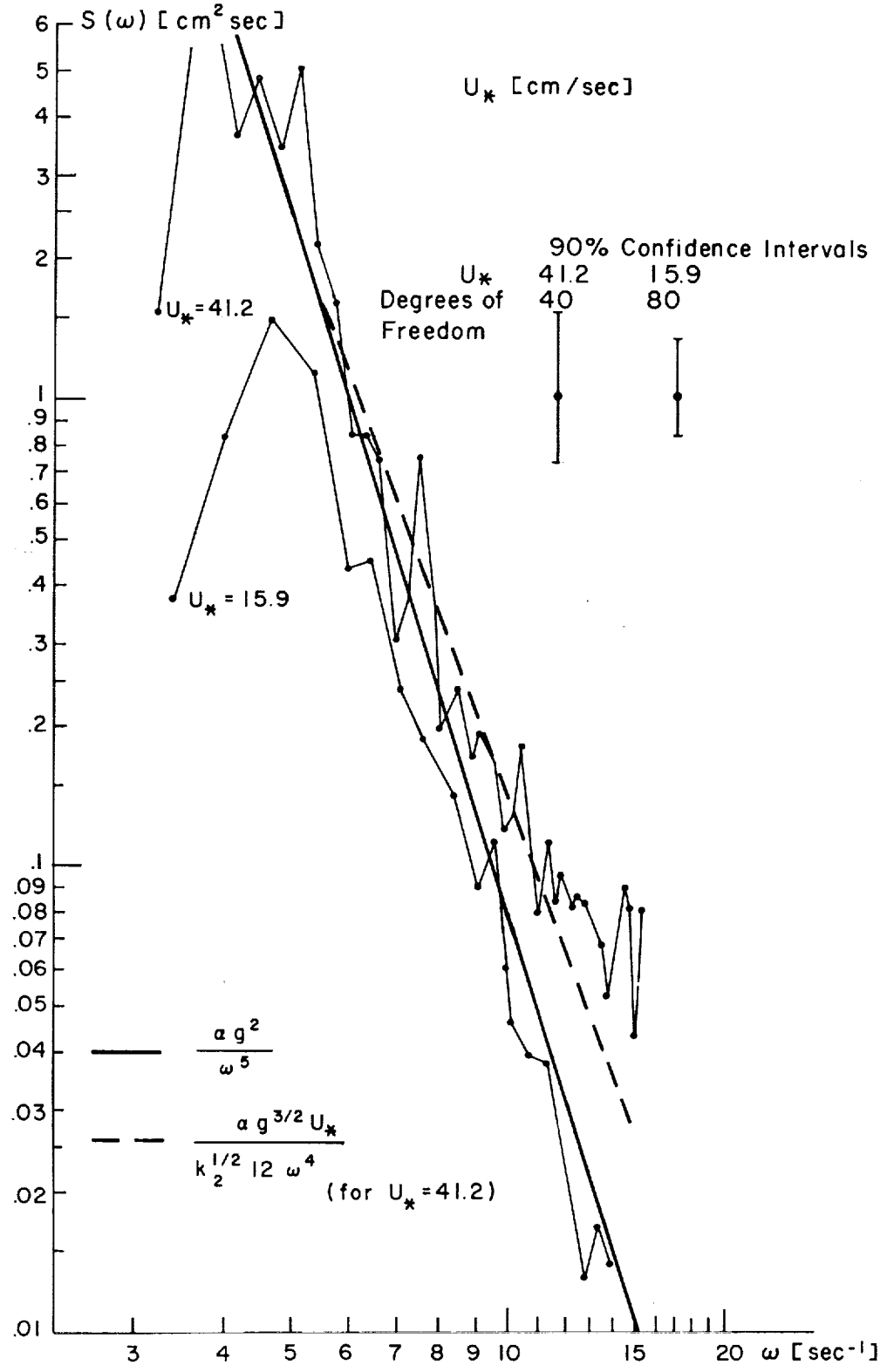

Fig. 7.1 Graphs of $S(\omega)$ versus ω for $u_* = 15.9$ and 41.2 cm/sec compared with estimated spectra to illustrate the Kitaigorodskii range.

The equilibrium ω^{-5} slope is well defined for $u_* = 15.9$ for the high frequency range, but the spectrum is low. Kinsman (1960) notes calibration problems for records 017 and 018 that could account for this. The $u_* = 41.2$ spectrum tracks the combined equilibrium and Kitaigorodskii ranges within sampling variability, except at high frequencies where sampling variability and aliasing clearly account for the difference between the computed spectrum and the theory. Normalizing the two spectra at f/f_{max} and averaging would have masked the simple wind speed dependence postulated by Kitaigorodskii and made it practically impossible to find.

The data of Saenger (1972) used to document the value of α also support the Kitaigorodskii range by showing its absence for frequencies less than 0.7 hertz. For the wind speeds for which the observations were made, the Kitaigorodskii range should not have been observed. There was no evidence of wind speed dependence in the equilibrium range for wind speeds corresponding to u_* greater than 12.

These results suggest that there is indeed an equilibrium range, but that both frequency boundaries shift toward lower frequencies with increasing wind. The Kitaigorodskii range may have been present in those observations that reached high enough frequencies, but the data analysis procedures were not designed to find it.

The "variable" constant for the equilibrium range thus appears to be the result of how much of a u_* dependent contribution at high frequencies was averaged into the computation after perhaps an f/f_{max} frequency shift, and the variable exponent appears to be dependent on how many spectra had an ω^{-5} dependence and how many had an ω^{-4} dependence as masked by noise and sampling variability. The "constant" also appears to be fetch dependent

because shorter fetches imply smaller and more response wave recording systems that obtain data for higher wave frequencies to yield spectral values that include the Kitaigorodskii range. *

Comparison of theory with the Leykin-Rosenberg data

Leykin and Rosenberg (1970) averaged the spectra that were estimated by combining them into five groups according to different ranges of wind velocity. In turn, these five averaged spectra were normalized by dividing them by the variance to obtain

$$S_{rel}(f) \doteq S(f)/\sigma^2 \tag{7.20}$$

This result was in turn multiplied by f^4, and $S_{rel}(f) \times f^4$ was plotted on a logarithmic scale versus f on a linear frequency scale and shown as Figure 5 in the cited paper.

The values of $S_{rel}(f)$ are quite sensitive to what happens at low frequencies and depend on such things as whether or not the point plotted at 1 hertz has a band width from 0.5 to 1.5 hertz or some other width. It is thus not possible, without the original data, to reproduce their data reduction procedure by comparable calculations on the theoretical spectra.

The function, $f^4S(f)$, was computed by means of appropriate transformations on the defining equations for a single wind speed within the range of the grouped winds of Leykin and Rosenberg (1970). The result was then multiplied by that factor that would make it agree with the corresponding graph of Leykin and Rosenberg at 3 hertz.

The results for wind speed ranges of 2 to 4, 6 to 8, and 8 to 11 m/s as calculated for 3.5, 5.5 and 8.5 m/s are shown in Figure 7.2. The agreement for the 2 to 4 and 6 to 8 m/s is quite good with the theoretical curves coming close to the observations over the range from 2 to 6 hertz.

* R.A. Stacy will have additional results on this range in the near future.

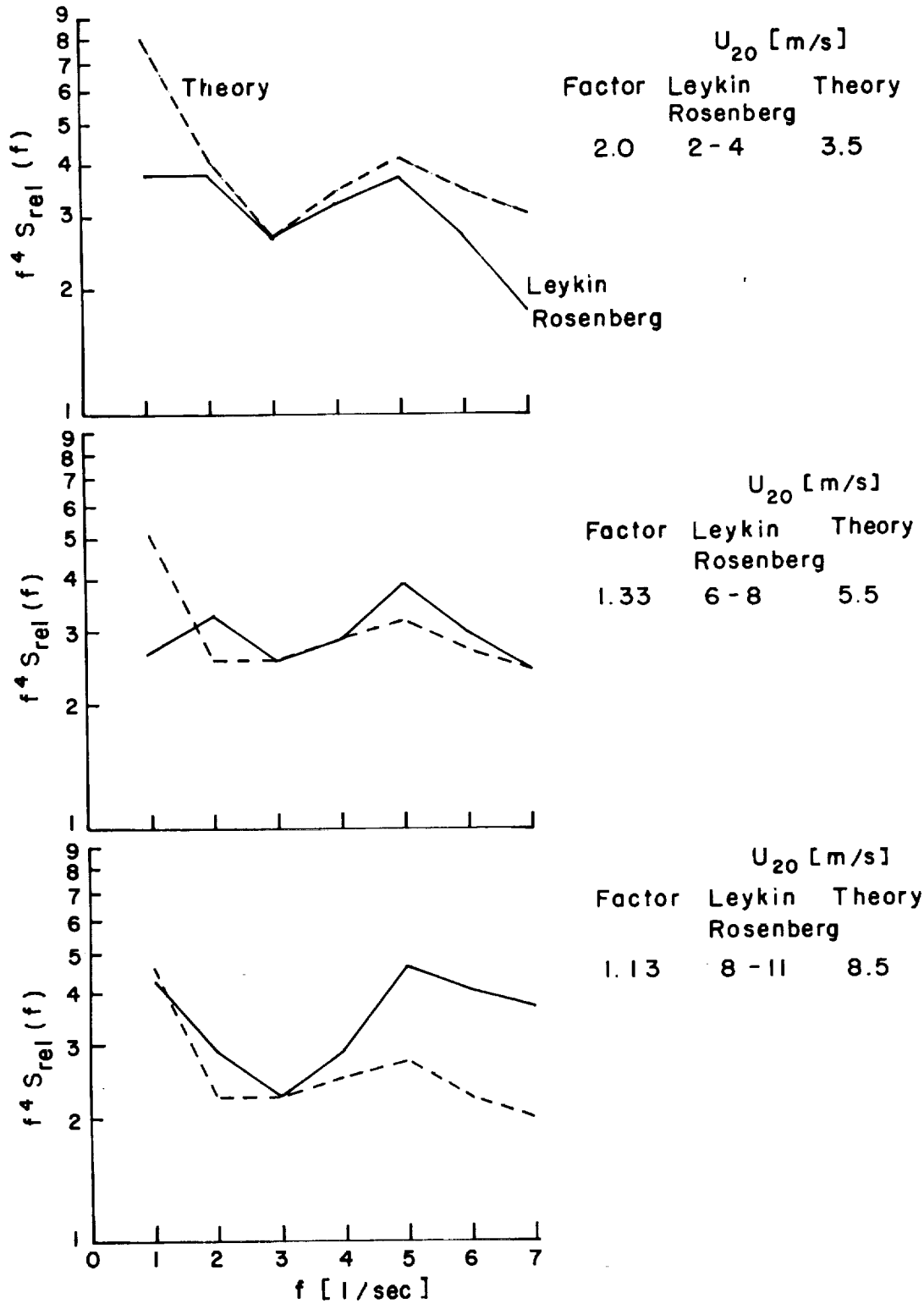

Fig. 7.2 Comparison of $f^4 S_{rel}(f)$ versus f as given by Leykin and Rosenberg with theoretical values.

Division of both curves by f^4 would result in the value at $f = 7$ being about 4×10^{-4} lower than the value at $f = 1$ so that even the curves for winds from 8 to 4 m/s are in fair agreement.

Additional supporting data

Quantitative data are difficult to obtain to support these two ranges. Much of the data has been processed in one way or another so as to make it difficult to go back to the basic observations and test these new spectral forms. Two sources can be cited, however, that give quantitative support for these ranges. One source is the figure given by Hess, Hidy and Plate (1969), and the other source is the graphs of the original spectra used to prepare the report by Dobson (1970).

The figure in Hess, Hidy and Plate includes $\omega = 6\pi$ and $\omega = 10\pi$ in its range from $\omega = 0.2$ to $\omega = 100$. The scatter of points between $\omega = 2\pi$ and $\omega = 6\pi$ shows a tendency to behave more like ω^{-4} than ω^{-5} as $\omega = 6\pi$ is approached from the left. The scatter of points between $\omega = 6\pi$ and $\omega = 10\pi$ illustrates the combined effect of wind speed variability in the Leykin-Rosenberg range and short fetches. Above $\omega = 10\pi$, if the spectra obtained from Toba and Sutherland were used, they would show the strong wind speed dependence obtained in the section on the capillary range.

The data used by Dobson (1970) consisted of stereophotogrammetric values of $\eta(x, y)$ along a line on the wavy surface. Spectra of these values were computed from observations made as the wind varied from 7 to 10 knots to 16 to 18 knots.

The resulting spectra are difficult to interpret. It would be necessary to define $S(\ell, m)$ by means of equations (2.4) through (2.9) over five regions defined by circles in the ℓ, m plane. Then it would be necessary

to evaluate $S(\ell^*)$ as given in equation (1.16) for those line sections in the upwind-downwind direction by an integration over m broken up into pieces corresponding to each spectral range of definition. Since angular effects, to be treated later, are not well known, the final result would be complicated by its analytical representation of the form used for the angular effects.

The original spectra, despite all of these qualifications, and except for some stray constant that cannot be explained, show what would be expected on the basis of the proposed wind speed dependent spectra. They follow an $(\ell^*)^{-2.5}$ law instead of an $(\ell^*)^{-3}$ law. They are wind speed dependent in that the spectrum for 16 to 18 knots is appropriately higher than the spectrum for 7 to 10 knots.

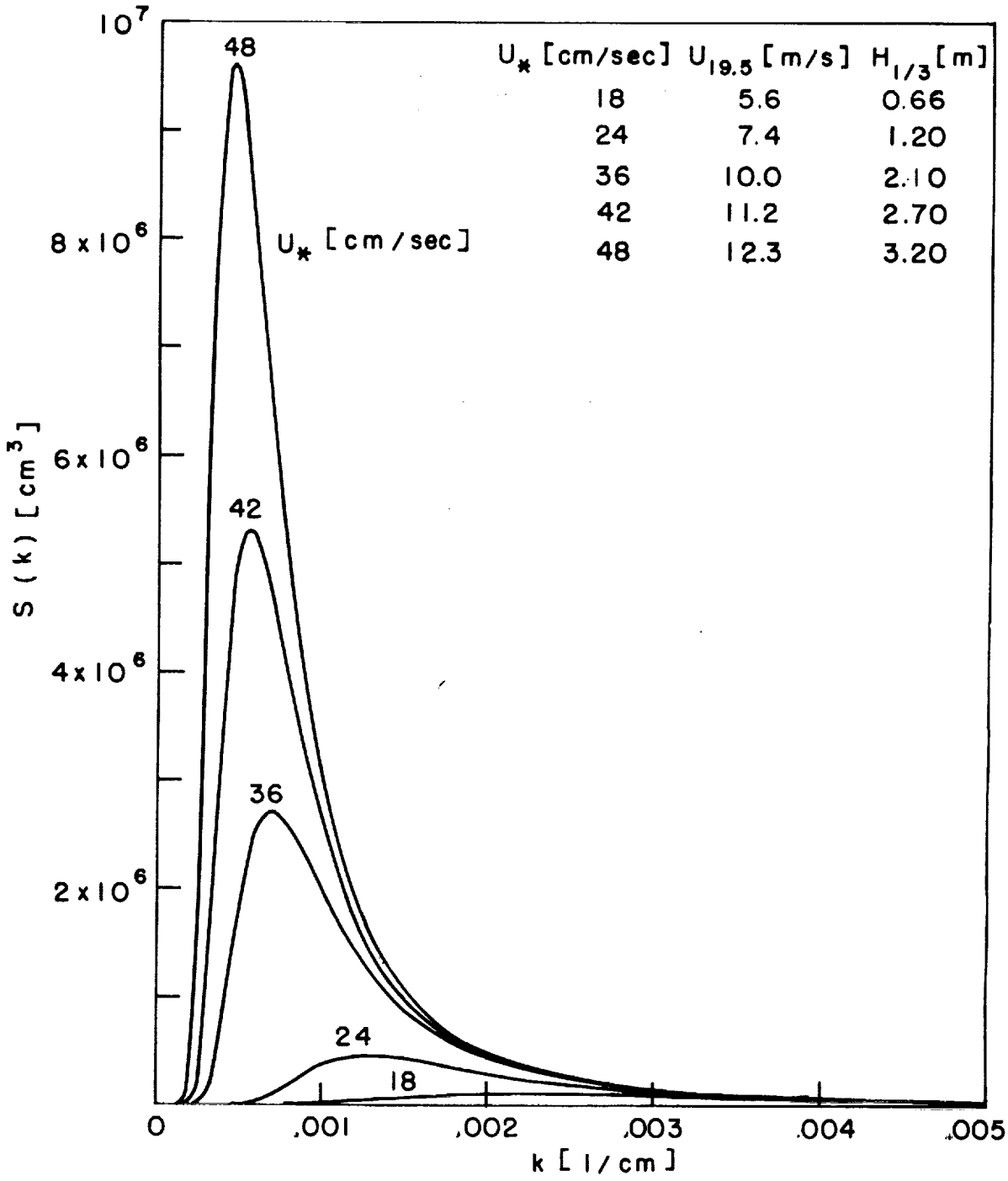

Fig. 8.1 S(k) versus k for light wind speeds. The graphs are area preserving.

be closely estimated simply by setting k_1, or k_2, equal to infinity.

$$\sigma^2 = \frac{\alpha U_{19.5}^4}{4\beta g^2}\left[1 - \frac{\beta g^2 u_*^4}{U_{19.5}^4 k_2^2 u_{*m}^4}\right] = \frac{\alpha U_{19.5}^4}{4\beta g^2} - \frac{\alpha}{4k_2^2}\frac{u_*^4}{u_{*m}^4} \tag{8.3}$$

Figure 8.2 shows graphs of, and portions of the graphs of S(k) versus k plotted on logarithmic scales for u_* equal to 12, 24, 48, 96, and 192 cm/sec so that the 19.5 meter wind varies from 3.5 to 34.3 m/s. The graphs for u_* = 12, 24, and 48 cm/sec are complete. For u_* = 12, $S_1(k)$ extends to $k \cong 0.35$, there is no Kitaigorodskii range, and the other three ranges follow. This is the lowest spectrum described by this theory, and it corresponds to a significant wave height of 25 cm. For a wind slightly lower than this, with no "gusts" above u_* = 12, the capillary range would drop by four orders of magnitude.

For u_* = 24, $S_1(k)$ extends to $k \cong 0.09$, the Kitaigorodskii range shows up out to $k \cong 0.35$. Because of the different behavior of $S_2(k)$ and $S_4(k)$, where one is a function of u_* and the other a function of $D(u_*)$, the break in slope of the Leykin-Rosenberg range is pronounced at first, then less pronounced, and finally more pronounced.

The graphs of the spectra for u_* = 96 and u_* = 192 are incomplete. Only the part of $S_1(k)$ for which it is essentially equal to $\alpha/2k^3$ is shown. The Kitaigorodskii range begins at $k \cong 0.007$ for u_* = 96 and $k \cong 0.0018$ for u_* = 192. A wind of 20.6 m/s (38.5 knots) and waves 9 meters (29.5 feet) in significant height can be expected once in a while.

However, a wind of 34.3 m/s (66.6 knots) and waves 24.9 meters (81.6 feet) are not to be expected because the fetch and the duration are far too large and never occur. The $S_1(k)$ part of the spectrum would not

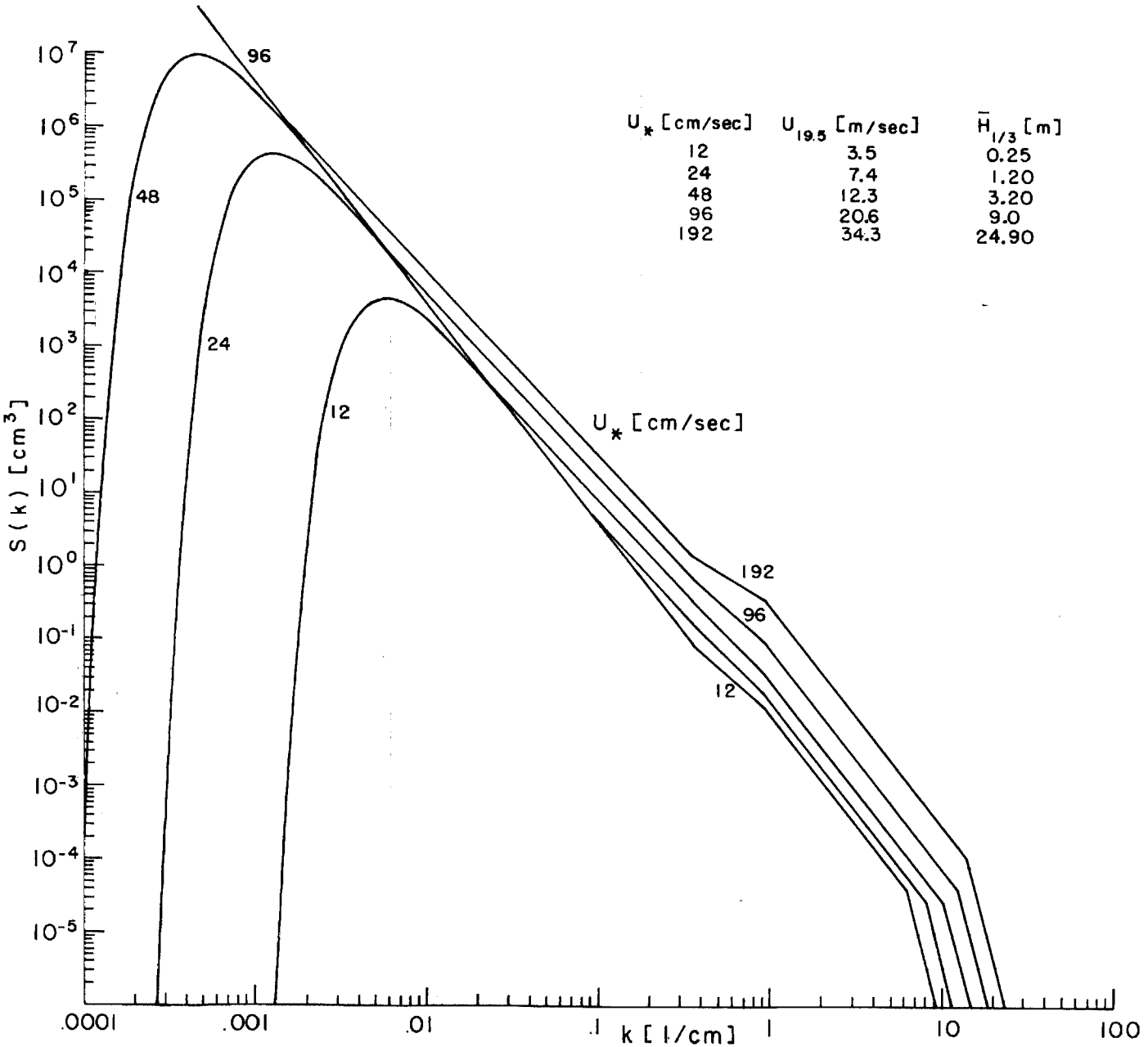

Fig. 8.2 S(k) versus k with both scales logarithmic for an extreme range of wind speeds.

have the required duration and fetch to be generated. The interval of "small scale isotropic turbulence" covers a large range and could conceivably be generated in hurricanes. This concept may be closer to reality at these high winds than any effort to define a single valued surface, $\eta(x, y, t)$, as shown, for example, in the photographs of waves for winds of 60 knots and over in Neumann and Pierson (1966). Just as there is a lower bound on u_* at 12 cm/sec for which these results apply, there is an upper bound, less well defined, where the concept of a wind roughened sea surface no longer applies.

Figure 8.3 shows graphs for only a small range of wind speeds. They are plotted on a logarithmic k scale and a linear kS(k) scale so that area is preserved. Since, from Figure 8.2, $S_2(k) \cong 30$ at $k = 0.1$, $kS_2 \cong 3$ at $k = 0.1$ and even for an extreme wind a graph of the spectrum would hardly move away from the horizontal axis at $k = 0.1$. Effects of higher winds would show on these graphs at $k = 0.02$, however.

An important feature of Figure 8.3 is that it shows that the contribution to the variance of the sea surface elevation comes from wave numbers smaller than 0.1 and that for most wind speed wave numbers larger than 0.01 contribute a very small percentage.

Slope Spectra

Figure 8.4 shows area preserving graphs of the slope spectra as u_* varies from 12 to 48 cm/sec corresponding to winds that vary from 3.5 to 12.3 m/s. Important contributions to the slope variance are produced by spectral components with wave numbers that vary all the way from 10^{-4} to 30.

For the gravity wave-gravity equilibrium range $k^3S_1(k)$ essentially rises to the constant value of $a/2$ for the equilibrium gravity range and becomes horizontal until the Kitaigorodskii range rises from it. The contributions of the $k^3S_2(k)$ and $k^3S_3(k)$ ranges to the slope variance are substantial, but the most important contribution comes from the capillary range for which equation (8.4) applies.

$$k^3S_4(k) = \frac{aD(u_*)}{2} \tag{8.4}$$

If $U_{19.5}$ were simply a constant multiple of u_*, the spectra would not bunch together with increasing u_* on the left and the contribution of $S_1(k)$ from $k = 0$ to $k = k_1$ to the slope variance would be a constant. As a result of equations (3.1) and (3.2), however, the contribution of $S_1(k)$ to the slope decreases with increasing wind speed. The values of k_1 can be located on the line, $a/2$, as the points where the Kitaigorodskii range begins.

Other graphs to attempt to illustrate properties of the slope spectra were prepared but are not included in this report. A simple linear plot is very misleading and difficult to graph.

Both Figures 8.2 and 8.4 show how the equilibrium gravity range depends on wind speed. The upper end of its range is given by k_1 and the lower end depends on how closely equation (2.5) is required to approach $a/2k^3$. The lower end of the range also decreases with increasing wind speed.

Curvature spectra

Figure 8.5 shows area preserving graphs of $k^5S(k)$ on a linear scale versus k on a logarithmic scale so as to illustrate the range of wave numbers that make important contributions to the curvature of the sea surface. The range is from $k \cong 1$ to $k \cong 10\pi$, corresponding to wavelengths of about 6 cm to 0.2 cm. The peak varies from $k \cong 2\pi$ to 4π, or wave-

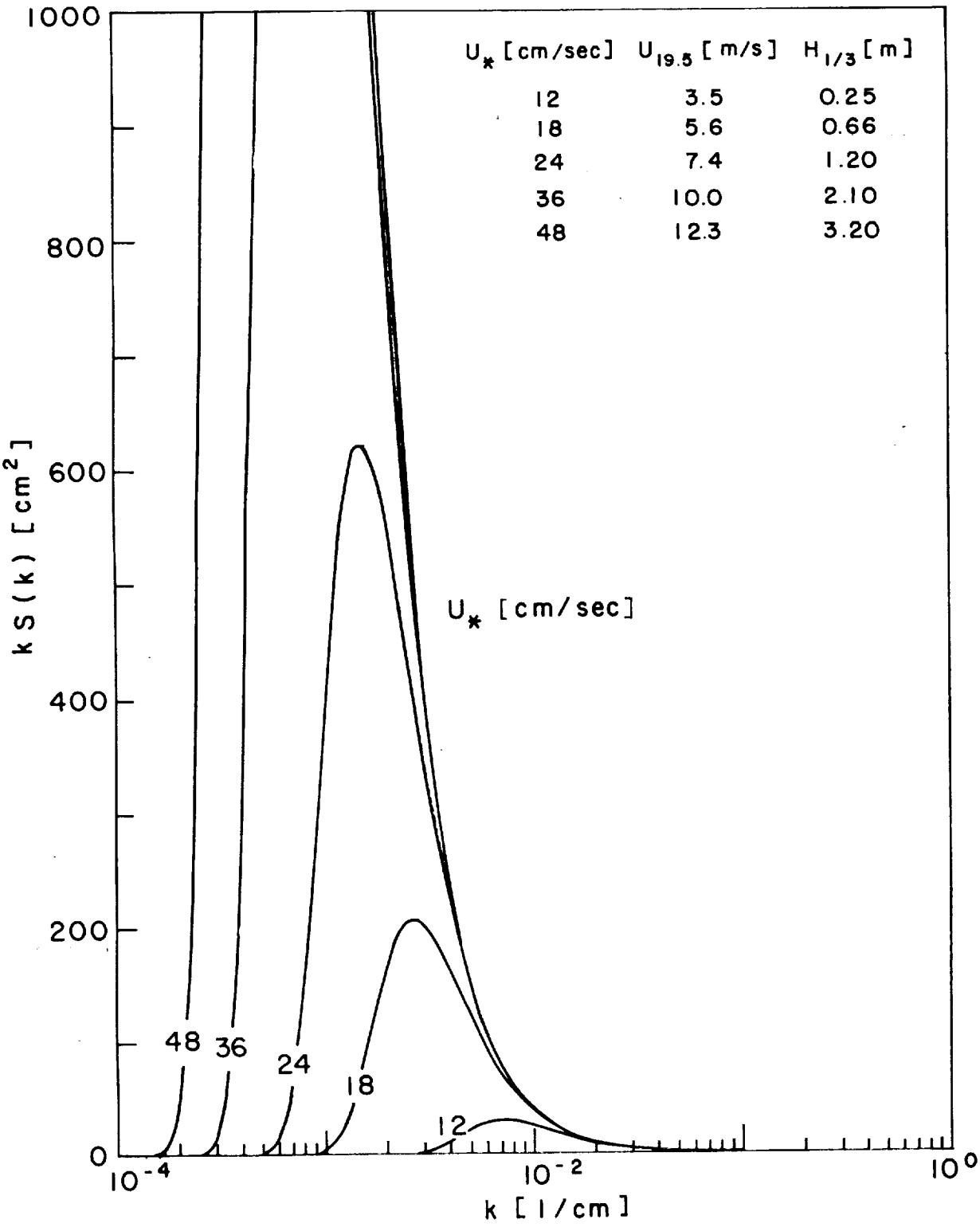

Fig. 8.3 kS(k) versus logk for a small range of wind speeds. The graphs are area preserving.

lengths of 1 cm to 0.5 cm.

An important feature of this spectrum is that higher moments exist. The k^{-9} behavior for the Cox viscous cutoff range ensures that moments up to the seventh can be found. Whether or not they have any real physical meaning is, of course, a question. Quantitative measurements of sea surface curvature do not seem to be available.

The three figures that show area preserving graphs of the elevation, slope, and curvature spectra (Figures 8.3, 8.4, and 8.5) should be compared. The elevation and curvature spectra each cover about two orders of magnitude on the wave number scale, but these two ranges are separated by more than one order of magnitude. In contrast, the slope spectra cover five orders of magnitude with important effects from waves from 100 meters long to one centimeter long.

Figure 8.6 shows graphs of curvature spectra ($k^4 S(k)$ versus k) on linear vertical and horizontal scales. The only important ranges, as far as curvature is concerned, are the capillary and viscous cutoff ranges and all the other spectral ranges are to the left of $k \cong 0.92$ where the curves stop. The left hand portion of each spectrum is simply a straight line with a slope that depends on $D(u_*)$, which, of course, increases with increasing wind speed.

The curvature spectra given by Figures 8.5 and 8.6 show the spectra of the "mean" curvature, which is an invariant property of the surface with reference to rotation, as defined by Longuet-Higgins (1962). Many other moments of $S(\ell, m)$ up to the fourth can be combined, as shown by Longuet-Higgins, to obtain the curvatures in various directions and other invariant properties of curvature with reference to rotation.

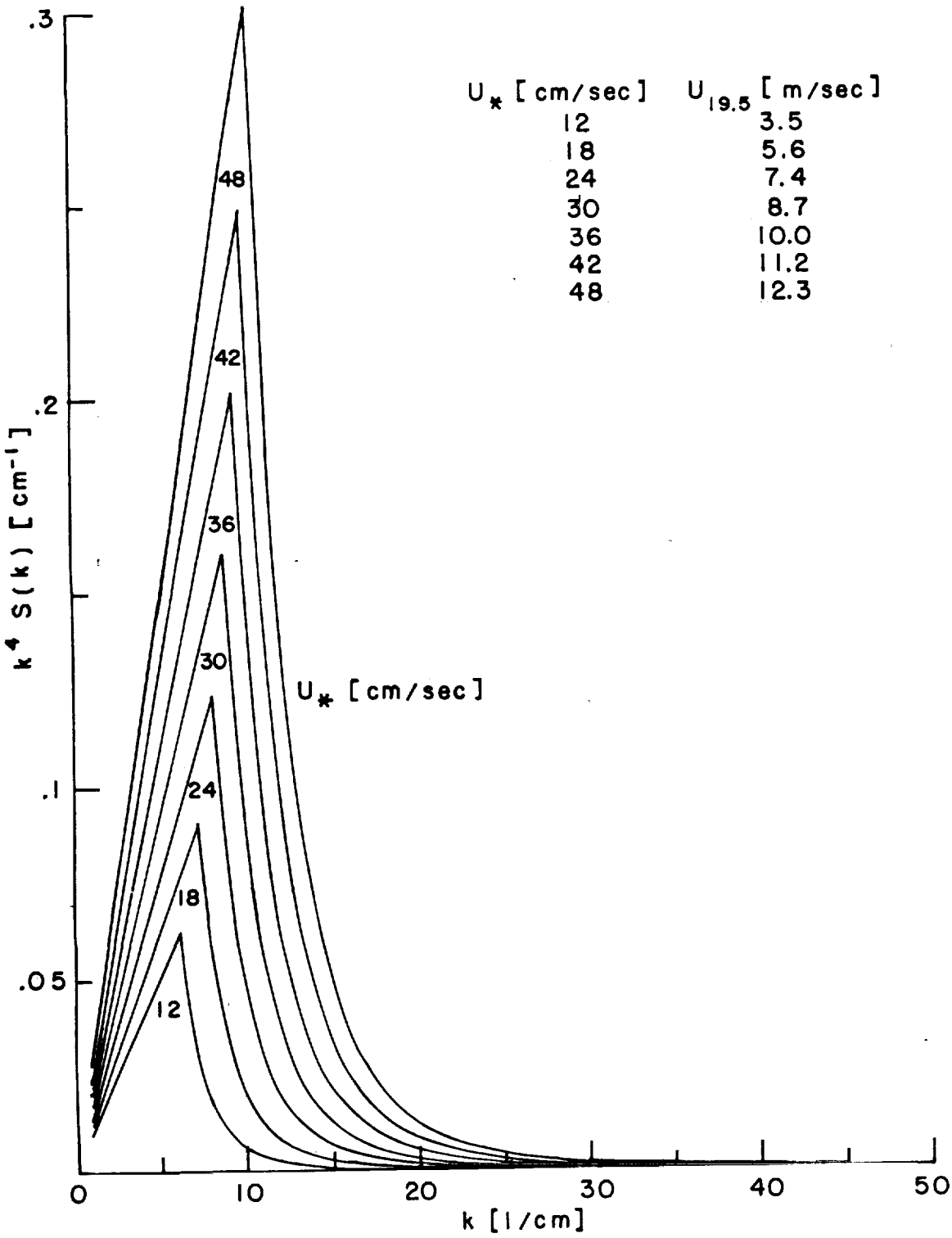

Fig. 8.6 $k^4S(k)$ versus k. The graphs are area preserving.

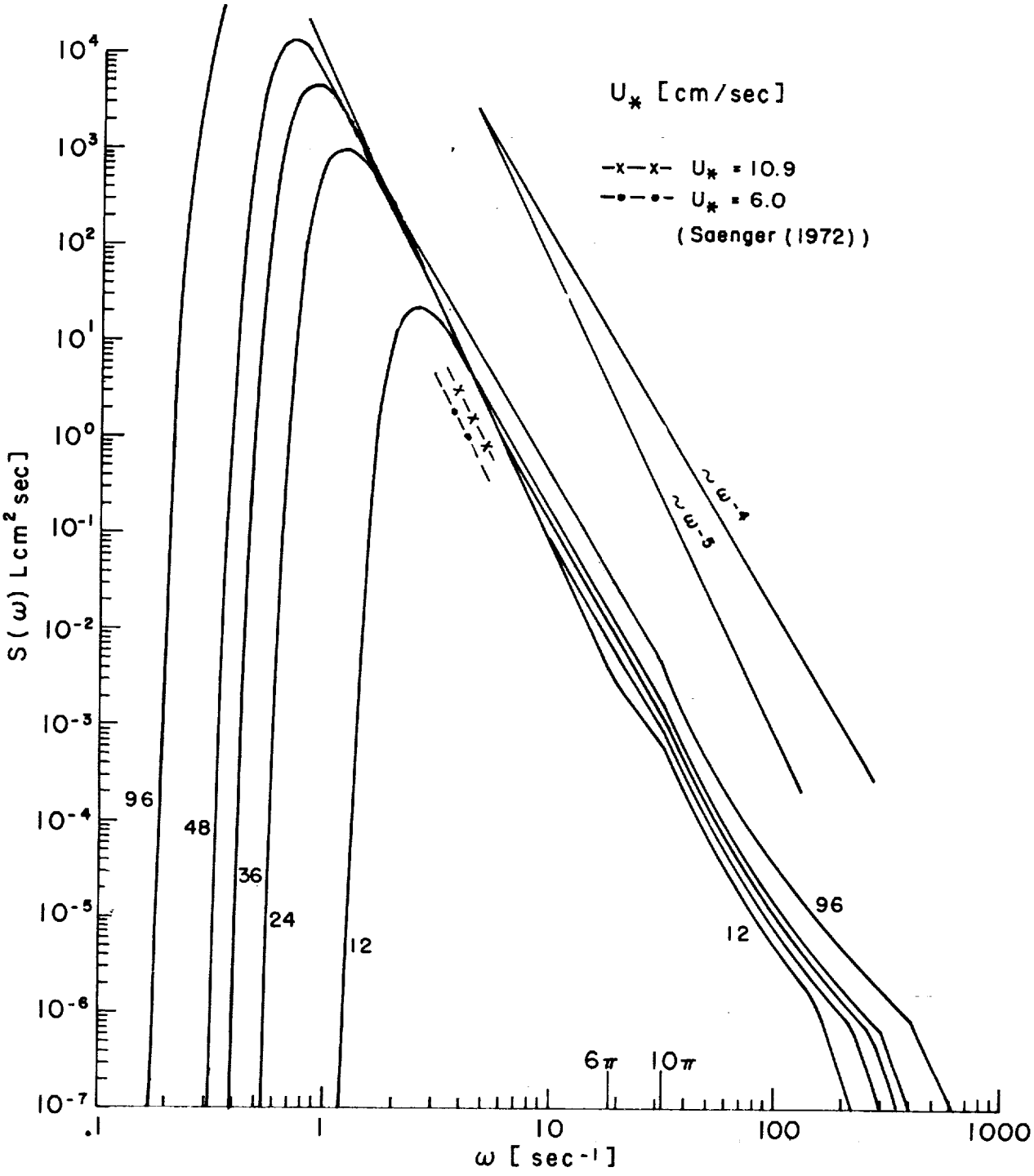

Fig. 8.7 $S(\omega)$ versus ω on logarithmic scales.

Frequency spectra

Figure 8.7 shows the spectra that result from transforming the equations for $S_1(k)$ through $S_5(k)$ (equations (2.4) through (2.9)) from wave number space to frequency space by means of the general relationship given by equation (1.15). Straight lines in wave number space become curved lines in frequency space when capillary effects become important. The spectra cover 12 orders of magnitude for the range of u_* used and 3.5 orders of magnitude over frequency. The two small segments near $\omega = 5$ show the results of Saenger (1972) for light winds of 6 knots (3.08 m/s) and 3 knots (1.54 m/s) which correspond to $u_* = 10.9$ and 6 cm/sec as discussed in the section on the gravity wave-gravity equilibrium range.

Kondo et al. (1973) have measured frequency spectra for a fetch of 40 km and a wind at 10 meters of 6.1 m/s and for a fetch of 30 km and a wind of 12.4 m/s. They report that "Our field results do not indicate a capillary saturation limit, at least within the range of winds encountered (about 1-16 m/sec at 10 m)". Two spectra are shown that cover 9 orders of magnitude in $S(\omega)$ over the range from $\omega = 6$ to $\omega = 200$. The similarities to Figure 8.7 are striking except that the spectra are higher and grow by more than the results of this study indicate they should. Waves in the capillary band seem to be too high to be realistic.

ANISOTROPY, SUN GLITTER AND RADAR BACKSCATTER

Introduction

The data on the form of $F(k, \Phi)$ such that $S(k, \Phi) = S(k) F(k, \Phi)$ can be found, now that $S(k)$ has been defined and illustrated over its five wave number ranges, comes from a wide variety of sources. It was originally intended to separate radar backscatter results from actual wave measurements in discussing $F(k, \Phi)$, but the radar measurements provide additional useful information on $F(k, \Phi)$ that can be incorporated into an understanding of the angular properties of the spectrum. Combining various sources that provide information on angular effects provides some information about $F(k, \Phi)$ for high wave number ranges, but full details are lacking.

The available data sources and data analyses that provide some information on angular effects are those of Coté et al. (1960), Longuet-Higgins, et al. (1963), Toba as given in Figures 5.8, 5.9, and 5.10, Cox and Munk (1954) (on sun glitter), Leykin and Rosenberg (1971), Bradley (1971) (on the MSC radar backscatter measurements), Valenzuela, Laing and Daley (1971) (which provides a partial verification of the form of $S(k)$), and unpublished radar backscatter data provided by Dr. J. W. Wright.

Taken altogether the data provide a fairly consistent description of some of the angular effects. They also indicate the need for further measurements and for careful interpretation of radar sea return measurements for winds from 3.5 to 10 m/s, or so. For example, for light winds the strongest sea return may come from angles that are 30° or 45° away from the upwind downwind direction.

Further work on the form of either $S(\ell, m)$ or $S(k, \Phi)$ is needed. This is a difficult problem, but theories and techniques are available, such as those of Stilwell (1969).

Differences between measurements under laboratory and natural conditions

The major difference between laboratory and natural measurements is that there are atmospheric turbulent scales that are not reproduced in wind-water tunnels. The photographs in Figures 5.8, 5.9 and 5,10 show for nominal winds of 5.1 m/s that the capillary waves are not traveling in the wind direction but at angles of 30 to 45° to each side of the wind direction. This feature of the wave spectrum was predicted by the resonant theory of wave generation of Phillips (1957). The wind in the wind water tunnel blows dominantly down the tunnel with little lateral variation.

In contrast, winds over the ocean vary from side to side about the average wind direction by amounts that would smear any well-defined two-peaked form for the angular variation of the spectrum for a given wave number, especially if the spot illuminated by the radar is large. Some of the effects of turbulence on radar sea return measurements were discussed by Pierson and Moore (1972), but this particular effect was not mentioned.

Turbulence is studied in terms of the horizontal, transverse and vertical components of the instantaneous wind. The transverse component would have an important effect on the capillary range by producing small local patches of short waves traveling in different directions for each patch. Studies of angular effects for $S(k, \Phi)$ for both natural conditions and under laboratory conditions are needed to clarify these features of the problem.

Theoretical considerations

For wave numbers corresponding to $k > k_1$ equation (2.3) needs to be replaced by equation (2.14) which is repeated here as equation (9.1) as defined over $-\frac{\pi}{2} < \Phi < \frac{\pi}{2}$ and by zero otherwise.

$$F(k, \Phi; u_*) = \frac{1}{\pi}\left[1 + \sum_{n=1}^{N} a_n(k, u_*) \cos 2n\Phi\right] \tag{9.1}$$

This form is inconvenient if the spectrum is required in the form $S(\ell, m)$. Moreover, so little is known about the a_n that it will only be possible to determine something about a_1 and a_2. Equation (9.1) is therefore specialized immediately to equation (9.2).

$$F(k, \Phi; u_*) = \frac{1}{\pi}\left[1 + a_1(k, u_*) \cos 2\Phi + a_2(k, u_*) \cos 4\Phi\right] \tag{9.2}$$

This can be rewritten as equation (9.3).

$$\begin{aligned} F(k, \Phi; u_*) &= \frac{1}{\pi}\left[1 + a_1(k, u_*)[2\cos^2\Phi - 1]\right. \\ &\quad \left. + a_2(k, u_*)[8\cos^4\Phi - 8\cos^2\Phi + 1]\right] \\ &= \frac{1}{\pi}\left[(1 - a_1(k, u_*) + a_2(k, u_*))\right. \\ &\quad \left. + (2a_1(k, u_*) - 8a_2(k, u_*))\cos^2\Phi + 8a_2(k, u_*)\cos^4\Phi\right] \end{aligned} \tag{9.3}$$

Equation (2.3) is a special case of this more general expression. For small k, for example, $a_1 = \frac{4}{3}$ and $a_2 = \frac{1}{3}$.

Each of the various spectral ranges can now be expressed as $S(\ell, m)$ where

$$S_i(\ell, m)\, d\ell\, dm = \frac{S_i((\ell^2 + m^2)^{\frac{1}{2}})}{(\ell^2 + m^2)^{\frac{1}{2}}} \cdot F((\ell^2 + m^2)^{\frac{1}{2}},\ \tan^{-1}(\tfrac{m}{\ell}))\, d\ell\, dm \tag{9.4}$$

because

$$S_i(\ell, m)\, d\ell\, dm \sim \frac{S_i(k)\, F(k, \Phi)}{k}\, k\, dk\, d\Phi \tag{9.5}$$

The results for the Kitaigorodskii range, the Leykin-Rosenberg range and the capillary range are given by equations (9.6), (9.7), and (9.8).

$$S_2(\ell, m) = \frac{a u_*}{2k_2^{\frac{1}{2}} u_{*m}} \frac{1}{(\ell^2 + m^2)^{7/4}} \cdot F(\ell, m) \tag{9.6}$$

$$S_3(\ell, m) = \frac{a D(u_*)}{2k_3^{p} (\ell^2 + m^2)^{(4-p)/2}} \cdot F(\ell, m) \tag{9.7}$$

$$S_4(\ell, m) = \frac{a D(u_*)}{2(\ell^2 + m^2)^2} \cdot F(\ell, m) \tag{9.8}$$

$F(\ell, m)$ is given by equation (9.9).

$$F(\ell, m) = \frac{1}{\pi} \Big[(1 - a_1((\ell^2 + m^2)^{\frac{1}{2}}, u_*) + a_2((\ell^2 + m^2)^{\frac{1}{2}}, u_*) + (2a_1((\ell^2 + m^2)^{\frac{1}{2}}, u_*) - 8a_2((\ell^2 + m^2)^{\frac{1}{2}}, u_*) \frac{\ell^2}{\ell^2 + m^2} + 8a_2((\ell^2 + m^2)^{\frac{1}{2}}, u_*) \frac{\ell^4}{(\ell^2 + m^2)^2} \Big] \tag{9.9}$$

For vv polarization, and upwind downwind conditions, Valenzuela et al. (1971) give the following equation for $\sigma^\circ_{vv}(\theta; u_*, k_o)$ after correction for a spectrum defined only over half a plane in ℓ-m space.

$$\sigma^\circ_{vv}(\theta; u_*, k_o) = 8\pi k_o^4 \cos^4\theta\, |G(\varepsilon, \theta)|^2 S(2k_o \sin\theta, 0) \tag{9.10}$$

For crosswind conditions, a similar equation results in which $S(2k_o \sin\theta, 0)$ is replaced by $S(0, 2k_o \sin\theta)$.

In equation (9.10), $|G(\varepsilon, \theta)|^2$ is given by equation (9.11).

$$|G(\varepsilon, \theta)|^2 = \left| \frac{(\varepsilon - 1)[\varepsilon(1 + \sin^2\theta) - \sin^2\theta]}{[\varepsilon \cos\theta + \sqrt{\varepsilon - \sin^2\theta}\,]^2} \right|^2 \tag{9.11}$$

Equations (9.6), (9.7), (9.8), and (9.9) can be substituted into equation (9.10) so as to obtain expressions for σ°_{vv} for each range of definition. For the capillary range and upwind-downwind conditions, the result is equation (9.12) which is independent of wave number except for $a_1(2k_o \sin\theta, u_*)$ and $a_2(2k_o \sin\theta, u_*)$.

$$\sigma^\circ_{vv}(\theta; k_o, u_*) = \frac{aD(u_*)}{4} |G(\varepsilon, \theta)|^2 (\cot\theta)^4 \cdot$$
$$[1 + a_1(2k_o \sin\theta, u_*) + a_2(2k_o \sin\theta_1 u_*)] \tag{9.12}$$

For crosswind conditions in the capillary range, the result is equation (9.13).

$$\sigma^\circ_{vv}(\theta; k_o, u_*) = \frac{aD(u_*)}{4} |G(\varepsilon, \theta)|^2 (\cot\theta)^4 \cdot$$
$$[1 - a_1(2k_o \sin\theta, u_*) + a_2(2k_o \sin\theta, u_*)] \tag{9.13}$$

Angular effects for the gravity wave-gravity equilibrium range

Equation (2.3) appears to be a good representation for angular effects in the gravity wave-gravity equilibrium range for $0 < k < k_1$ for the idealized conditions discussed in the introduction. As k approaches k_1, only the second term is important. Near the peak of the spectrum the $(\cos\Phi)^4$ term dominates. This equation is a modification of an equation given by Cote et al. (1960) to permit some simplifications in planned applications to studies in radar backscatter, which will use the recent results of Jackson (1972).

The use of the series of buoys developed at the National Institute of Oceanography in Great Britain as described in Neumann and Pierson (1966) and by Longuet-Higgins et al. (1963) has resulted in an alternate empirical expression for the portion of the spectrum for fully developed wind seas of the form

$$F(k,\Phi) = C_q[\cos(\Phi/2)]^{q(k)} \tag{9.14}$$

such that the integral from $-\pi$ to π is one and the expression is defined over the full angular range.

Near the peak of the spectrum q is typically 20, and it decreases as a function of k (or ω) to values of about 5 or 10 toward high wave number (or frequency). It is interesting to note that

$$(\cos\Phi/2)^{20} \cong (\cos\Phi)^4 \tag{9.15}$$

For example, the left hand side at $\Phi = \pi/2$ equals $(\sqrt{2}/2)^{20}$ or 2^{-10} and the right-hand side is zero. At $\Phi = \pi/3$, $(\cos\Phi/2)^{20}$ equals $(\sqrt{3}/2)^{20}$, or $(3/4)^{10}$ or $(9/16)^5 = (17.6)^{-1}$ and $(\cos\Phi)^4$ equals $(1/2)^4 = (16)^{-1}$.

Instead of a discontinuity at $\Phi = \pm\pi/2$ for the higher wave numbers in this range the actual function probably fairs smoothly to zero by being smaller than the values given in the equation inside the range of definition and small, but non-zero, for some fraction of a radian outside of the range of definition. Or in other terms, owing to the lateral gustiness of the wind, there may be some spectral components traveling opposite to the average wind direction.

Sun glitter

The measurements of sun glitter by Cox and Munk (1954) can be used to check the reality of the slope spectrum given by Figure 8.4

and to learn about anisotropy in the spectrum for the spectral range that provides the dominant contribution to the slope.

The data tabulated by Cox and Munk (1959) provide information on the wind speed at two elevations, on wave height, and on the sea surface slope variance in the upwind-downwind (σ_u^2) and crosswind (σ_c^2) directions. It was shown that the slopes had a nearly Gaussian distribution except that the upwind-downwind distribution had a peak toward the upwind direction. Slight nonlinearities are therefore evident in the slope properties, but to a fair degree of approximation $k^2S(k)$ does describe the slope spectrum.

The tabulated data in Cox and Munk (1954) give estimates of the significant wave height for each measurement. A plot of wave height versus wind speed from these data shows practically no correlation between the wave height and the wind speed and a very large scatter. For the conditions of the measurements, the gravity wave part of the spectrum was controlled by conditions other than the local wind such as swell from a distance and short fetches.

This wave height variability had little effect on the slope variance, although it probably accounts for some of the scatter. Figure 8.4 shows that the gravity wave range could be quite different from the idealized fully developed wind sea condition as far as slope is concerned and yet the effect on slope variance would be small.

If S(k) is the amplitude spectrum, the total slope variance integrated over Φ is given by equation (9.16).

$$\sigma_s^2 = \int_0^\infty k^2 S(k)\, dk \tag{9.16}$$

Figures 9.1 and 9.2 compare the slope variance of this spectral model with measurements of Cox and Munk (1954) as a function of both

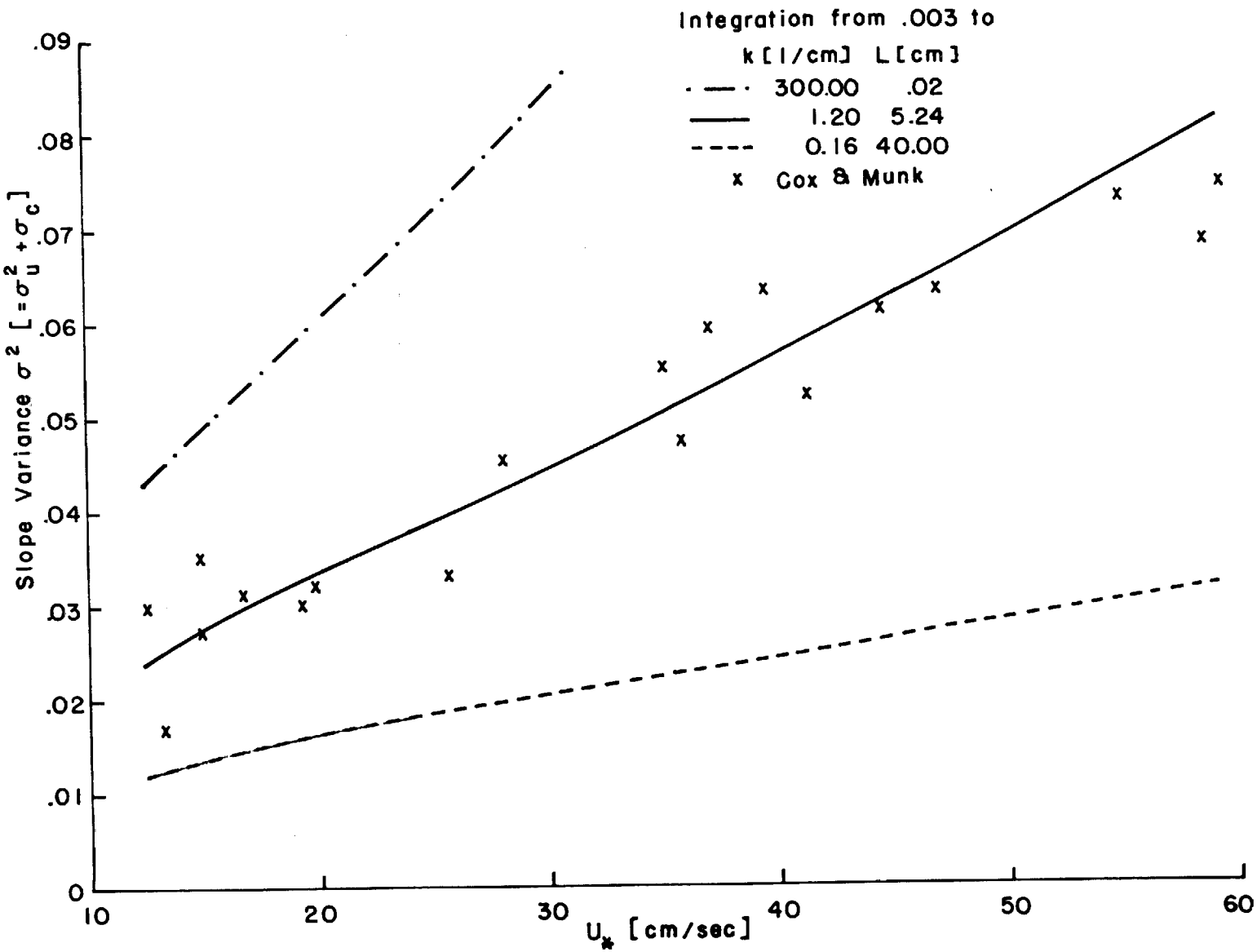

Fig. 9.1 Slope variance versus u_* from the theoretical spectra compared with measurements by Cox and Munk.

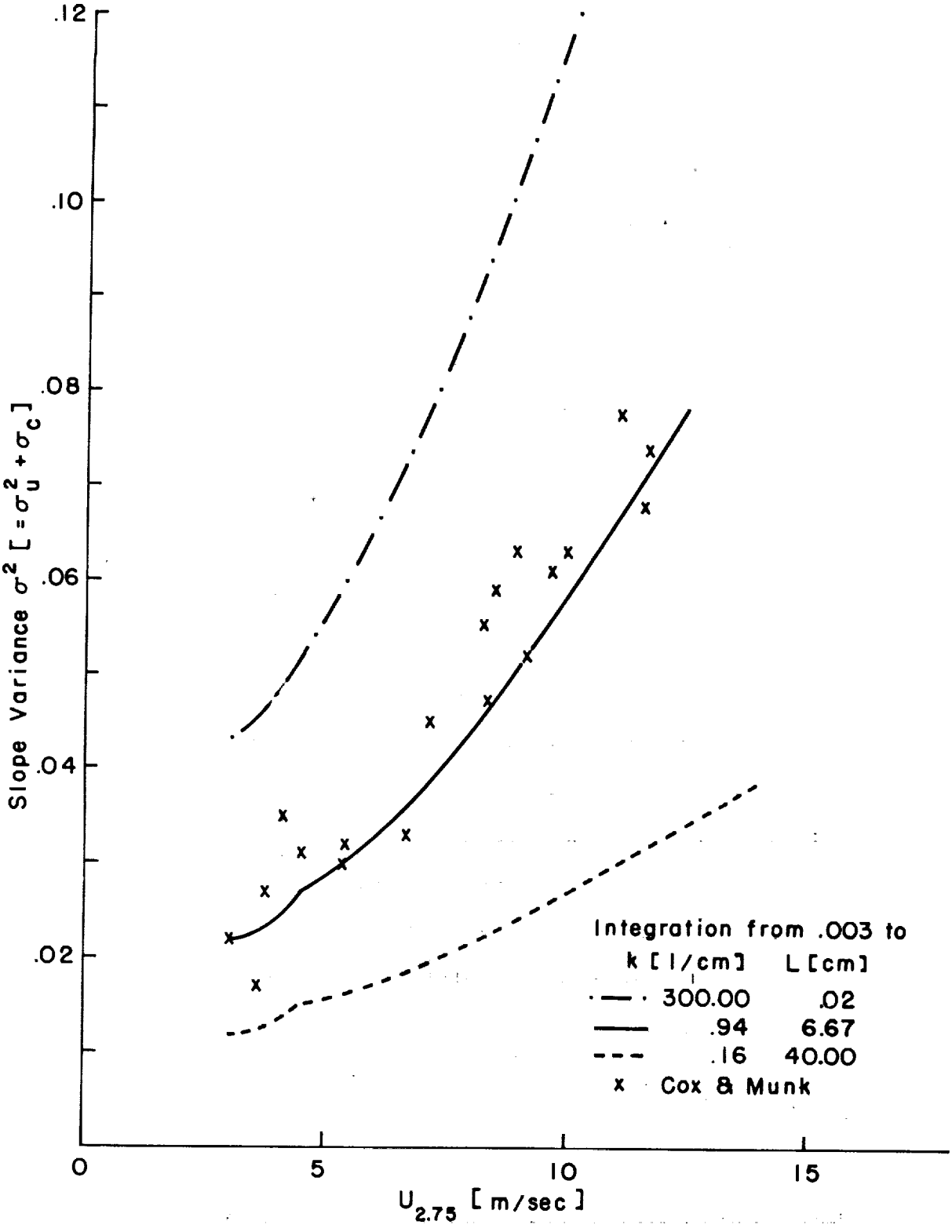

Fig. 9.2 Slope variance versus u_* from the theoretical spectra compared with measurements by Cox and Munk.

u_* and $U_{2.75}$ (one of the heights at which Cox and Munk measured the winds). Integration of the spectrum from $k = .003\ cm^{-1}$ to $k = 300\ cm^{-1}$ (essentially $k = 0$ to ∞) yields variances at least a factor of two high. Cox and Munk (1954) stated that the resolvability of their system was about 40 cm. Integration to this value yields variances a factor of two low. These results illustrate that the optics of their system probably imposed a high frequency filter on the sea surface reflection. The other line in the figures represents a compromise in the high wave number cut-off. Figure 9.2 shows the variance computed by integration only to $k_3 = .9419\ cm^{-1}$ (i.e., no capillary or Cox viscous cut-off waves are involved). This range of integration still does not produce enough slope variance. Figure 9.1 shows that the integration to $k = 1.2\ cm^{-1}$ (which includes some of the capillaries) produces a reasonable fit to the data.

Cox and Munk (1954) cite other investigations that yielded sea surface slopes a factor of two larger than the values that they obtained. The theoretical spectra are producing results of the right order of magnitude for slope, and the two bounds illustrated bracket the Cox and Munk data. It is not inconceivable that the system used by Cox and Munk imposed a low pass filter on the slopes at a wave number of $1.2\ cm^{-1}$, which corresponds to a wavelength of 5.2 cm.

The upwind-downwind slope variance is given by equation (9.17). In the absence of more detailed knowledge of the variation of a_1 and a_2 with wave number, they are assumed to be independent of wave number.

$$\sigma_u^2 = \int_{-\infty}^{\infty}\left[\int_0^{\infty} \ell^2 S(\ell,m)\, d\ell\right] dm = \int_{-\pi/2}^{\pi/2}\left[\int_0^{\infty} k^2 \cos^2\Phi S(k)\, F(k,\Phi) dk\right] d\Phi$$

$$\cong \int_0^{\infty} k^2 S(k)\, dk \int_{-\pi/2}^{\pi/2} \frac{1}{\pi}[1 + a_1 \cos 2\Phi + a_2 \cos 4\Phi]\cos^2\Phi\, d\Phi$$

$$\cong \sigma_s^2 \left[\frac{1}{2} + \frac{a_1}{4}\right] \tag{9.17}$$

Similarly for the crosswind slope variance,

$$\sigma_c^2 = \sigma_s^2\left[\frac{1}{2} - \frac{a_1}{4}\right] \tag{9.18}$$

There is no information on a_2 in these two variances and $\sigma_u^2 + \sigma_c^2 = \sigma_s^2$ as it should.

From Cox and Munk (1954),

$$\sigma_c^2 = 3 \times 10^{-3} + 1.92 \times 10^{-3} U \tag{9.19}$$

and

$$\sigma_u^2 = 3.16 \times 10^{-3} U \tag{9.20}$$

where U is in meters/sec at 41 feet (12.5 meters). It follows that equation (9.21) holds,

$$\frac{\sigma_u^2}{\sigma_c^2} = \frac{3.16U}{3 + 1.92\,U} = \frac{1 + \frac{a_1}{2}}{1 - \frac{a_1}{2}} \tag{9.21}$$

and therefore

$$a_1 = \frac{2.48U - 6}{5.08U + 3} \tag{9.22}$$

If a_2 were zero, a wind at 12.5 meters of 2.42 m/s would produce isotropy. A wind of 3.5 m/s yields an a_1 of 0.112. A wind of 20 m/s yields an a_1 of 0.42. The angular variation becomes more pro-

nounced with increasing wind speed.

Wind Water Tunnel Measurements of Slope and Curvature

Wu (1971) has measured the probability density function for upwind-downwind slopes, including skewness, and functions related to surface curvature distributions in a wind water tunnel. The slope distributions were close to normal, but also showed some non-linear properties unexplainable by our model.

The upwind-downwind slopes measured by Wu (1971) exceeded the upwind-downwind slopes measured by Cox and Munk by about 50%, even without the gravity wave part of the spectrum being present. From Figure 9.8 and equations 9.17 and 9.18 and from Figure 8 of Wu, the total slope would be about 0.06 at $U_* \cong 27$ and 0.114 at $U_* \cong 40$. These values would plot favorably on Figure 9.1 in terms of the total slope variance predicted by the spectra of this theory.

Wu (1971) also found that as the free stream wind speed, U_o, increased from about 2 to 3 m/s, the average radius of curvature decreased from 4 to about 0.8 cm. For U_o greater than 3 m/s, the average radius of curvature decreased slowly and linearly with wind speed. The curvature spectra in Figure 8.6 have this property.

Sea return data from the Manned Spacecraft Center Program

A study by Bradley (1971) has analyzed the results of sea return measurements for a vertically polarized fan beam scatterometer at 13.3 GHz. It was not possible to obtain absolute values of $\sigma^\circ_{vv}(\theta)$ but

$$10 \log_{10} \frac{\sigma^\circ_{vv}(35^\circ)}{\sigma^\circ_{vv}(10^\circ)},$$

which is called a normalized scattering cross section, was obtained and tabulated for Missions 119 and 156. The results of Bradley (1971) for these two missions were also given by Pierson and Moore (1972) and interpreted in another context.

The measurements of interest here were made at a radar wavelength of 2.25 cm at an angle off the vertical of 35°. This corresponds to a capillary wavelength of 1.96 cm, or a wave number of 3.2 cm^{-1}. This water wavelength is near the center of the capillary band and the radar backscatter should be describable by equations (9.11), (9.12) and (9.13).

For upwind and crosswind conditions the results of Bradley at 35° can be summarized by equations (9.23) and (9.24) with U in knots at 19.5 meters.

$$10 \log_{10}[\sigma^\circ_{vv}(35^\circ)/\sigma^\circ_{vv}(10^\circ)]_u = -34.42 + 14.93 \log_{10} U \qquad (9.23)$$

$$10 \log_{10}[\sigma^\circ_{vv}/35^\circ)/\sigma^\circ_{vv}(10^\circ)]_c = -35.51 + 12.62 \log_{10} U \qquad (9.24)$$

From equations (9.12) and (9.13) and equations (9.23) and (9.24),

$$\frac{\sigma^\circ_{35^\circ u}/\sigma^\circ_{10^\circ u}}{\sigma^\circ_{35^\circ c}/\sigma^\circ_{10^\circ c}} \cong \frac{\sigma^\circ_{35^\circ u}}{\sigma^\circ_{35^\circ c}} = \frac{1 + a_1 + a_2}{1 - a_1 + a_2} = \frac{10^{-3.442}}{10^{-3.551}} \frac{U^{1.493}}{U^{1.262}} \qquad (9.25)$$

which reduces to

$$\frac{1 + a_1 + a_2}{1 - a_1 + a_2} = 1.28U^{0.23} \tag{9.26}$$

and a_1 is given by

$$a_1 = (1 + a_2)\frac{1.28U^{0.23} - 1}{1.28U^{0.23} + 1} \tag{9.27}$$

From equation (9.12),

$$10 \log_{10} \frac{\sigma^\circ_{vv}(35^\circ)_u}{\sigma^\circ_{vv}(10^\circ)_u} = 10 \log_{10}\left[\frac{aD(u_*)}{4}|G(\varepsilon, \theta)|^2 \cdot \cot^4\theta[1 + a_1 + a_2]\right]$$
$$- 10 \log_{10} \sigma^\circ_{vv}(10^\circ)_u \tag{9.28}$$

The left-hand side of equation (9.28) represents the values of σ°_{vv} tabulated by Bradley (1971). The right-hand side is the sum of a number of logarithms. Of these, a, $|G(\varepsilon, \theta)|^2 (\cot\theta)^4$ are known, and $\sigma^\circ_{vv}(10^\circ)$ is believed to be nearly a constant but is not known for these measurements. Equation (9.28) can be rewritten as equation (9.29).

$$10 \log_{10} \frac{\sigma^\circ_{vv}(35^\circ)_u}{\sigma^\circ_{vv}(10^\circ)_u} = K + 10 \log_{10} D(u_*)(1 + a_1 + a_2) \tag{9.29}$$

The values tabulated by Bradley should differ from

$$10 \log_{10} D(u_*)[1 + a_1 + a_2]$$

only by some unknown constant. It is tempting to use equations (9.22) and (9.27) to solve for both a_1 and a_2. However, since the equations apply to different ranges, and since the true situation is undoubtedly quite complicated, it will be assumed that a_2 is zero.

Table 9.1 shows how this unknown constant was determined and how $D^*(u_*)[1 + a_1]$ and $D^*(u_*)$ were calculated. A conversion from knots

Table 9.1. Results of Bradley and other supplemental values to yield $D^*(u_*) \cdot (1+a_1)$ and $D^*(u_*)$ as estimated from radar sea return data.†

Set	Wind speed (knots)	Wind speed (m/s)	u_*	Normalized scattering cross section	Normalized cross section +24.21 db	$D^*(u_*) \cdot (1+a_1)$	$1+a_1$	$D^*(u_*)$	$D^*(u_*)$ assuming $1+a_1 = 1.414$
1	6	3.08	10.9	-23.17	1.04	1.2706	1.298	0.98	0.338
2	6	3.08	10.9	-21.23	2.98	1.986	1.298	1.53	1.40
3	10	5.14	16.7	-20.02	4.19	2.624	1.372	1.92	1.85
4	10	5.14	16.7	-21.04	3.17	2.075	1.372	1.51	1.47
5	12	6.95	22.5	-18.02	6.19	4.16	1.386	3.01	2.84
6	15	8.7	29.9	-16.65	7.56	5.70	1.410	4.04	4.04
7	15	8.7	29.9	-17.47	6.74	4.72	1.410	3.34	3.34
8	16	9.3	32.7	-16.25	7.96	6.25	1.414	4.42	4.42
9	16	9.3	32.7	-15.01	9.20	8.32	1.414	5.87	5.87
10	16	9.3	32.7	-16.88	7.33	5.41	1.414	3.82	3.82
11	16	9.3	32.7	-15.50	8.71	7.43	1.414	5.25	5.25
12	17	9.85	35.4	-15.70	8.51	7.10	1.415	5.00	5.00
13	17	9.85	35.4	-16.85	7.16	5.20	1.415	3.67	3.67
14	22	11.3	42.8	-13.67	10.54	11.325	1.444	7.85	8.00
15	22	11.3	42.8	-14.97	9.24	8.39	1.444	5.80	5.93
16	22	11.3	42.8	-15.69	8.52	7.11	1.444	4.93	5.00
17	22	11.3	42.8	-15.52	8.69	7.41	1.444	5.14	5.22
18	31	15.8	67.2	-11.23	12.98	19.86	1.476	13.45	14.00
19	32	16.5	71.1	-10.96	13.29	21.33	1.477	14.45	14.90
20	33	17.0	74.0	-12.15	12.06	16.07	1.482	10.82	11.35

†The cross section values are in db.

to meters per second is shown in the second column of the table. The value of u_* from a neutral atmosphere is shown in the third column. The normalized values given by Bradley are shown in the fourth column. The antilogs of the four values tabulated for 16 knots were found to be 0.0237, 0.0316, 0.0204 and 0.0282. These average to the value 0.026 and $D^*(u_*)$ from Figure 5.6 or equation (2.12) is 4.85 for this wind speed at 19.5 meters and $1+a_1$ equals 1.414. Therefore $0.026x = 4.84\ (1.414)$ and $x = 187\ (1.414)$ for the unknown constants (as far as these measurements are concerned) in equation (9.29). The addition of 24.21 db to Bradley's values ought to produce a number equal to $10 \log_{10} D^*(u_*)(1 + a_1)$. This value is shown in the fifth column and the appropriate antilog is tabulated in the sixth column.

The next column shows the value of $(1 + a_1)$ calculated from equation (9.26) with a_2 set equal to zero. The next but last column shows the value of $D^*(u_*)$ obtained by dividing $D^*(u_*)(1 + a_1)$ by $(1 + a_1)$. The last column shows the results of assuming that a_1 is a constant equal to 0.414.

Sixteen of these twenty values of $D^*(u_*)$ obtained in this way, with the correction for variable a_1, where the asterisk designated that it was calculated from sea return data and not wave data, are plotted on Figure 5.6 as given in the section on the capillary portion of the spectrum. The lowest four values do not fit on the scale used, and the ones for 6 knots, or 3.08 m/s, would not be expected to do so.

The points for 9.3 m/s ought, of course, to straddle the curve for $D^*(u_*)$ because these points were used to determine the unknown constant. The interesting feature of this calculation, however, is that

these calculated values of $D^*(u_*)$ also fit the $D(u_*)$ curve at 11.3 and 15.8 to 17 m/s about as well as the values of $D(u_*)$ found from measurements of the capillary spectrum in wind-water tunnels by Toba and Sutherland.

$D^*(u_*)$ is also plotted against u_* in Figure 5.2. Some values are not shown because the points are too crowded together on this scale. The points for u_* between 10 and 20 cm/sec seem to be lower than the cluster of seven NYU values and $D^*(u_*)$ obtained from the radar data is lower than the values given by the defining equation for $D(u_*)$. This discrepancy will be explained on the basis of the behavior of a_2 to be described later.

The distance covered by the aircraft in a typical data run for these missions was more than 10 km, or 10^4 meters, compared to typical wind water tunnel fetches of 10 meters. If the values of $D^*(u_*)$ given in Table 9.1 were plotted on Figure 5.3, the figure would have to be extended at least 1.5 orders of magnitude to the left and the points would form a separate isolated pattern paralleling the wind tunnel points over a completely different range of $(u_*^2/gF)^{\frac{1}{2}}$. This strongly suggests that capillary waves do not know the difference between a fetch of 10 meters and a fetch of 10 kilometers, or more.

This result lends support to the argument that capillary spectra on the open ocean are quite similar to those measured in wind water tunnels and provides an important link between laboratory and open ocean measurements. It is unfortunate that a primary calibration for σ°_{vv} was not possible in the MSC program. However, the agreement, once the data are fitted at 16 knots, is striking. The alternate hypothesis that $D(u_*)$ on the open ocean differs by say, a factor of ten from $D(u_*)$ in wind water

tunnels leads to great logical inconsistencies.

It should be noted that $U_{19.5}$ is not linearly related to u_* so that the curvature in the graph for $D(u_*)$ in Figure 5.6 need not necessarily show that

$$\sigma^\circ \sim (U_{19.5})^{1.49} \tag{9.30}$$

does not hold, as found by Bradley (1971). The range from 7, or 8, m/s to 18 m/s can be fitted to a $U^{1.49}$ power law. The low values for 6 and 10 knots in Table 9.1 , which may be in part due to going below the critical speed of 3.5 m/s, make the data fit this exponential law approximately over its full range.

Spectra deduced from radar sea return

In this section, an attempt is made to relate wave number spectra as deduced by Valenzuela, Laing and Daley (1971) to the preceding results. Radar sea return data were used to calculate wave spectra by means of the assumption that σ°_{vv} (the normalized radar cross section) is given by Bragg scattering theory. Points were obtained for the wave spectra (in units of cm^4) for a range of more than 10^7 and for a range of 10^2 in wave number by applying the theory to four different radar frequencies and a variety of depression angles. The values that were obtained correspond to $S(\ell,0)$ for upwind down wind conditions for values of ℓ that correspond to $2k_o \sin\theta$ when k_o is the wave number of one of the four different radars and $\sin\theta$ is the angle off the vertical, which was varied between 30° and 60°.

For a set of observations for which the wind (probably at 19.5 meters) varied from a maximum of 23 to 24 m/s to a minimum of 2.5 m/s, $W(\ell, 0)$ was calculated from equation (9.31).

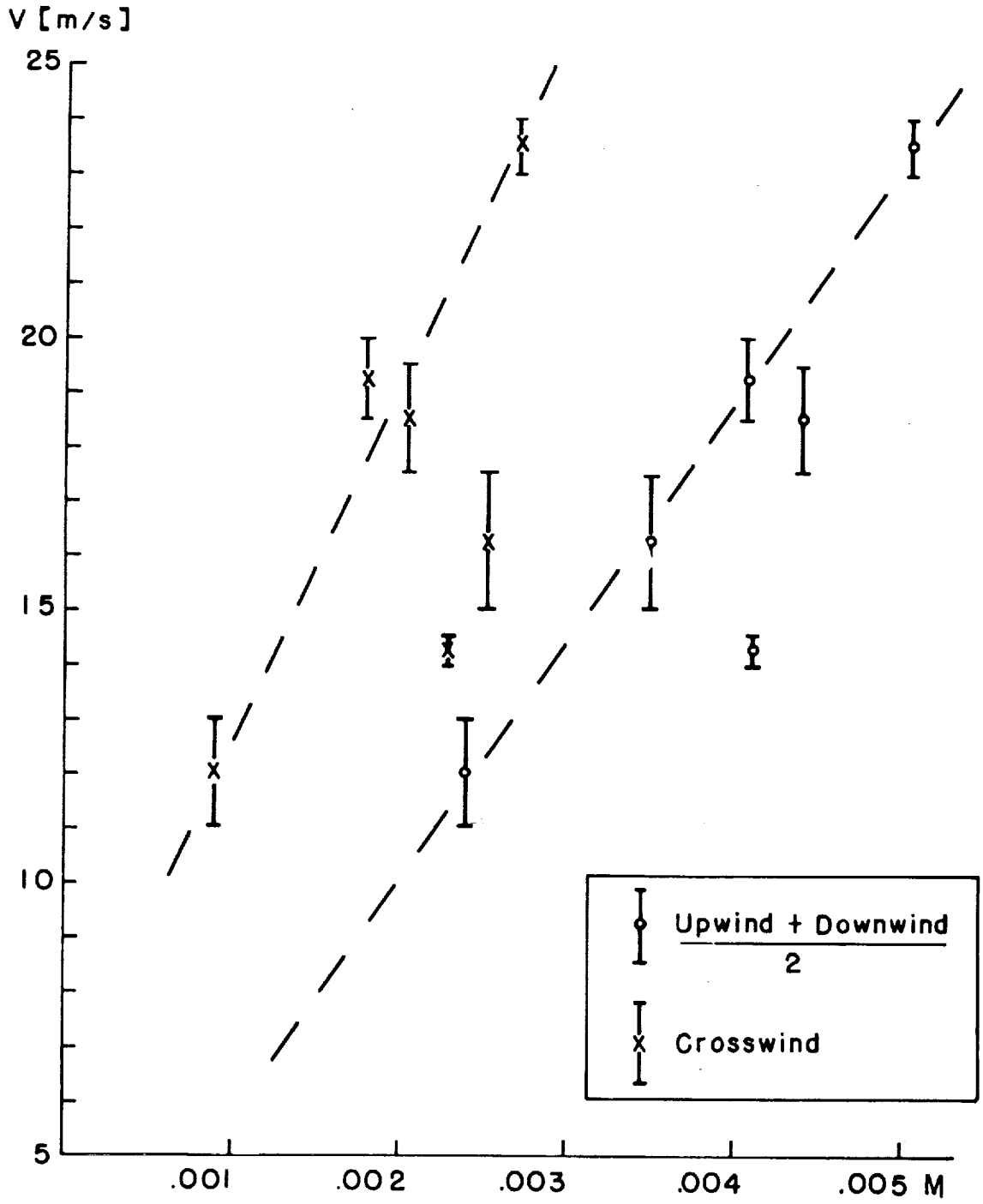

Fig. 9.3 Values of M as a function of V.

$$a_1 = \frac{1}{3} \tag{9.37}$$

Equation (9.8), for example, becomes equation (9.38).

$$S_4(\ell, 0) = \frac{a}{2} \frac{4}{3\pi} \frac{D(u_*)}{\ell^4} \tag{9.38}$$

Figure 9.4 shows $S(\ell, 0)$ plotted versus ℓ on a db scale (or equivalently a double log scale) for $U_{19.5}$ equal to 3.5 m/s, 12 m/s, and 23.5 m/s. The lowest curve represents the spectrum for the minimum wind speed for which the capillary waves have a substantial amplitude. To the left of the $\ell = 0.35$ line, the spectrum shows the saturation value of the Phillips equilibrium range for the gravity wave range. There is no Kitaigorodskii range.

The middle curve is the curve for a wind of 12 m/s to correspond to the data for a wind between 11 and 13 m/s. The Leykin-Rosenberg range continues into the Kitaigorodskii range without much change in slope. The Kitaigorodskii range will intersect the line with a slope of -4, and labeled 1.71×10^{-3} (ℓ^{-4}), at a point just to the left of -12 db.

The upper curve is for a wind of 23.5 m/s (for the range from 23 to 24 m/s). The three different slopes for $S_2(\ell)$, $S_3(\ell)$, and $S_4(\ell)$ are clearly evident.

The data from Valenzuela et al. (1971), as given in Figure 2 of that paper, do not fit these curves. The data appear to be about 11 db too low, a factor of about 4π, after reduction by 3 db to account for the difference in definition. A total discrepancy of about 11 db would yield a factor of 12 so that the waves over the range of definition would be only 29% as high as calculated from wind-water tunnel measurements.

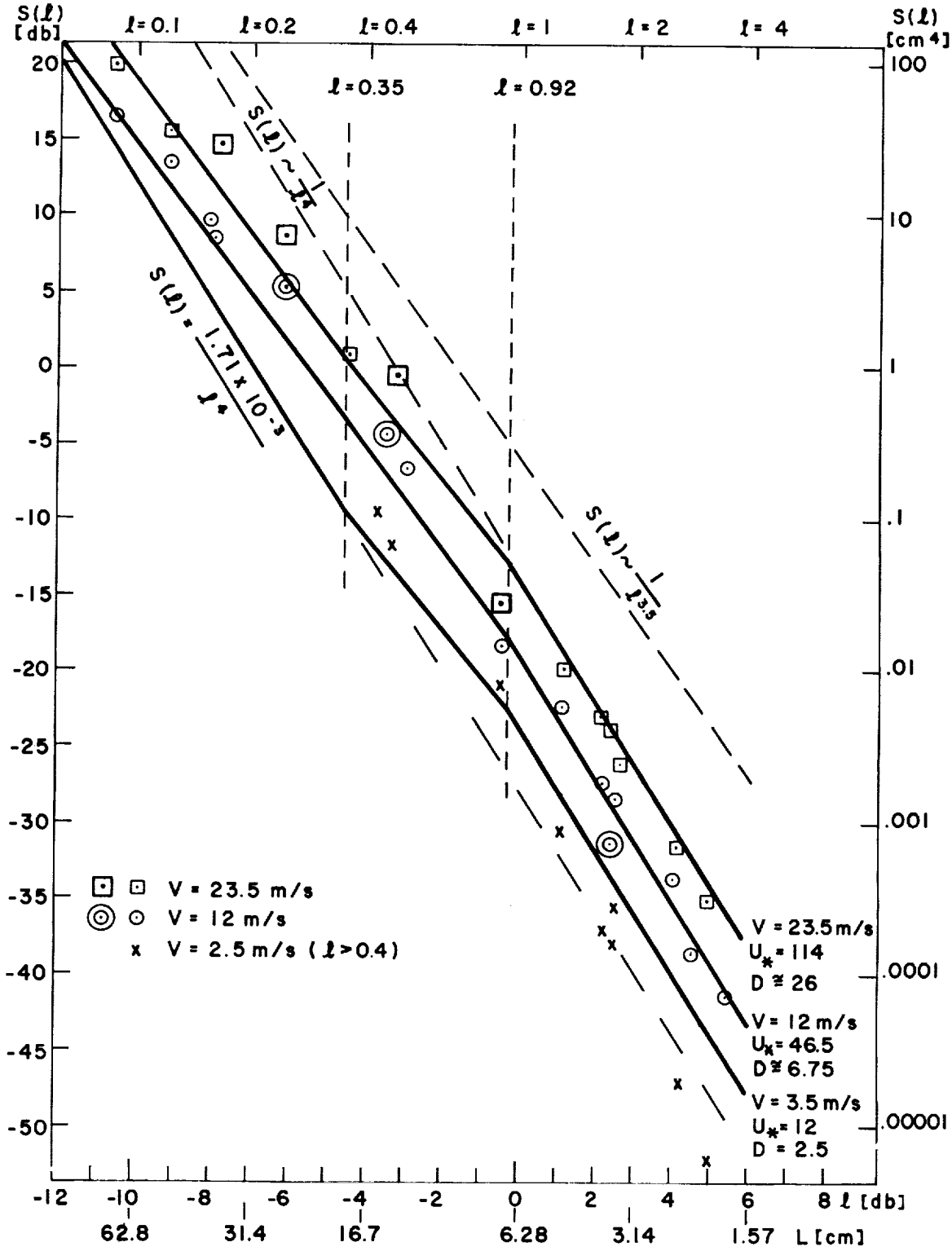

Fig. 9.4 $S(\ell, 0)$ versus ℓ in db and on logarithmic scales for winds of 3.5, 12, and 23.5 m/s compared with data from Valenzuela et al. (1971).

The 11 db discrepancy does not seem to be explainable on the basis of any inconsistencies in the basic definitions of either the wave spectrum or the normalized radar cross section. Guinard et al. (1971) have given details on how the radar data were processed and definition of σ° given by their equation 3 is the appropriate one for the calculation. Some other definitions do not include the 4π.

The 11 db discrepancy appears to be present in the originally reported values of σ°_{vv} (Daley et al., 1970). After adding +3.2 db to account for differences between median and average values and for one-way versus two-way beam widths as Valenzuela et al. (1971) did also,* the tabulated values at $\theta = 60^\circ$ are about 11 db lower than the values measured by Wright in a wind-water tunnel (Table 9.3) for nearly the same radar frequency. $D(u_*)[1 + a_1]$ calculated from equation (9.39) (with 19.42 replacing 20.32) is 0.85 for 11 m/s and 1.91 for 23.5 m/s.

However, once 8 db are added to the values plotted in Figure 2 of Valenzuela et al. (1971) (3 db are already there), the result is shown by the coded points on figure 9.4. The small squares and the large squares are for the 23 to 24 m/s winds; the circles and double circles are for the 11 to 13 m/s winds, and the x's are for the 2.5 m/s winds. Since the M values for the 17.5 to 19.5 m/s and 18.5 to 20 m/s cases lie between the values for the two cases used, similar results would be expected for these measurements also.

Of the thirteen points for the 23 to 24 m/s winds, nine are quite close to the theoretical curve. The six points in the capillary range fit an ℓ^{-4} line very well. Three of the remaining points fall close to the Kitaigorodskii range. The sharp break in slope from one side of the line $\ell = 0.92$ to the other is quite evident.

*Personal communication from Dr. J. W. Wright.

Of the fifteen point for the 11 to 13 m/s winds, twelve points come close to the theoretical curve. The capillary range is clearly one with an ℓ^{-4} slope. Four points come close to the Kitaigorodskii range near $\ell = 0.1$.

The large squares and double circles do not come close to the theoretical curves. For $\ell \cong 0.3$ and 0.5, the poorly fitting points are paired and they are the right distance apart so that a shift of 3 db would put them on the correct line.

The x's are for a wind of 2.5 m/s. They fall below the curve for 3.5 m/s. They should be expected to be even less than shown. A few isolated patches of wind above 3.5 m/s could produce the observed results for the points plotted. The x's in the original paper for low wave numbers are up above the curve for a wind of 12 m/s and do not agree with any particular theory.

It appears that the values of the slope found by Valenzuela et al. (1971) are fictitious combinations of values composited out of the ranges given by equations (9.6), (9.7) and (9.8). Apart from a discrepancy of 11 db, the data fit the theory given in this paper quite well since 75% of the points for winds of 12 and 23.5 m/s are close to the theoretical curves. The data also show clearly the -4 slope at the high wave number end and the -3.5 slope at the low wave number end.

In view of these results, the other results given in this study, the other conclusions of Valenzuela et al. are very much to be questioned. The conclusion that for light winds, σ° is proportional to $e^{-c/v}$, based on Pierson and Moskowitz (1964), is doubtful since the exponential term in Pierson and Moskowitz only affects very long waves. The behavior with σ° proportional to $U^{2\nu}$ and 2ν given by 0.455 for X band (8.9 GHz)

and 0.619 for C band (4.455 GHz) is also much too low because these bands are in the capillary and Leykin-Rosenberg ranges, which are strongly wind speed dependent. If Bragg scattering provides a valid sea return theory for angles off the vertical of 20° or 30°, or more, than one would expect, for radar wave numbers greater than about one, that the wind speed dependence would be described by Fig. 5.6.

Radar backscattering data obtained in a wind water tunnel

Dr. J.W. Wright has made some absolute measurements of σ°_{vv} as a function of wind speed for a value of θ equal to 60° and a radar frequency of 9.375 GHz in a wind-water tunnel at a fetch of 39 feet. The results were given in preliminary form, as provided by Dr. Wright in Pierson and Moore (1972). They are subject to modifications as the study by Dr. Wright continues, but these preliminary results seem to be explainable in an absolute quantitative sense by the capillary portion of the spectrum proposed by equations (2.8) and (9.8).

The frequency of 9.375 GHz and the angle of 60° yield the result that $k = 2k_o \sin 60° = 3.40$ and the water wavelength involved is 1.85 cm. This wave number is in the capillary range defined by equation (2.8) and shown in Figure 8.2.

For this frequency, $\varepsilon = 54 - i\,38.5$, $|G(\varepsilon, \theta)|^2 = 20.32$, and $(\cot \theta)^4$ at 60° equals 1/9. Since the wave number is fixed, a_1 and a_2 in equation (9.12) can only be functions of u_*.

Equation (9.12) therefore becomes equation (9.39).

$$\sigma^{\circ}_{vv}(u_*) = \frac{a}{36}\,(20.32)\,D(u_*)[1 + a_1(u_*) + a_2(u_*)] \tag{9.39}$$

The only remaining problem is to relate the free stream wind speeds (converted from feet/min to meters/sec), as measured in the wind-water tunnel to u_* values. Values of the free stream wind speed (U_∞) reported by Toba and Sutherland (1967) and measured at N. Y. U. for various fetches are given along with the resulting values of u_* in Table 9.2. If it is assumed that similar wind profiles would be observed in Wright's facility the values of u_* can be extracted from these data.

A plot of u_* versus U_∞ using these values has considerable scatter. The extrapolation of the wind profile toward the surface and the estimate of its slope to find the stress at the surface is a source of this scatter. Quite a bit of the scatter of $D(u_*)$ plotted against u_* in the section on the capillary wave spectrum is probably attributable to this scatter.

To determine the values of u_* to use with Wright's data, u_* was plotted against U_∞ from Table 9.2. A best fit curve and curves for upper and lower bounds on the scatter of points were drawn. The values of U_∞ from Wright were entered on the graph and a lower bound, best fit, and upper bound value for u_* was determined for each U_∞.

The result is shown in Table 9.3. The first column is U_∞ and the next three columns are the lower bound, best fit and upper bound values of u_*. The fourth column shows the measured values of σ°_{VV} obtained by Wright.

These values are plotted in Figure 9.5. The best fit line is the solid line and the two bounds are the dashed lines connecting the x's. The break in the curve does not come at $u_* = 12$; it could range from $u_* = 5$ to $u_* = 11$ with the best fit corresponding to $u_* = 8$.

Table 9.2. Values of U_∞ (m/s) (the free stream wind speed), fetch and u_* (cm/s) from three wind-water tunnels.

Source	Fetch (ft)	U_∞	u_*
NYU	20.7	1.46	5.9
"	20.7	2.74	12.3
"	20.7	4.15	18.9
Toba	32.8	5.1	33.5
"	44.6	5.1	36.7
"	32.8	6.1	39.4
"	44.6	6.1	38.9
"	32.8	7.5	47.8
"	44.6	7.5	48.9
"	32.8	8.7	54.8
"	44.6	8.7	61.5
"	32.8	9.7	64.8
"	44.6	9.7	73.7
"	32.8	10.8	81.7
"	44.6	10.8	92.6
"	32.8	11.2	113.0
"	44.6	11.2	102.0
"	32.8	12.1	112.0
"	44.6	12.1	114.0
Sutherland	28.8	6.74	56.1
"	43.8	7.10	56.7
"	28.8	9.64	80.2
"	43.8	10.1	74.1
"	28.8	12.1	102.4
"	43.8	12.65	107.3
"	28.8	15.36	177.0
"	19.1	15.27	166.1

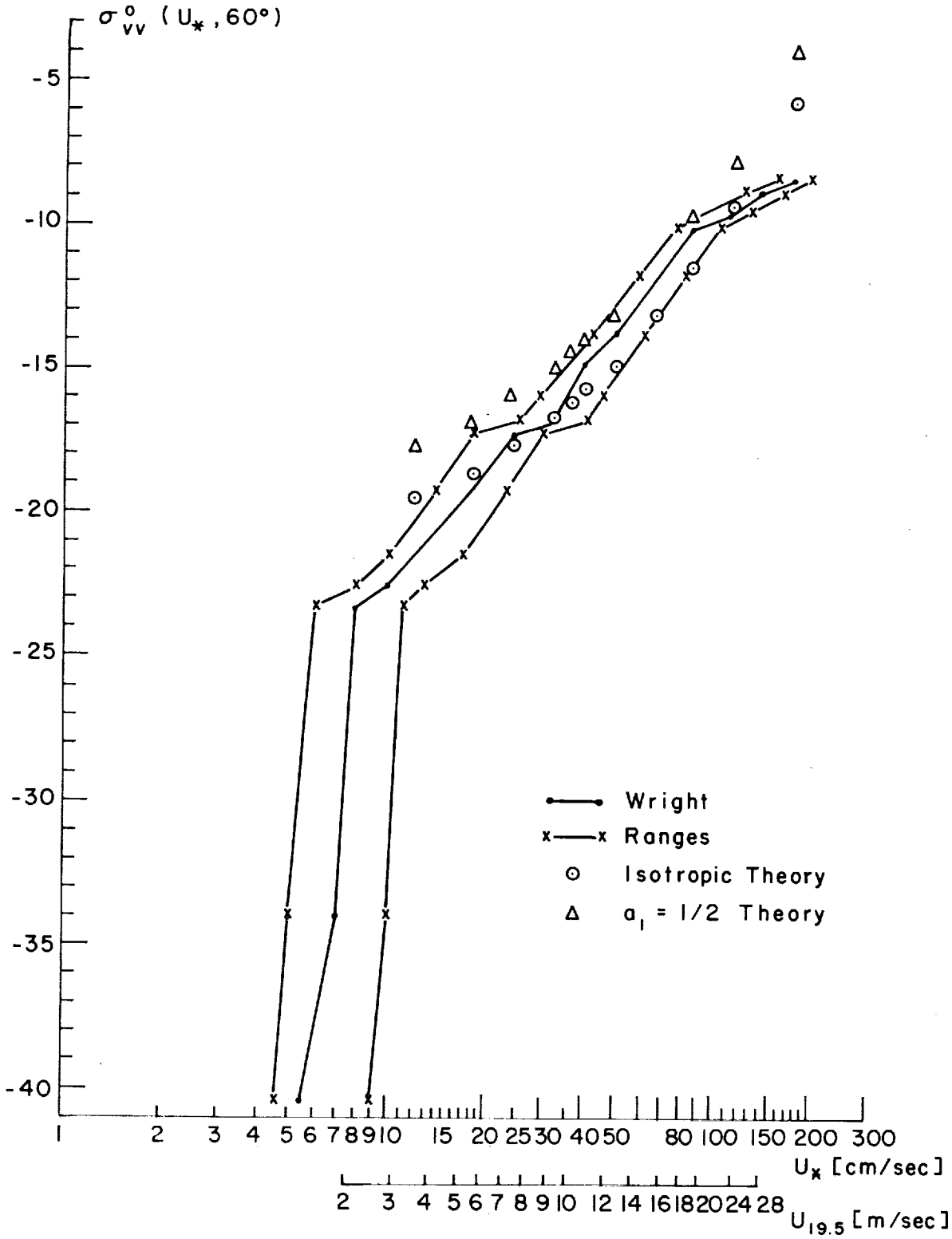

Fig. 9.5 $\sigma^{\circ}_{vv}(u_*, 60°)$ obtained by Wright as a function of u_* and various theoretical curves (see text).

Table 9.3. Analysis of scattering cross-section data obtained by J. W. Wright.

Free stream wind speed u_∞(m/s)	Range of u_*			$\sigma^\circ_{vv}(60°)$ (Wright)	Isotropic theory Best u_*	$a_1 = \frac{1}{2}$ $a_2 = 0$	u_* dependent a_1 and a_2
	Lower	Best	Upper				
1.63	4.5	5.5	9	-40.6			
1.753	5	7	10	-33.9			
2.03	6	8	11	-23.3			
2.44	8	10	13	-22.6			
2.95	10	12	17	-21.5	-19.42	-17.66	-21.06
3.76	14	18	23	-19.2	-18.63	-16.87	-19.43
4.57	18	24	30	-17.3	-17.66	-15.90	-17.77
5.59	25	32	41	-16.9	-16.63	-14.87	-16.45
6.10	29	36	46	-15.9	-16.20	-14.44	-15.92
6.60	33	40	50	-14.7	-15.80	-14.04	-15.42
7.62	42	50	61	-13.8	-14.80	-13.04	-14.19
9.14	58	67	81	-11.7	-13.09	-11.33	-12.11
10.67	75	86	102	-10.1	-11.36	- 9.60	-10.0
12.19	98	112	128	- 9.4	- 9.42	- 7.66	
13.72	123	140	158	- 8.9	- 7.58	- 5.82	
15.49	158	175	196	- 8.4	- 5.69	- 3.93	
16.76				- 8.1			
18.18				- 7.8			
19.05				- 7.7			

(The last four columns are in db.)

Along with the previously mentioned results of Cox (1958), this is an indication that the critical u_* may be somewhat smaller than 12. The critical value depends on the stability of the air in the tunnel and other factors such as the amount of artificial turbulence in the air flow. Perhaps the results of previous sections could be extended to u_* values as low as 9 cm/sec and still give useful results.

As given in the sixth column of Table 9.3, the circles on Figure 9.4 show the result of evaluating equation (9.39) for a_1 and a_2 equal to zero using the best estimate of u_*. Bragg scattering theory would yield these results if the wave number spectrum were isotropic over a half-plane in ℓ-m space.

The triangles on Figure 9.4 show the results of evaluating equation (9.39) for $a_1 = \frac{1}{2}$ and $a_2 = 0$. These values are tabulated in the seventh column of Table 9.3.

The isotropic theoretical values fit the data obtained by Wright near $u_* = 25$ and 30 cm/sec. From u_* equal to 30 to u_* equal to 80, the anisotropic and isotropic theoretical points bracket the observed values and the observed values increase from values near the isotropic values to values near the $a_1 = \frac{1}{2}$ values over this range.

Above $u_* = 80$, the curves diverge. It is understood that there were breaking waves in the experiment. Since $u_* = 80$ corresponds to winds of 18 m/s ($\sim$ 36 knots) there may be other important effects over the ocean that would modify sea return results. For such high winds, passive microwave techniques show promise of being a useful indicator of wind speed. It should be noted that the results of Bradley (1972) extend to this range also.

Between $u_* = 12$ and $u_* = 25$, the measured values fall below the values computed for an isotropic spectrum. Either the values of $D(u_*)$ are too high, or the spectrum is anisotropic with an angular variation such that the value of $S(\ell, 0)$ in the upwind-downwind direction is less than that which would be predicted for an isotropic spectrum.

The second alternative is to be preferred both from the resonance theory of wave generation of Phillips (1957) which predicts a bimodal distribution of spectral values for light winds and from photographs such as Figures 5.8, 5.9, and 5.10 that clearly show dominant trains of capillary waves traveling at angles to the wind direction. This same phenomenon has been documented many times in the scientific literature.

The function $F(k, \Phi; u_*)$, defined previously, depends only on u_* and Φ since k is fixed. It is repeated here as equation (9.40).

$$F(k, \Phi; u_*) = \frac{1}{\pi} [1 + a_1(u_*) \cos 2\Phi + a_2(u_*) \cos 4\Phi] \tag{9.40}$$

Since the values of σ°_{vv} from equation (9.39) are only in the upwind-downwind direction, this reduces to equation (9.41). (The π vanished when equation (9.39) was derived.)

$$F(0; u_*) = \frac{1}{\pi} [1 + a_1(u_*) + a_2(u_*)] \tag{9.41}$$

With two free parameters to pick up as a function of u_* it is not at all difficult to obtain a close fit to the measured values of Wright. For example, a_1 and a_2 can be defined by equations (9.42) and (9.43).

$$a_1 = \begin{cases} 0 & 12 < u_* < 25 \\ \left(\frac{u_* - 25}{80 - 25}\right)\frac{1}{3} & 25 \leq u_* < 86 \end{cases} \tag{9.42}$$

$$a_2 = \begin{cases} -\left(\frac{25 - u_*}{25 - 12}\right)0.315 & 12 < u_* < 25 \\ 0 & 25 \leq u_* < 86 \end{cases} \tag{9.43}$$

These wind speed dependent coefficients were used to evaluate equation (9.39) as u_* varied from 12 to 86 and the results are given in the last column of Table 9.3. The theoretical values differ from the measured absolute values by at most 0.7 db and in general by less than 0.4 db.

Figure 9.6 shows the values obtained by Wright connected by a solid line, the values for the isotropic assumption as x's connected by a dashed line, the values for $a_1 = \frac{1}{2}$ and $a_2 = 0$ as x's, and the values computed from equations (9.39), (9.42) and (9.43) as circles. The agreement for the circles is good from $u_* = 12$ to $u_* = 85$, corresponding to winds at 19.5 meters of 3.5 m/s to about 19 m/s.

Figure 9.7 shows $F(k, \Phi; u_*)$ for this particular k as a function of Φ for different values of u_* ranging from 12 to 80. Within an ability to resolve such a complicated function by two harmonics, the curves shown are quite reasonable as a possible variation of $F(k, \Phi; u_*)$. Actually the bimodal peak for low u_* values is probably not at plus and minus $\pi/4$. It is wind speed dependent according to Phillips (1957). Many harmonics would be needed to describe $F(k, \Phi; u_*)$ over an adequate range of u_* and k, even for the relatively simple conditions found in wind-water tunnels.

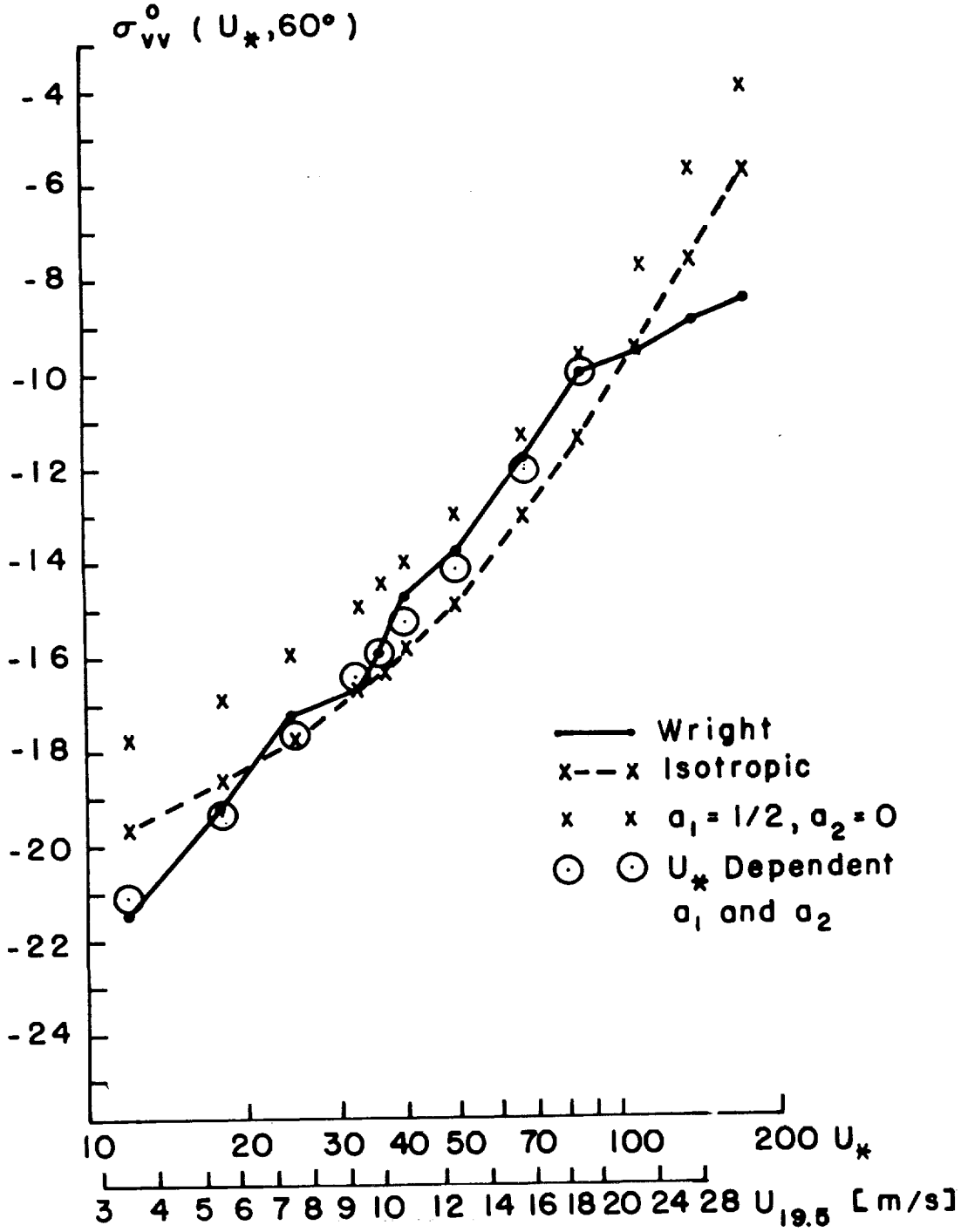

Fig. 9.6 Comparison of theoretical and observed backscattering values.

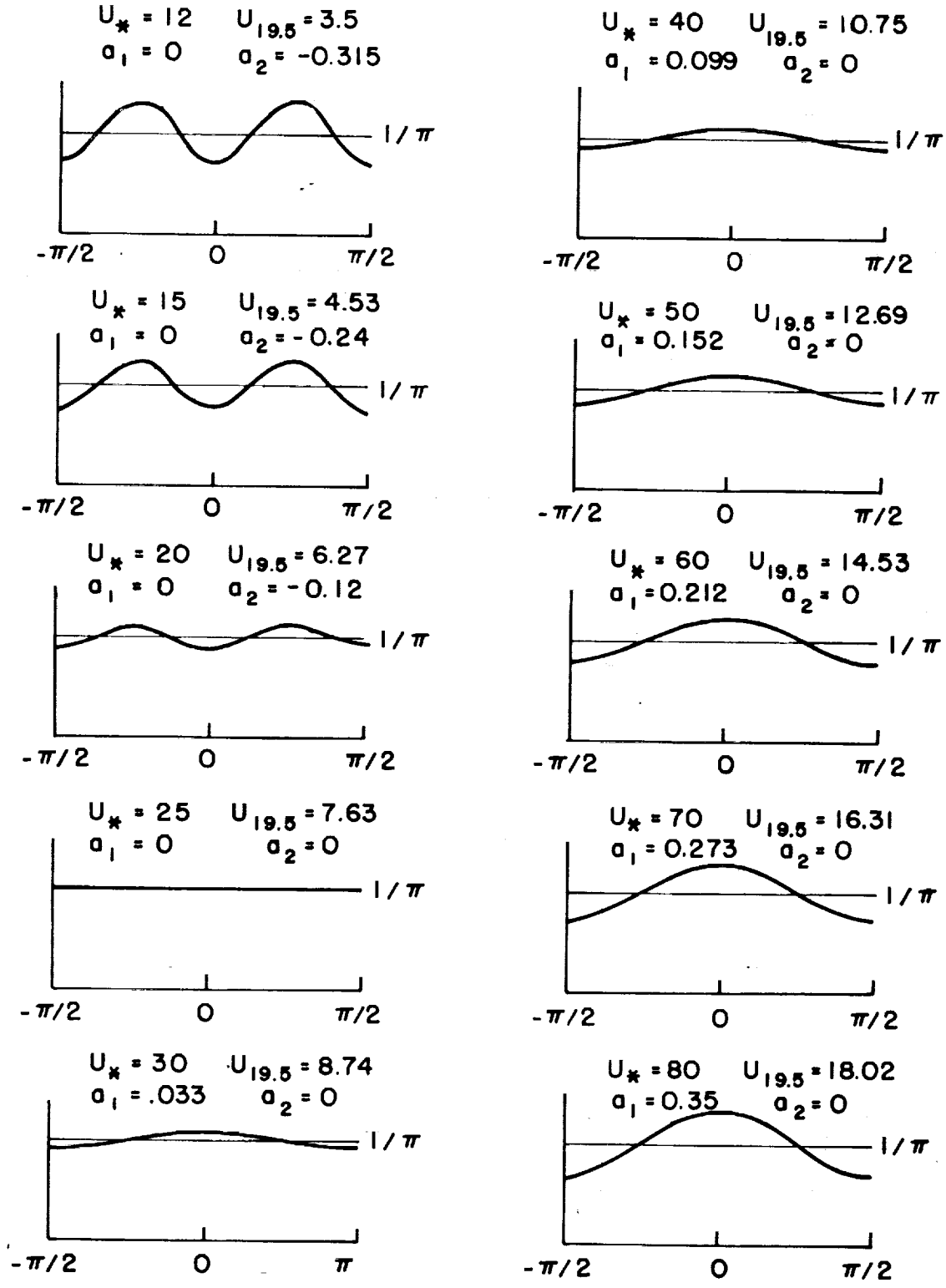

Fig. 9.7 Graphs of $F(k, \Phi, u_*)$ for different u_* and $k = 3.40$.

Measuring $\sigma^{\circ}_{vv}(\theta; u_*, k_o, \Phi)$ by varying Φ in, say, 10° steps over this same range of U_∞ from zero to 90° could provide some extremely valuable results. It is encouraging, however, that reasonable quantitative agreement between a fairly simple theory for radar backscatter and known and reasonably assumed properties of the capillary wave spectrum has been found.

It should also be noted that if a_2 varies over the ocean in roughly the same way that it varies in equation (9.43), the values of $D(u_*)$ would be computed to be too low in the analysis of the results of Bradley (1971). The triangles in Figure 5.2 for low u_* values would then move up closer to the data points obtained by New York University.

Field measurements by Leykin and Rosenberg

Leykin and Rosenberg (1971) determined $F(k, \Phi; u_*)$ for one wind speed corresponding to a value in excess of $u_* = 12$. The wind was 5 m/s at 20 meters, and the water wavelength was 5 cm. $F(2\pi/5, \Phi; 13.4)$ was essentially a constant for $-\frac{\pi}{2} < \Phi < \frac{\pi}{2}$. This is still another indication that the spectrum in nature varies from nearly isotropic at low winds to a peaked form in the wind direction at high winds.

Summary of anisotropic properties

Five different sources have been used to find estimates of the anisotropic properties of the spectrum for high wave numbers. Three were for particular wave numbers as obtained from the results of Bradley, Wright, and Leykin and Rosenberg. The result obtained from Cox and Munk's data probably extends down into the Kitaigorodskii range, and the result obtained from Valenzuela et al. (1971) does extend to that range.

These five results for a_1 are shown in Figure 9.8 in which

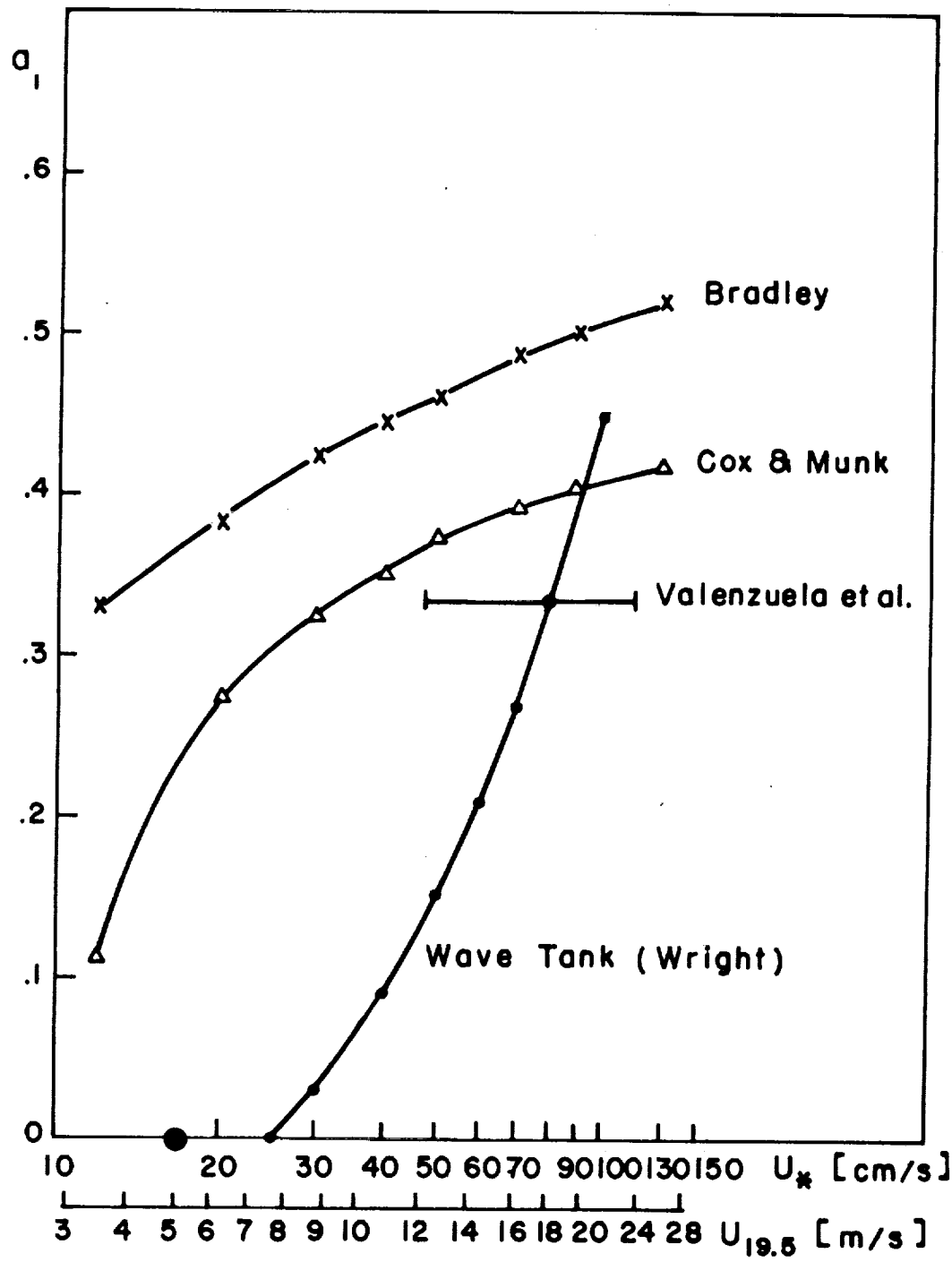

Fig. 9.8 a_1 as a function of u_* from five different sources.

equations (9.22), (9.26) (with $a_2 = 0$), and (9.37) are all referred to a common u_* and to $U_{19.5}$ for a neutral atmosphere, with appropriate changes for different anemometer heights and units. A correction for atmospheric stability effects has not been made for the Cox and Munk result. The dot at $U_{19.5} = 5$ m/s is from Leykin and Rosenberg's result.

The difference between the wave tank result and the open ocean results could be explainable on the basis of the lateral component of the turbulent wind, which would tend to remove the bimodal peak for low winds. For winds of 12 to 20 m/s, or so, a_1 is between 1/3 and 1/2. The ratio $(1 + a_1)/(1 - a_1)$ is between 2 and 3, and thus crosswind radar backscatter values should run 3 db to 4.8 db below upwind-downwind values over this range. This, in fact, appears to be what does happen. The next generation of radars and radar-radiometers should be able to pin down a_1 to a smaller range.

For low winds, the different sources yield quite variable predictions. This variability is probably a function of atmospheric stability and $\sigma_u/\bar{U}$ (see Pierson and Moore, 1972), which can be parameterized in terms of atmospheric turbulence theories.

CONCLUSION

The wave number and frequency spectra of a wind roughened sea have been described and documented. More and better data are needed to improve on these results, in particular with reference to the values of k_2 and k_3. Also other data not available to us should be used to check these various ranges in greater detail, especially with reference to the Kitaigorodskii and Leykin-Rosenberg ranges. Ways to study the shorter waves in wave number space should be developed for open ocean conditions.

The results of this study can be used as a framework for deeper theoretical investigations of the generation and properties of the shorter waves.

Radar backscattering data yield results that agree with Bragg scattering theory applied to the wave number spectra proposed for the high wave number ranges for laboratory backscatter measurements.

An unequivocal agreement between radar backscatter measurements over the ocean and the spectra given in this paper has not been established. If the tabulated results of Daley et al. (1970) are correct, $S_2(k)$, $S_3(k)$, and $S_4(k)$ would have to be a factor of about 12 (or 4π) lower than the values given. Such a reduction would be difficult to reconcile with the substantial overall internal consistency of the proposed spectra and the other data sources that were used. In contrast, the results of Kondo et al. (1973) are higher over the capillary range and provide support for the argument that the capillary spectrum does not decrease with increasing fetch.

Acknowledgements

This research was supported by the Langley NASA AAFE program under contract NAS 1-10090.

We wish to thank the many scientists who provided us with their basic data in original form. They were Dr. C. S. Cox, Mrs. E. B. Dobson, Dr. B. Kinsman, Dr. A. Schooley, Dr. A. J. Sutherland (with the help of Mr. T. R. Mogel), Dr. Yoshiaki Toba, and Dr. J. W. Wright.

We also wish to acknowledge the many other scientists who documented their reports to such an extent that it was possible to use their published results in this research.

The NYU wind-water tunnel data on the capillary spectra were obtained under contract Nonr 285(26), supported by the Electronics Branch of the Office of Naval Research and initiated on 1 April 1956. There were a number of reports on the work completed at that time that were published, but the full data analysis was not published. It is fortunate that the basic data were available from this earlier research and that the data complemented the data made available by Drs. Toba and Sutherland.

REFERENCES

Adamo, L.C., L. Baer, and J.P. Hosmer (1968): Icosohedral-gnomonic projection and grid of the world ocean for wave studies. J. Geophys. Res., 73(16), 5125-5132.

Barnett, T.P. (1970): Wind waves and swell in the North Sea; an international field study. E⊕S Trans. Amer. Geophys. U., 51(7), 544-550 (July).

Bradley, G.A. (1971): Remote sensing of ocean winds using a radar scatterometer. Tech. Report 177-22, The University of Kansas Center for Research. 191 pp. MSC, NASA Contract NAS-9-10261.

Bunting, D.C. (1970): Evaluating forecasts of ocean wave spectra. J. Phys. Res., 75(21), 4131-4143.

Bunting, D.C., and L. Moskowitz (1970): An evaluation of a computerized numerical wave prediction program for the North Atlantic Ocean. TR-209, U.S. Naval Oceanographic Office, Washington, D.C.

Burling, R.W. (1959): The spectrum of waves at short fetches. Deutsch. Hydrogr. Z., 12, (44-64), 96-117.

Cardone, V.J. (1969): Specification of the wind field distribution in the marine boundary layer for wave forecasting. Geophysical Sciences Lab. Report TR-69-1, New York University.

Chang, M.S. (1968): Mass transport in deep water long crested random gravity waves. J. Geophys. Res., 74(6), 1515-1536.

Chia, R.C. (1968): The theory of radar backscatter from the sea. Ph.D. Thesis, The University of Kansas.

Claassen, J.P., and H.S. Fung, R.K. Moore and W.J. Pierson (1972): Radar Sea Return and the Radscat Anemometer. International Conference Record IEEE Pub. 72-CHO 660-1, OCC Newport, R.I., pp 180-185.

Coté, L.J., J.O. Davis, W. Marks, R.J. McGough, E. Mehr, W.J. Pierson, J.F. Ropek, G. Stephenson, and R.C. Vetter (1960): The directional spectrum of a wind generated sea as determined from data obtained by the Stereo Wave Observation Project. Meteor. Papers, 2(6), 88 pp. New York University Press.

Cox, C.S. (1958): Measurements of the slopes of high frequency wind waves. J. Mar. Res., 16, 177-225.

Cox, C.S., and W.H. Munk (1954): Statistics of the sea surface derived from sun glitter. J. Mar. Res., 14(2), 198-277.

Daley, J.C., W.T. Davis, and N.R. Mills (1970): Radar sea return in high sea states. NRL Report 7142, Naval Research Lab., Washington, D.C. 47 pp.

DeLeonibus, P.S., J.F. Boogaard, R.J. Shiel, and B.E. Olson (1973): Observations of wave spectra in the Norwegian Sea with a bow-mounted wave height sensor. J. Geophys. Res. Vol. 78 No. 15.

Dobson, E.B. (1970): Measurements of the fine-scale structure of the sea. J. Geophys. Res., 75(15), 2853-2856.

Ewing, J.A. (1969): Some measurements of the directional wave spectrum. J. Mar. Res., 27, 163.

Guinard, N.W., J.T. Ransome, Jr., and J.C. Daley (1971): Variation of the NRCS of the sea with increasing roughness. J. Geophys. Res., (Oceans and Atmosphere), 76(6), 1525 -1538.

Hasselmann, K. (1962): On the non-linear energy transfer in a gravity wave spectrum. Part 1. J. Fluid Mech., 12, 481-500.

Hasselmann, K. (1963): On the non-linear energy transfer in a gravity wave spectrum. Parts 2. J. Fluid Mech., 15, 275-281. Part 3, Ibid., 15, 385-398.

Hess, G.D., G.M. Hidy, and E.J. Plate (1969): Comparison between wind waves at sea and in the laboratory. J. Mar. Res., 27(2), 216-225.

Hicks, B.L. (1960): The generation of small water waves by the wind 1, Comparison of data from different sources. Coordinated Science Laboratory Report M86, Univ. of Illinois, Urbana, Ill. Jan. 1960.

Jackson, F.C. (1973): A curvature-corrected Kirchoff formulation for radar sea return from the near vertical. NASA CR-11 2263.

Kinsman, B. (1960): Surface waves at short fetches and low wind speeds--a field study. Chesapeake Bay Institute, Tech. Rept. 19, Parts I, II and III. Reference 60-1.

Kinsman, B. (1961): Some evidence of the effect of nonlinearity on the position of the equilibrium range in wind-wave spectra. J. Geophys. Res., 66(8), 2411-2415.

Kinsman, B. (1965): Wind Waves; Their Generation and Propagation on the Ocean Surface. Prentice-Hall, Englewood Cliffs, N.J.

Kitaigorodskii, S.A. (1962): Applications of the theory of similarity to the analysis of wind generated wave motions as a stochastic process. Akad. Nauk, SSSR, Bull. Sci. Geophys , Ser. No. 1, pp. 73-80.

Kondo, J., Y. Fujinawa and G. Naito (1973): High Frequency Components of Ocean Waves and Their Relation to the Aerodynamic Roughness. J. Phys. Oceanog., Vol. 3 No. 2, pp. 197-202.

Leykin, I.A. and A.D. Rosenberg (1970): Study of the high frequency portion of the spectra of sea waves. Izv. AN SSSR, Fisiki Atmosfery i okeana, 6(12), 791-794.

Leykin, I.A. and A.D. Rosenberg (1971): Measurement of the angular spectra of the high frequency portion of swell. Izv. AN SSSR. Fisiki Atmosfery i okeani, 7(1), 102-106. English Translation, pp. 72-75.

Longuet-Higgins, M.S. (1962): The statistical geometry of random seas, pp. 105-143 of Hydrodynamic Instability. Proc. of Symposia in Applied Mathematics, vol. 13, U.S.A. :American Mathematical Society.

Longuet-Higgins, M.S., D.E. Cartwright, and N.D. Smith (1963): Observations of the directional spectrum of sea waves using the motions of a floating buoy. In Ocean Wave Spectra, Proceedings of a Conference. Prentice-Hall, Englewood Cliffs, N.J.

Longuet-Higgins, M.S. (1963): The effects of non-linearities on the statistical distribution of the theory of sea waves. J. Fluid Mech., 17, pt. 3, pp. 459-480.

Longuet-Higgins, M.S. (1963): The generation of capillary waves by steep gravity waves. J. Fluid Mech., 16(1), 138-159.

Longuet-Higgins, M.S. (1069): On wave breaking and the equilibrium spectrum of wind-generated waves. Proc. Roy. Soc., Ser. A, 310(1501), 6 May 1969, 151-159.

Martin, J.J. (1966): Acoustic reverberation at the sea surface. Surface and sublayer spectra vis-á-vis scattering and reflection. IDA Paper P-284, Institute for Defense Analyses, Research and Engineering Support Division, DDC No. AD645 541.

Martin, J.J. (1969): Capillary wave spectrum from sound reverberation measurements. IDA Note N-631, Institute for Defense Analyses.

Miles, J.W. (1957, 59, 59, 62): On the generation of surface waves by shear flow. J. Fluid Mech., Part 1, 1957, 3, 184-204; Part 2, 1959, 6, 568-582; Part 3, 1959, 6, 583-598; Part 4, 1962, 13, 433-448.

Mitsuyasu, H. (1968): A note on the non linear energy transfer in the spectrum of wind generated waves. Research Institute for Applied Mechanics XVI 54 251-264 Kyushu University.

Moskowitz, L., W.J. Pierson, and E. Mehr (1962, 1963): Wave spectra estimated from wave records obtained by the OWS Weather Explorer and the OWS Weather Reporter (I and II). Prepared for the U.S. Naval Oceanographic Office, Research Division, School of Engineering and Science, New York University.

Moskowitz, L. (1964): Estimates of the power spectrums for fully developed seas for wind speeds of 20 to 40 knots. J. Geophys. Res. 69(24), 5161-5179.

Neumann, G., and W. J. Pierson (1966): Principles of Physical Oceanography. Prentice-Hall, Englewood Cliffs, N. J. 545 pp.

Ocean Wave Spectra, Proceedings of a Conference (1963). Prentice-Hall, Englewood Cliffs, N. J.

Phillips, O. M. (1957): On the generation of waves by turbulent wind. J. Fluid Mech., 2, 417-445.

Phillips, O. M. (1958): The equilibrium range in the spectrum of wind generated waves. J. Fluid Mech., 4, 426-435.

Phillips, O. M. (1960): On the dynamics of unsteady gravity waves of finite amplitude. Part I, J. Fluid Mech. 9, 193-217.

Phillips, O. M. (1961): On the dynamics of unsteady gravity waves of finite amplitude. Part 2, J. Fluid Mech., 1, 143-155.

Phillips, O. M. (1966): The Dynamics of the Upper Ocean. Cambridge University Press.

Pierson, W. J., and L. Moskowitz (1964): A proposed spectral form for fully developed seas based on the similarity theory of S. A. Kitaigorodskii. J. Geophys. Res., 69(24), 5181-5190.

Pierson, W. J. (1964): The interpretation of wave spectra in terms of the wind profile instead of the wind measured at a constant height. J. Geophys. Res., 69(24), 5191-5203.

Pierson, W. J., L. Tick, and L. Baer (1966): Computer based procedures for preparing global wave forecasts and wind field analyses capable of using wave data obtained by a spacecraft. Sixth Symposium Naval Hydrodynamics, Office of Naval Research, Department of the Navy ACR 136.

Pierson, W. J. (1971): Spectral wave forecasts. Proc. 8th Annual Military Oceanography Conference. U.S. Navy, Postgraduate School, Monterey, California.

Pierson, W. J., F. C. Jackson, R. A. Stacy, and E. Mehr (1971): Research on the problem of the radar return from a wind roughened sea. Advanced Applications Flight Experiments Principal Investigators' Review, Oct. 5-6, 1971. NASA Langley Research Center, pp. 83-114.

Pierson, W.J., and V.J. Cardone (1971): Radar satellite oceanography and ocean dynamics. Final Report on Contract N623-6-70-A-0075, Task Order .0005, with supplemental material on Task Order 7, for the period 1 July 1970 to 1 December 1971. New York University, School of Engineering and Science, Department of Meteorology and Oceanography.

Pierson, W.J., and R.M. Moore (1972): The extrapolation of laboratory and aircraft radar sea return data to spacecraft altitudes. In Proc. Fourth Annual Earth Resources Review, MSC, Houston, Texas

Saenger, R.A. (1972): Measurement of the roughness and directional properties of the ocean surface in support of the NRL low frequency underwater surface-scattering experiment. O P 70-61-04 GSL Report TR-72-6 New York University, Dept. of Meteorology and Oceanography. AD 752065.

Schule, J.J., L.S. Simpson, and P.S. DeLeonibus (1971): A study of fetch-limited wave spectra with an airborne laser. J. Geophys. Res., 76 (18), 4160-4171.

Stilwell, D., Jr. (1969): Directional energy of sea waves from photographs. J. Geophys. Res., 74(8), 1974-1986.

Sutherland, A.J. (1967): Spectral measurements and growth rates of wind generated water waves. Tech. Rept. No. 84, Dept. of Civil Engineering, Stanford University, 64 pp.

Tucker, M.J. 91956): A shipborne wave recorder. Trans. Inst. Naval Arch. 98, 236-250 (London).

Valenzuela, G.R., M.B. Laing, and J.C. Daley (1971): Ocean spectra for the high-frequency waves as determined from airborne radar measurements. J. Mar. Res., 29(2), 69-84.

Wright, J.W. (1968): A new model for sea clutter. IEEE Trans. Antennas Propagat., 16(2), 217-233.

Wu, Jin (1971): Slope and Curvature Distribution of Wind Disturbed Water Surface. J. Opt. Soc. America, Vol. 61, No. 7, pp. 852-858.

*U.S. GOVERNMENT PRINTING OFFICE: 1973-739-155/71